An Approach to Using Finite Element Models to Predict Suspension Member Loads in a Formula SAE Vehicle

By
Lane Thomas Borg

Thesis submitted to the faculty of the
Virginia Polytechnic Institute and State University
in partial fulfillment of the requirements for the degree of
Master of Science
In
Mechanical Engineering

Robert L. West, Committee Chair

John B. Ferris, Committee Member

Matthew A. Merkle, Committee Member

May 28, 2009

Blacksburg, Virginia

Keywords: Suspension design, vehicle dynamics, finite elements, Formula SAE

An Approach to Using Finite Element Models to Predict Suspension Member Loads in a Formula SAE Vehicle

Lane Thomas Borg

ABSTRACT

A racing vehicle suspension system is a kinematic linkage that supports the vehicle under complex loading scenarios. The suspension also defines the handling characteristics of the vehicle. Understanding the loads that the suspension carries in a variety of loading scenarios is necessary in order to properly design a safe and effective suspension system. In the past, the Formula SAE team at Virginia Tech has used simplified calculations to determine the loads expected in the suspension members. This approach involves several large assumptions. These assumptions have been used for years and the justification for them has been lost.

The goal of this research is to determine the validity of each of the assumptions made in the method used for calculating the vehicle suspension loads by hand. These assumptions include modeling the suspension as pinned-pinned truss members to prevent bending, neglecting any steering angle input to the suspension, and neglecting vertical articulation of the system. This thesis presents an approach to modeling the suspension member loads by creating a finite element (FE) model of the entire suspension system. The first stage of this research covers the validation of the current calculation methods. The FE model will replicate the suspension with all of the current assumptions and the member loads will be compared to the hand calculations. This truss-element-based FE model resulted in member loads identical to the hand calculations.

The next stage of the FE model development converts the truss model to beam elements. This step is performed to determine if the assumption that bending loads are insignificant is a valid approach to calculating member loads. In addition to changing the elements used from truss to beam element, the suspension linkage was adapted to more accurately model the methods by which each member is attached to the others. This involves welding the members of each control arm together at the outboard point as well as creating a simplified version of the pull rod mounting bracket on the upper control arm. The pull rod is the member that connects the ride spring, damper, and anti-roll bar to the wheel assembly and had previously been mounted on the upright. This model reveals reduced axial components of load but increases in bending moments sizable enough to reduce the resistance to buckling of any member in compression.

The third stage of model development incorporates the steer angle that must be present in loading scenarios that involve some level of cornering. An analysis of the vehicle trajectory that includes the effects of slip angle is presented and used to determine the most likely steer angle the vehicle will experience under cornering. The FE model was

adapted to include the movement of the steering linkage caused by driver input. This movement changes the angle of the upright and steering linkage as well as the angle at which wheel loads are applied to the suspension. This model results in a dramatic change in member loads for loading cases that involve a component of steering input.

Finally, the FE model was further enhanced to account for vertical movement of the suspension as allowed by the spring and damper assembly. The quasi-static loading scenarios are used to determine any member loading change due to vertical movement. The FE model is also used to predict the amount of vertical movement expected at the wheel center. This data can be used by the suspension designer to determine if changes to the spring rate or anti-roll bar stiffness will result in a more desirable amount of wheel movement for a given loading condition. This model shows that there is no change in the member loads due to the vertical movement of the wheel.

This thesis concludes by presenting the most important changes that must occur in member load calculations to determine the proper suspension loading under a variety of loading scenarios. Finally, a discussion of future research is offered including the importance of each area in determining suspension loads and recommendations on how to perform this research.

Acknowledgements

This research could not have occurred without the help of many individuals. I would like to express my immense gratitude to my committee chair, Dr. Robert West, for all of his help with modeling using finite elements as well as his patience while dealing with my remote work location. I would also like to thank Dr. John Ferris and Mr. Matt Merkle for joining my committee and being a part of this project. In addition, I would like to convey my appreciation to John Fratello, suspension designer VT-FSAE 2009, for all of the information and insight he provided me about the 2009 car and the current design processes. I wish John and the rest of the VT-FSAE team the best and hope for a successful competition in May, 2009. Also, I would like to thank The Goodyear Tire & Rubber Co. for allowing me to work on this project while working full time in at the San Angelo Proving Grounds. Lastly, I would like to thank my family for all of their support in everything I do.

Table of Contents

List of Figures viii
List of Tables x
Glossary xiii
Chapter 1 - Introduction 1
1.1 Needs Statement and Overview of the Problem 1
1.2 Hypothesis and Concept for Solution 2
1.3 Research Objectives 3
1.3.1 Validate/Disprove Current Loading Calculation Methods 3
1.3.2 Determine if FE Models are a More Thorough Method for Load Calculations 3
1.3.3 Create a FE Model that Accounts For More Parameters 4
1.3.4 Determine the Key Aspects of the Analysis 5
1.4 Scope of Project 5
1.4.1 Validate the Current Calculations used to Determine Suspension Loads 5
1.4.2 Develop a FE Model of the Suspension that Accurately Loads the Suspension Members 5
1.5 Organization of Thesis 6
Chapter 2 – Literature Search and Background 7
2.1 Elastic Kinematics 7
2.1.1 Suspension Kinematics/Load Transfer 7
2.1.2 Large Displacement, Small Strain FE 12
2.1.3 Abaqus Elements including Connectors 12
2.2 Suspension Loading and Dynamics 13
2.2.1 Tire Loads at the Contact Patch (Tire Consortium Data) 13
2.2.2 Forces in the Suspension 21
2.2.3 Suspension Movement and Articulation 25
2.2.4 Examples of Finite Elements in Suspension Design 28
Chapter 3 – Suspension System and Load Calculations 30
3.1 Suspension Design 30
3.1.1 Background on Short Long Arm (SLA) Suspension 30
3.1.2 Components of Suspension (Members, Springs, Damper, Tire, etc.) 32
3.1.3 Major Areas of Concern with Loading 36
3.2 Conventions Used in Thesis 37
3.2.1 Coordinate Systems 37
3.2.2 Member Nomenclature 39
3.3 Load Calculations 40
3.3.1 Outline of Method (Hand Calculations) 40
3.3.2 Results of the Hand Calculations 44
3.4 Assumptions of the Hand Calculations and where Improvement is Needed 46
3.4.1 Members Modeled as Beams Instead of Trusses 46
3.4.2 Forces and Members Rotated with Steered Tire 48
3.4.3 Suspension Articulates Vertically with Load Transfer 49
Chapter 4 – Development of FE Model 51
4.1 Truss Model Design 51

4.1.1 Explanation of the Need for a Large Displacement/Small Strain Model 51
4.1.2 Pin-Pin Six Member Truss Model 52
4.1.3 Discussion of Connector Elements (*Join)..... 55
4.1.4 Calculations of Forces at the Contact Patch for Loading Scenarios..... 56
4.1.5 Results of Truss Model for Key Loading Scenarios..... 60
4.2 Beam Model Development 61
4.2.1 Trusses Converted to Beams/Explanation of Geometry Changes 61
4.2.2 Comparison of Truss Model to Beam Model 65
4.3 Steered Model 69
4.3.1 Slip Angle vs. Steered Angle and Effect on Direction of Travel..... 69
4.3.2 Outline of Steer Angle through Typical Course Radii..... 70
4.3.3 Articulate Model across a Range of Steering Angles 77
4.4 Sprung Model..... 82
4.4.1 Explanation of Load Transfer and Installation Ratio..... 82
4.4.2 Adjusting Steered Model to Contain Spring/ARB Forces..... 84
4.4.3 Vertical Articulation Analysis 88
4.5 Validation of FE Model through Vertical Movement Comparison 91
4.5.1 Concept of Model Validation..... 91
4.5.2 Vertical Validation Analysis Data and Discussion..... 92
Chapter 5 – Final FE Model versus Calculations 95
5.1 Comparison of FE Model Results versus Calculations..... 95
5.1.1 Truss Model 95
5.1.2 Beam Model..... 96
5.1.3 Steered Model 104
5.1.4 Sprung Model..... 105
5.1.5 Vertical Articulation from the Sprung Model Compared to On-Vehicle Measurements 107
5.2 Discussion of Significant Effects..... 107
5.2.1 Concern between Hand Calculations and FE Model 107
5.2.2 The Significance of Bending and Factors to Address..... 108
5.2.3 The Effect of Vertical Suspension Movement..... 109
Chapter 6 – Conclusions and Recommendations..... 110
6.1 Discussion of Hand Calculation Assumptions..... 110
6.1.1 Pin-Pin Truss Members..... 110
6.1.2 Analysis Can Ignore Bending and Buckling in Members 110
6.1.3 Analysis Performed without Steer Angle 111
6.1.4 Analysis Performed at Ride Height 112
6.2 Final Effects on Suspension Loading 113
6.2.1 Beam Members Change Loads 113
6.2.2 Suspension Steering Changes Loads 114
6.3 Recommendations..... 114
6.3.1 Validate Loading with On-Car Testing and/or Test Rig..... 114
6.3.2 Improving the Realism of the Components in the Model (Gussets, Crimped Tubes, etc.)..... 115
6.3.3 Dynamic Loading of Suspension..... 116
6.3.4 Bearing Hysteresis 118

References 119
Appendix A: Programming Code 120
A-1 MATLAB m-file to Calculate Member Loads 120
Appendix B: Member Load Data 123
B-1 Member Load Comparison of Hand Calculations and Truss Model 123
B-2 Complete Member Load Comparison of Hand Calculations, Truss Model, and Beam Model 124
B-3 Full Data for Beam Models 125
B-4 Complete Member Loads using the Steered Model 127
B-5 Complete Member Loads using the Sprung Model 128
Appendix C: Complete Wheel Load Data 130
C-1 Wheel Center Loads for All Wheels and All Loading Scenarios 130
Appendix D: Steer Angle Calculations 132
D-1 Steer Angle versus Lateral Movement of Tie Rod Calculations 132
D-2 Steer Angle versus Radius of Travel Data 136

List of Figures

Figure 2.1. Example of a short-long arm suspension from the front view. 8
Figure 2.2. Variables and dimensions associated with lateral load transfer [6]. 11
Figure 2.3. Calspan TIRF tire measurement machine [9]. 14
Figure 2.4. Tire contact patch under slip angle. 16
Figure 2.5. Example graph of lateral force versus vertical load across a range of slip angles [6]. 17
Figure 2.6. Lateral force versus slip angle for the same tire as Figure 2.5. 18
Figure 2.7. Examples of tire camber angle conventions from the front view of the vehicle. 19
Figure 2.8. Lateral force versus slip angle with various camber angles applied to the tire [6]. 20
Figure 2.9. Diagram of forces and moments on a tire in the SAE standard system [6]... 21
Figure 2.10. View of front right suspension from the front middle of the vehicle. 22
Figure 2.11. Diagram of steering linkage movement to driver inputs. 26
Figure 2.12. FBD of the upright. 27
Figure 3.1. SLA suspension in the front view. 30
Figure 3.2. Kingpin geometry [6]. 31
Figure 3.3. Corner suspension assembly with all components labeled. 33
Figure 3.4. FBD of the front upright showing wheel center forces and suspension reaction forces. 34
Figure 3.5. Degrees of freedom on the suspension upright. 35
Figure 3.6. SAE Car Coordinate System [3]. 38
Figure 3.7. Abaqus coordinate system shown on a CAD model of the 2009 VT-FSAE vehicle. 39
Figure 3.8. Definition of suspension point nomenclature represented graphically. 40
Figure 3.9. Suspension point labeling convention. 42
Figure 4.1. Truss element FE model as viewed from the right front view of the vehicle looking towards the left rear showing boundary conditions and loads for a left hand cornering scenario. 53
Figure 4.2. The cross-section and photo of a typical spherical bearing. 55
Figure 4.3. FBD of upright showing wheel center forces as they are applied to the upright. 59
Figure 4.4. View comparing the pull rod mount in the Truss Model to a photograph of the same area from the completed 2009 VT-FSAE car. 62
Figure 4.5. Beam element FE model showing the modified pull rod mount area to accurately represent the load path of the pull rod through the upper control arm. 63
Figure 4.6. Beam element FE model with modified pull-rod mount as viewed from the front right with chassis mount boundary conditions and loading for a left hand corner. 64
Figure 4.7. Beam element FE model with modified pull-rod mount as viewed from the front middle of the vehicle with chassis mount boundary conditions and loading for a left hand corner. 65

Figure 4.8. Layout and dimensions of the FSAE skid pad course modified to show the calculated path of the vehicle CG travel in red [4]. 71
Figure 4.9. Steering diagram used to account for the effect of slip angle on the radius of vehicle travel. 73
Figure 4.10. Modified two wheeled vehicle steering angle effect diagram. 74
Figure 4.11. Modified two wheeled vehicle steering angle effect diagram. 75
Figure 4.12. Diagram showing the triangles used to calculate the radius of travel, *R*..... 76
Figure 4.13. Comparison of member axial force with steering angle for left hand cornering with expected load transfer. 78
Figure 4.14. Highlighted member MN on FE model. 78
Figure 4.15. Member PO highlighted on the FE model. 82
Figure 4.16. CAD model of the bellcrank with labeled connection points. 85
Figure 4.17. Bellcrank, spring, and ARB as added to the vertically articulated model... 86
Figure 4.18. Vertical displacement at the wheel center under the steered loading scenarios over the steer angle sweep. 89
Figure 4.19. Amount of ride spring compression under the steered loading scenarios over the steer angle sweep. 89
Figure 4.20. Movement of wheel center when steered. 90
Figure 4.21. FBD of upright showing wheel center forces as they are applied to the upright. 91
Figure 4.22. Plot of the tire load versus spring force for the theoretical, measured, and Sprung Model. 93
Figure 5.1. Visual representation of buckling failure in member JK in cornering at 11 degrees of steer. 99
Figure 5.2. Member JK highlighted on the FE model. 101
Figure 5.3. Diagram of suspension from the front middle labeling each member. 103
Figure 6.1. Highlighted member MN on FE model. 111
Figure D.1. Geometry of steering linkage in the top view (not to scale). 132
Figure D.2. Steering arm detail showing the notation for steered calculations. 133
Figure D.3. Diagram of the tie rod movement under steering in the top view. 134
Figure D.4. Geometry of the triangle formed when the tie rod is displaced due to a steering input. 135

List of Tables

Table 2.1. Dimensions of an example FSAE vehicle. 9
Table 2.2. More detailed specifications for the example FSAE vehicle. 11
Table 3.1. Suspension points for the front right corner of the 2009 VT-FSAE car. 44
Table 3.2. Wheel center loading for the front right corner of the suspension. 45
Table 3.3. Critical member loads for each suspension member for the seven loading scenarios as determined by the hand calculations. 46
Table 4.1. Truss element specifications for the Truss Model. 53
Table 4.2. Section properties for each member of the Truss Model and the Beam Model. 54
Table 4.3. Material properties of AISI 4130 steel. 54
Table 4.4. Constraints on the Truss Model. 55
Table 4.5. Contact patch loads for each loading scenario as given by the FSAE TTC data for the Goodyear D2692 20x7.0-13 tire. 58
Table 4.6. Wheel center loads for each loading scenario in the car coordinate system. 58
Table 4.7. Comparison of maximum member loads from hand calculations and truss model. 61
Table 4.8. Beam element specifications for the Beam Model and all subsequent stages of the FE Model. 64
Table 4.9. Boundary conditions on the Beam Model. 65
Table 4.10. Comparison of maximum compressive and tensile loads with hand calculations, truss elements, and beam elements. 66
Table 4.11. Maximum and minimum loads in each member for the beam element model. 67
Table 4.12. Suspension member sections as specified by the suspension designer for the 2009 VT-FSAE car. 68
Table 4.13. Comparison of internal axial forces for the Beam Model with unit sections and Beam Model with proper sections. 68
Table 4.14. Comparison of member stresses in the Beam Model with unit sections and with proper sections. 68
Table 4.15. Slip angle values for the three loading scenarios that involve cornering. 70
Table 4.16. Load transfer data for a left hand corner with expected load transfer as provided by the suspension designer. 72
Table 4.17. Boundary conditions for the Steered Model. 77
Table 4.18. Axial forces in members in steered loading scenarios for each of the model stages with the critical member load in cornering highlighted in orange. 79
Table 4.19. Comparison of member stresses in cornering loading scenarios for the non-steered Beam Model and the Steered Model. 80
Table 4.20. Comparison of the critical loads with hand calculations, exclusion of the 5g bump scenario, and accounting for steer angle and slip angle in the steered loading scenarios. 81
Table 4.21. Boundary conditions on the Sprung Model. 87
Table 4.22. Comparison of maximum member loads for all Abaqus models and hand calculations. 88
Table 4.23. Vertical articulation results for all loading scenarios. 90

Table 4.24. Vertical validation analysis data for the theoretical, measured, and Sprung Model. 93
Table 5.1. Summary of results comparing the hand calculated member loads to the truss FE model. 95
Table 5.2. Summary of all internal loads from the beam element FE model. 96
Table 5.3. Factor of safety in buckling and critical member for all loading scenarios. 99
Table 5.4. Comparison of factors of safety in buckling between the hand calculations and Abaqus. 100
Table 5.5. Yielding and buckling factors of safety in member JK. 101
Table 5.6. Factors of safety for all loading scenarios in each member. 102
Table 5.7. Comparison of hand calculations to the axial force in the beam element FE model with the percent difference of the beam element FE model to the hand calculations. 103
Table 5.8. Summary of maximum axial forces in the suspension members through a steer angle sweep. 104
Table 5.9. Vertical articulation results for all loading scenarios. 106
Table 5.10. Minimum factors of safety for each member in each stage of FE model development. 108
Table B.1. Axial loads as calculated by the Truss Model compared to the hand calculations with the percent difference for all loading scenarios. 123
Table B.2. Comparison of the hand calculations, the Truss Model, and the Beam Model with unit sections for all loading scenarios. 124
Table B.3. Complete internal member loads for the Beam Model with unit sections. 125
Table B.4. Complete member loads for the Beam Model with proper designed cross-sections. 126
Table B.5. Internal axial forces, bending moment magnitudes, and shear force magnitudes for the suspension members as calculated by the Steered Model. 127
Table B.6. Internal axial forces, bending moment magnitudes, and shear force magnitudes for the suspension members as calculated by the Sprung Model for the steered scenarios. 128
Table B.7. Internal axial forces, bending moment magnitudes, and shear force magnitudes for the suspension members as calculated by the Sprung Model for the non-steered scenarios. 129
Table C.1. Wheel center loads for left hand cornering at 1.4g with expected load transfer. 130
Table C.2. Wheel center loads for left hand cornering with full load transfer. 130
Table C.3. Wheel center loads for pure braking at 1.4g with expected load transfer. 130
Table C.4. Wheel center loads for pure braking with full load transfer. 130
Table C.5. Wheel center loads for combined left hand cornering and braking. 131
Table C.6. Wheel center loads for a 1.5g full vehicle skid. 131
Table C.7. Wheel center loads for a 5g bump at each corner. 131
Table D.1. Steer angle and radius of travel data for the left hand corner loading scenario. 136
Table D.2. Steer angle and radius of travel data for the left hand corner with full load transfer loading scenario. 137

Table D.3. Steer angle and radius of travel data for the left hand corner and braking combined loading scenario. 138

Glossary

Many unique terms are used in suspension design and discussion. Some of these terms stem from the world of high-performance driving; others are engineering vocabulary used when referring to specific vehicle behavior. The following list will act as a glossary to inform the reader of any new or unusual terms used in this research. Additional terms can be found in the SAE publication "Vehicle Dynamics Terminology – SAE J670" [1].

- Ackerman Steer Angle – "The angle whose tangent is the wheelbase divided by the radius of turn" [1].
- Ackerman Steer Angle Gradient – "The rate of change of Ackerman steer angle with respect to change in steady-state lateral acceleration on a level road at a given trim and test conditions" [1].
- Anti-Geometry – Suspension geometry that reduces the tendency of the vehicle to pitch under longitudinal accelerations (anti-squat for acceleration and anti-dive for braking).
- ARB – Acronym for Anti-Roll Bar (or sway bar), a device that adds roll resistance to the vehicle, but does not add ride resistance.
- Camber Angle – "The inclination of the wheel plane to the vertical. It is considered positive when the wheel leans outward at the top and negative when it leans inward" [1].
- Capacity – Often lateral capacity, or traction capacity, is the ability of the tire to provide a traction force to propel or corner the vehicle.
- Center of Tire Contact – "The intersection of the wheel plane and the vertical projection of the spin axis of the wheel onto the road plane" [1].
- Contact Patch – Area of tire tread that is in contact with the road surface and will change under different loading conditions.
- Instant Center – Of one suspension corner, this is the point about which the suspension will rotate when at a given position (the same as an instant center in kinematics).
- LCA – Lower Control Arm abbreviation.
- Overall Steering Ratio – "The rate of change of steering wheel angle at a given steering wheel trim position, with respect to change in average steer angle of a pair of steered wheels, assuming an infinitely stiff steering system with no roll of the vehicle" [1].
- Oversteer (loose) – "A vehicle is oversteer at a given trim if the ratio of the steering wheel angle gradient to the overall steering ratio is less than the Ackerman steer angle gradient" [1].
- PR – Pull (or push) Rod abbreviation, this is the member that connects the spring/damper to the wheel and tire assembly.
- Roll Center – "The point in transverse vertical plane through any pair of wheel centers at which lateral forces may be applied to the sprung mass without producing suspension roll" [1].
- Roll Center Migration – The amount the roll center of a vehicle axle will move under suspension articulation, this is ideally zero.
- Roll Rate – The resistance of an axle to body roll of the vehicle.

- Slip Angle – "(α) The angle between the X' axis and direction of travel of the center of tire contact" [1].
- Sprung Mass – "Considered to be a rigid body having equal mass, the same center of gravity, and the same moments of inertia about identical axes as the total sprung weight" [1].
- Sprung Weight – "All weight which is supported by the suspension, including portions of the weight of the suspension members" [1].
- Steer angle – "The angle between the projection of a longitudinal axis of the vehicle and the line of intersection of the wheel plane and the road surface" [1].
- Steering Wheel Angle Gradient – "The rate of change in the steering wheel angle with respect to change in steady-state lateral acceleration on a level road at a given trim and test conditions" [1].
- Suspension Compression (bump) – "The relative displacement of the sprung and unsprung masses in the suspension system in which the distance between the masses decreases from that at static condition" [1].
- Suspension Rebound (Extension) – "The relative displacement of the sprung and unsprung masses in a suspension system in which the distance between the masses increased from that at static condition" [1].
- Take a set – A driving term used to describe the point at which the vehicle/suspension has reached a steady state condition in a corner.
- Tire carcass – The structure of the tire including the tire bead, plies, belts or breakers, and any other structural component of the tire that supports the tread cap.
- Tire load – The vertical load a tire is supporting in any given loading condition.
- Static Toe Angle – "The static toe angle of a wheel, at a specified wheel load or relative position of the wheel center with respect to the sprung mass, is the angle between a longitudinal axis of the vehicle and the line of intersection of the wheel plane and the road surface. The wheel is 'toed-in' if the forward portion of the wheel is turned toward a central longitudinal axis of the vehicle and 'toed-out' if turned away" [1].
- TR – Tie Rod abbreviation, this is the arm that controls steering input in the front suspension.
- Tread (tread cap) – "The peripheral portion of the tire, the exterior of which is designed to contact the road surface" [1].
- Trim – "The steady-state (that is, equilibrium) condition of the vehicle with constant input which is used as the reference point for analysis of dynamic vehicle stability and control characteristics" [1].
- UCA – Upper Control Arm abbreviation.
- Understeer (push, tight) – "A vehicle is oversteer at a given trim if the ratio of the steering wheel angle gradient to the overall steering ratio is greater than the Ackerman steer angle gradient" [1].
- Unsprung Mass – "The unsprung masses are the equivalent masses which reproduce the inertia forces produced by the motions of the corresponding unsprung parts" [1].
- Unsprung Weight – "All weight which is not carried by the suspension system, but is supported directly by the tire or wheel and considered to move with it" [1].

- Wheel Rate (Suspension Rate) – “The change of wheel load, at the center of the tire contact, per unit vertical displacement of the sprung mass relative to the wheel at a specified load” [1].

Chapter 1
Introduction

1.1 Needs Statement and Overview of the Problem

The Virginia Tech Formula SAE team would like to further the understanding of suspension systems by performing a thorough structural analysis of the internal suspension member loads in the expected loading scenarios. A detailed analysis of the member loads will aid in further improving the design of the suspension components and the chassis, giving the team advantages in both the design competition as well as performance improvements for the dynamic events. Several assumptions made in the current method of load calculation need to be verified and if proven unacceptable, new assumptions or methods are to be provided to properly calculate suspension member loads.

Auto racing began shortly after the invention of the automobile. Since then, motorsports has grown into an extremely popular activity all over the world. Technological advances have propelled the sport to speeds that have not been seen before. Races can be won by thousandths of a second forcing engineers and race teams to spend large amounts of resources on finding the last little bits of speed within their vehicles. The Formula SAE competition as of 2009 falls into the category of formula car racing. A formula car is an open wheeled vehicle with only one seat, typically in the middle of the vehicle. Formula cars are purpose built for racing with very few compromises.

In the world of formula racing, the pinnacle of technology exists in Formula 1. These cars are capable of cornering at nearly 5g and reach speeds as high as 200 MPH. Formula 1 teams will spend millions of dollars for fractions of a second in lap times. Part of improving lap times of any racing vehicle is to optimize the suspension. The suspension controls the attitude of the tire to the road surface through the design of the linkage kinematics. The suspension also reacts to the loads created by the tire. The loads will force the suspension to elastically deform. This compliance will change the orientation of the tire to the road. To control and predict this compliance, race engineers will thoroughly analyze the suspension members.

Depending on the racing series, a simplified method of load calculation can be utilized to minimize the time and effort required to determine the suspension loads. One simplified method often used assumes that the suspension can be represented by a truss structure consisting of six independent members. This structure is essentially a static space truss [1]. A space truss eliminates several of the variables that could be present in the suspension; the most prominent of which is any bending moment. It is also assumed that a space truss is constrained such that there is no displacement of the structure. A suspension will have a great deal of displacement, a small amount due to the internal strain in the members in the form of compliance, as well as the large displacement caused by the wheel movement relative to the chassis.

The other typical analysis method seen in the automotive industry is creating all suspension parts in an FE model and loading the entire assembly with the expected tire loads or road inputs. This method is often used to determine stress concentrations in the individual parts and not to determine loads within each member. The reason for looking at stress concentrations over member loads is due to the nature of production vehicle suspension designs. Suspension parts in these vehicles are typically designed to meet certain fatigue and cost criteria at the sacrifice of some high performance potential.

Racing vehicles are likely designed using a finite element based technique; however the secrecy that surrounds the world of motorsports makes the specific processes used proprietary and rarely published in publically accessible documents. The overall purpose of this research is to make information on structural suspension analyses of racing vehicles available to the public. The dominant mechanics of the common racing type suspension will be investigated and areas for future research will be determined from these results.

1.2 Hypothesis and Concept for Solution

Many assumptions have been made in the past while calculating member loads for common suspension loading scenarios. To provide research that will determine whether each assumption is valid, an Abaqus finite element (FE) model will be developed in stages. The first stage will establish how accurately the current theoretical calculations determine suspension loading under similar loading conditions with a geometry representative of the existing assumptions. Subsequent stages will add features to the model to determine if any change occurs in the member loads compared to the simple hand calculations when accounting for the assumptions in question. The main assumptions to be examined are (1) that bending moments within each member can be neglected, (2) that geometry changes due to steering have no effect on the member loads, and (3) that geometry changes from vertical displacement of the suspension have no effect on the member loads.

The first stage beyond the basic model (Truss Model) will implement elements capable of handling forces and moments other than a single axial force. This Beam Model stage of development will allow the determination of bending moments, torsion moments, and shear forces that may be present in some or all of the loading scenarios. One assumption of the Truss Model and hand calculations is that the axial forces dominate the mechanics of the system. This stage will determine if it is valid to assume that the axial force is the only significant factor of the internal member loads.

Steering angle will then be added to this model to create the Steered Model stage. The proper amount of rotation will be applied to the forces on the suspension to account for the slip angle of the tires and the steer angle of the wheel and tire. The suspension geometry will be constrained in a new, steered position. The Steered Model will then be used to determine if there are any changes to the member loads when accounting for a steer angle. A comparison will then be made between the non-displaced suspension and

the steered suspension. Any changes in loading will be investigated to determine the effect on the critical design load for each member.

Lastly, vertical displacement of the wheel will be added to the model. The Sprung Model will be the final stage of this research and will examine any changes in internal member forces due to vertical displacement of the suspension. This stage will also allow for a simple model validation by comparing the vertical displacement of the wheel in the FE model to an equivalent condition on the completed VT-FSAE vehicle. All of these stages of model development will be used to summarize changes in member loads due to each of the assumptions made using the space truss method. Each difference found, should any exist, will be discussed to determine the effects on the stresses of the members.

1.3 Research Objectives

1.3.1 Validate/Disprove Current Loading Calculation Methods

The primary goal of this research is to determine the accuracy of the current method for calculating member loads under quasi-static loading scenarios. There is a need to either validate the assumptions made with the current method or to understand why the assumptions are not valid and to develop methods that will account for the discrepancies. If all the existing assumptions can be validated, the hand calculations can continue to be used as a means of determining the member loads in the suspension.

The loading scenarios that will be used are the same as those used in the current hand calculations. There are seven common loading scenarios that represent common situations any given racing vehicle will see in a competition setting including cornering, braking, sliding, and hitting a bump. These loading scenarios are also used to make a valid comparison with the current calculation methods. Using different inputs would invalidate any comparison of the old methods to the new model. With similar initial loads on the structure, aspects of the model will be changed to determine which aspects of the suspension have the greatest effect on the internal member loads of each suspension component.

1.3.2 Determine if FE Models are a More Thorough Method for Load Calculations

The current method of calculating suspension loads makes more assumptions than desired about the structure. The new method to be developed needs to represent the suspension in a manner that correlates well with the hand calculation method. In order to make a meaningful comparison between the new model and the old calculation methods, the FE model must correlate with the hand calculations under a similar set of assumptions. This new method will need to decrease the amount of assumptions made in the calculation of the member loads by modeling the suspension geometry in a more realistic manner than used in the current methods. These assumptions center on the representation of the suspension geometry, specifically the assumption of no bending moments or other non-axial forces. Large displacements due to steering and vertical

movement are also neglected under the current analysis methods. While the contact patch loads are fairly well known, their effect on member loads may be incorrect due to the above assumptions. The new method will also need to be adaptable to changes in the suspension points such that future teams will be able to quickly and effectively determine the suspension loads for the new designs.

To determine the accuracy of this new model, two methods will be used. First, the Truss Model, a basic representation of the suspension, will be created and compared to the hand calculations. The Truss Model should produce member loads equal to those determined by the hand calculations. A FE model that results in equal loads to the hand calculations will validate the decisions made in designing the basic FE model.

Second, a comparison of vertical movement will be used to compare the final vehicle to the FE model. The resources to conduct a full strain gauge analysis of the suspension on the final vehicle are not available at this time and therefore, this research concentrates on investigating the effects of making certain assumptions about the suspension members. The simple vertical movement validation will need to suffice for now as a means of determining if the FE model is behaving in a roughly similar manner to the actual car. Once resources are available to utilize on-car strain gauges, future research should be arranged to compare the FE model developed here with the measurements from the vehicle.

1.3.3 Create a FE Model that Accounts For More Parameters

The current method of determining suspension loads assumes all members are constrained to prevent large displacements, but are allowed to experience small strains. The actual suspension members on the vehicle are required to allow the wheels to move vertically to absorb road disturbances and permit the vehicle to handle predictably. The front suspension must articulate while allowing the wheels to steer, adding an additional type of large displacement to the suspension geometry.

In addition to the changes in geometry as the suspension travels, some of the members, specifically the control arms, are going to be subjected to loads that are more complex than simple axial loads. These potential loads need to be understood before they are dismissed as insignificant. The most prominent of these loads are bending moments. These moments have the potential to greatly decrease the factor of safety of each suspension member when loaded. Other forces that may be present are transverse shear forces and torsion loads. It is expected that if these loads are present, they will have a much less significant effect when compared to the axial loads and bending moments. Before this claim can be made though, the shear forces and torsion loads must be determined. Currently these three types of loads are unknown and therefore cannot be dismissed until they have been determined.

1.3.4 Determine the Key Aspects of the Analysis

After investigating the different assumptions and determining what, if any effect, they have on the suspension loads, the most prominent effects will need to be accounted for in future design decisions. The dominant mechanics will be determined, specifically the effects of internal bending moments on the critical design loads of each member. Also, the effects of suspension articulation (large displacements) will be determined and the dominate mechanics of these scenarios will be investigated. The model used to determine these effects can then be used to model future suspension designs. This will allow future designers to fully account for the suspension loads and will allow for more thorough suspension and chassis designs. Ultimately, this will provide VT Motorsports and other FSAE teams with the ability to design increased performance into their vehicles.

1.4 Scope of Project

1.4.1 Validate the Current Calculations used to Determine Suspension Loads

Suspension designers and race engineers can devote entire careers to developing knowledge of suspension systems; therefore, the scope of this thesis must be limited to a reasonable scale. The most necessary information to verify in this research includes determining if the assumption of the hand calculations are valid, investigating a more accurate representation of the suspension geometry, and articulating the suspension appropriately for loading scenarios that require large suspension displacement. The intention of this work is also to provide a foundation for future graduate work that studies the effects of these and additional factors in more detail.

1.4.2 Develop a FE Model of the Suspension that Accurately Loads the Suspension Members

The current method of calculating suspension loads involves hand calculations and a large number of assumptions. This research will concentrate on validating the assumptions made when using the space truss as a basis for the calculations and examining any changes in member loads that occur in the FE model when more correctly modeling the real suspension. To that end, a complete corner assembly will be developed using finite element analysis software. The corner to be used will be the right front corner of the vehicle. This corner was chosen for two reasons. A front corner must be used to investigate loading changes with steering angle. The right side will be used since the team has chosen to perform all loading calculations with the right side of the suspension, so all cornering scenarios will involve left-hand turns which load the right-side suspension more heavily than right-hand turns. Loads will be identical on the left-hand side of the suspension in right-hand corners due to the symmetry of the suspension and vehicle designs as well as the symmetry of the loading scenarios. This corner assembly model will then be used to calculate suspension loads for the same loading scenarios as the hand calculations. Any differences in member loading will be investigated. The loading scenarios will also be studied to determine their validity in

calculating loads. Recommendations based on this research will be provided for future engineers to investigate and model.

1.5 Organization of Thesis

This thesis is organized into the following five chapters:

- Literature Search (Chapter Chapter 2)
- Basic Suspension System and Load Calculations (Chapter Chapter 3)
- Development of FE Model (Chapter Chapter 4)
- Final FE Model vs. Calculations (Chapter Chapter 5)
- Conclusions (Chapter Chapter 6)

The literature search in Chapter Chapter 2 describes research already performed in various areas of suspension design, vehicle dynamics, and finite element analysis. This background information will provide the basic knowledge used to develop the finite element model. Chapter Chapter 3 discusses the current type of suspension system; the components incorporated into it, and most importantly, outline the hand calculations used to determine suspension loads. The development of the finite element model for the suspension is covered in Chapter Chapter 4. This includes the Truss Model used to simulate the scenario of the hand calculations as well as the development of the model to represent a more realistic geometry through the Beam Model, Steered Model, and Sprung Model. Chapter Chapter 5 compares the results of this model in all stages of development to the hand calculations and discusses the significance of any differences as well as what those differences mean to the suspension design and the model development. Finally in Chapter Chapter 6, conclusions and recommendations are discussed. These recommendations include how the current method of calculating suspension loads needs to be changed as well as which assumptions are valid to use and why. Also presented are the recommended areas of future research and the potential benefits of such projects.

Chapter 2
Literature Search and Background

2.1 Elastic Kinematics

2.1.1 Suspension Kinematics/Load Transfer

Suspension loading requires the knowledge of suspension behavior, design techniques, and how each of these affects the dynamics of a racing vehicle. From Thomas Gillespie's Fundamentals of Vehicle Dynamics, "The primary functions of a suspension system are to:

- Provide vertical compliance so the wheels can follow the uneven road, isolating the chassis from roughness in the road.
- Maintain the wheels in the proper steer and camber attitudes to the road surface.
- React to the control forces produced by the tires-longitudinal (acceleration and braking) forces, lateral (cornering) forces, and braking and driving torques.
- Resist roll of the chassis.
- Keep the tires in contact with the road with minimal load variations." [3]

To accomplish these functions, the suspension needs to articulate such that the wheel and tire will move along the desired paths under loading (maintaining the proper attitude, or camber angle, to the road surface). This movement also allows for the vertical compliance needed to follow an uneven road surface. While a virtual rigid suspension such as those used on modern Formula 1 vehicles can provide some vertical compliance through the tire and suspension member deflection, this is more of an exception to the rule. For the purposes of the FSAE car, vertical compliance through suspension articulation will provide not only the needed movement to conform to irregularities in the road surface, but will also satisfy the SAE requirement that the suspension have ± 25.4 mm movement from the static position with driver aboard [4].

While there are many different types of suspension systems, the vast majority of racing vehicles use some form of independent suspension, assuming the sanctioning body has not limited the choice of suspension geometry. The most widely utilized type of independent suspension is the double wishbone, or short-long arm (SLA) suspension [5]. This design is essentially a four bar linkage in the front view, with two control arms (a-arms) comprising two of the moveable links such that they are able to resist forces out of the front view plane (longitudinal forces). Figure 2.1 shows an example of this suspension in the front view.

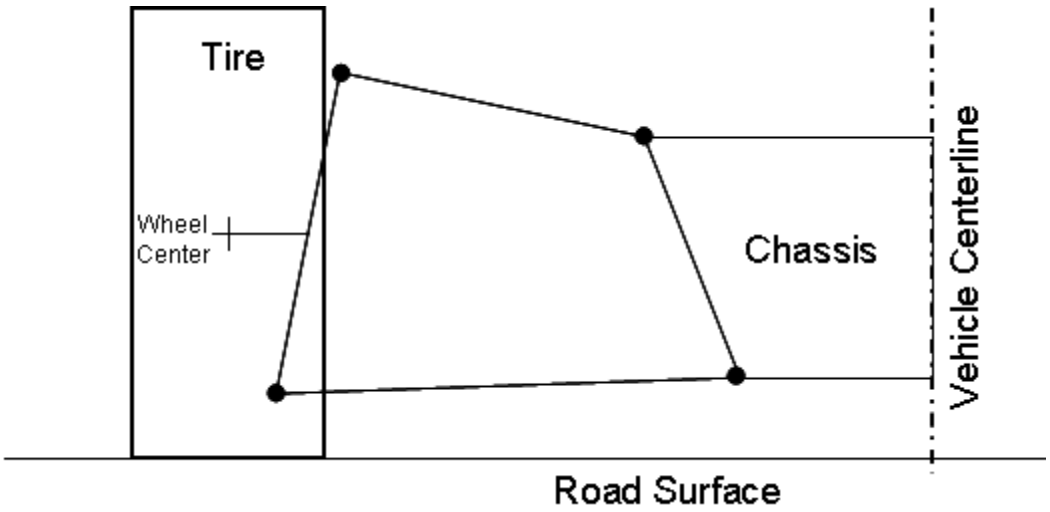

Figure 2.1. Example of a short-long arm suspension from the front view. Black dots represent joints between members.

Like any four bar linkage, the suspension will rotate about the instant center and this will dictate the attitude of the wheel and tire to the road surface. The suspension will move according to the instant center of the suspension linkage when subjected to variations in the road surface, such as bumps or cracks, as well as under chassis roll and pitch due to load transfer.

Load transfer occurs when the driver makes an input through one of the vehicle controls like the steering wheel, brakes, or accelerator. To use pure cornering as an example scenario, the lateral acceleration will result in a centrifugal force at the center of gravity acting in the opposite direction as the lateral loads at the tire contact patches. Since the center of gravity is not at ground level (in line with the lateral loads), a roll moment (M_x) results and there is lateral load transfer. Depending on the speed the vehicle is traveling about a given corner, the amount of load transfer can become a significant percentage of the total vehicle weight. The lateral load transfer is equal to

$$\Delta W_{lat} = \frac{W A_Y h}{t}, \tag{2.1}$$

where ΔW is the increase in the left side vertical load due to a right hand corner (or right side load increase due to a left hand corner), W is the vehicle weight, A_Y is the lateral acceleration in g's, h is the CG height, and t is the track width [6]. Note that Equation (2.1) assumes a vehicle that is symmetric in the front view, such that the vehicle has the same left and right side weights in a static position. Equation (2.1) can be applied to individual axles or to the vehicle as a whole if the track width is the same in the front as the rear.

As an example, the weight transfer of a small single seat racing car needs to be determined. This example FSAE vehicle has dimensions shown in Table 2.1. Please note that these are roughly typical dimensions but do not replicate any specific vehicle.

Table 2.1. Dimensions of an example FSAE vehicle. These dimensions are representative of an average FSAE vehicle, but do not reflect one specific vehicle.

Example FSAE Vehicle		
Spec	**Measurement**	
W	272.2	kg
h	304.8	mm
A_y	1.5	g
t_F	1219.2	mm

Prior competitions reveal a best time of just over 5 seconds wins the skid pad competition [7]. The SAE rules provide the dimensions of the skid pad, which when combined with the winning times, reveal that a lateral acceleration of just over 1.4g is fairly common in competition [4, 7]. Assuming the example FSAE car is designed and tuned well, it would be possible for it to corner at approximately 1.5g. The lateral load transfer of this example FSAE car from Table 2.1 using the front track width and with 1.5g lateral acceleration is determined by Equation (2.1) such that

$$\Delta W_{lat} = \frac{WA_Y h}{t} = \frac{272.2 * 1.5 * 304.8}{1219.2} = 102.1\,\text{kg}, \tag{2.2}$$

revealing that 102 kg is transferred off of the left side and onto the right side. Since the vehicle is assumed to be symmetric (with the CG on the vehicle center line in the front view), the original 136.1 kg on each side of the vehicle becomes 238.2 kg on the right side and just 34 kg on the left side during this type of a maneuver. That means one side of the vehicle is carrying 87.5% of the total vehicle weight, a significant amount. This scenario assumes there are no aerodynamic loads. The 2009 VT-FSAE vehicle does not use aerodynamic devices and therefore, this aspect of suspension loading is neglected for the time being. The above example is typical of the small formula style racing cars designed for the FSAE competition.

An equation similar to Equation (2.2) can be used to find the longitudinal load transfer due to braking and acceleration by substituting track width for wheelbase. Note that the CG is typically not located in the center of the wheelbase so the percent vehicle weight on each end will depend on the static weight distribution. A car heavily biased to the rear (a rear-engined Porsche 911 is a prime example) will have almost no weight on the front under acceleration but will have a very even weight distribution under braking. The longitudinal load transfer, Equation (2.3), is

$$\Delta W_{long} = \frac{WA_X h}{l}, \tag{2.3}$$

where ΔW is the increase in the rear axle vertical load, W is the vehicle weight, A_X is the longitudinal acceleration in g's with acceleration positive (and braking negative), h is the CG height, and l is the wheelbase.

The above methods are simplified slightly to ease the calculations and to accommodate limited knowledge of a car that has yet to be designed. As detailed in Milliken and Milliken [4], there is a more thorough method of calculating the lateral load transfer using several of the characteristics of the suspension, specifically the orientation of the Neutral Roll Axis (NRA) or simply roll axis [6]. From Race Car Vehicle Dynamics, the complex method of calculations involves "expressions [that] are cumbersome and [that] require a rather detailed knowledge of a car's geometry. These equations can be simplified if one uses the total vehicle CG and its height above the NRA" [6]. This example will use the simplified version of these calculations due to the lack of knowledge of the final vehicle specifications. The areas that remain unknown at this stage of the design cycle are the front and rear unsprung CG location, front and rear unsprung assembly weights, and the sprung assembly CG locations and weight. These values are unknown as they are part of an iterative process of suspension and vehicle design. The amount of load transfer the vehicle is subjected to will determine the size of the suspension members which will then change the unsprung weights, hence changing the load transfer. Since typical FSAE teams (and all but the highest level professional racing teams) do not have the resources to devote to iteratively calculating the load transfer with variations in suspension component designs, the simplified equations must be used. .

To simply the complex load transfer calculations, the roll axis must be known. The roll axis is simply the axis that connects the front and rear suspension roll centers. There is nothing that dictates that the front and rear roll centers must be at the same height. Creating an inclination of the roll axis will result in changes to the fundamental oversteer/understeer characteristics of the vehicle [6]. The basics of this method involve accounting for any inclination of the roll axis as well as the front and rear unsprung CG heights, and an offset total vehicle CG in the side view. This simplified method by Milliken and Milliken can account for some aspects of the vehicle being unknown at this stage of the design cycle. The simplified lateral load transfer per acceleration magnitude for the front is given by Equation (2.4) and for the rear by Equation (2.5) such that

$$\frac{\Delta W_F}{A_Y} = \frac{W}{t_F}\left[\frac{HK_F}{K_F + K_R} + \frac{b}{l} z_{RF}\right], \tag{2.4}$$

$$\frac{\Delta W_R}{A_Y} = \frac{W}{t_R}\left[\frac{HK_R}{K_F + K_R} + \frac{a}{l} z_{RR}\right], \tag{2.5}$$

where H is the vertical distance from the roll axis to the total vehicle CG, K is the roll stiffness in the front, K_F, or rear, K_R, ,b is the longitudinal distance from the rear axle to the CG, a is the longitudinal distance from the front axle to the CG, l is the wheelbase, and z is the height of the roll axis at the front, z_{RF}, or rear, z_{RR}. These variables are graphically represented in Figure 2.2.

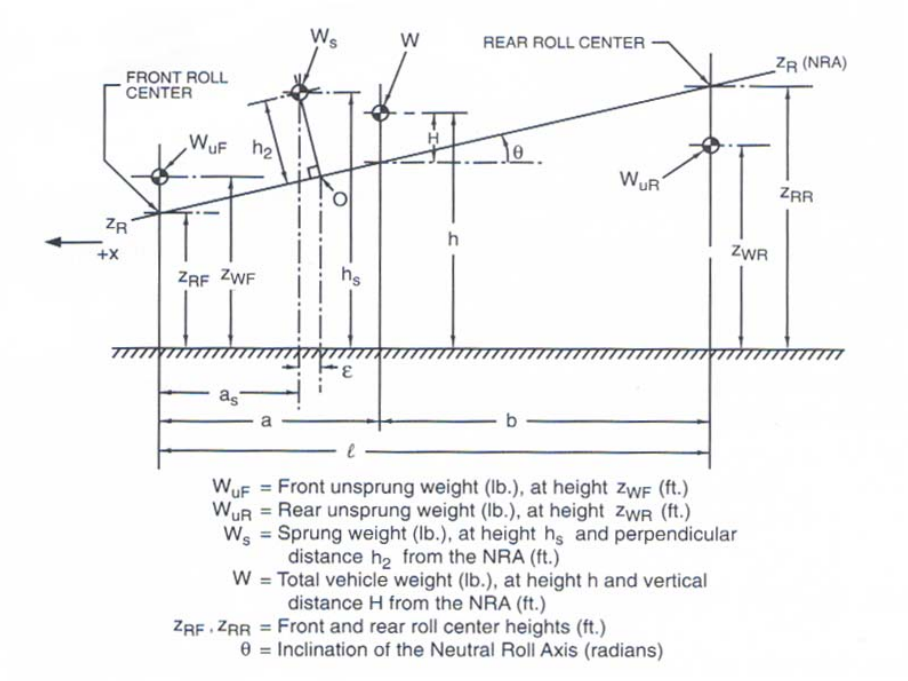

Figure 2.2. Variables and dimensions associated with lateral load transfer [6]. Reprinted with permission from SAE publication *Race Car Vehicle Dynamics* by Milliken and Milliken © SAE International.

Continuing with the example FSAE vehicle from Table 2.1, more detailed information about the vehicle is needed. Table 2.2 shows the complete specifications for the example FSAE vehicle.

Table 2.2. More detailed specifications for the example FSAE vehicle.

Example FSAE Vehicle		
Spec	**Measurement**	
W	272.2	kg
h	304.8	mm
A_y	1.5	g
t_F	1219.2	mm
t_R	1168.4	mm
H	272.5	mm
K_F	27116.4	N-m/rad
K_R	33895.4	N-m/rad
a	914.4	mm
b	762.0	mm
l	1676.4	mm
z_{RF}	25.4	mm
z_{RR}	38.1	mm

Equation (2.4) and Equation (2.5) calculate the load transfer as approximately 44.5 kg at the front and 60.3 kg at the rear. This results in a total vehicle load transfer of 104.8 kg, slightly higher than the simplified calculation in Equation (2.2), which resulted in 102.1

kg total lateral load transfer. This new value for lateral load transfer results in 88.4% of the load being carried by the outer tires in a steady state cornering scenario. This drastic amount of load transfer to the outer wheels is going to have later effects as the inboard tires carry such a small amount of the vehicle weight, they are essentially along for the ride, with the outboard tires providing the primary means of cornering force, and therefore dictating the vehicle corning behavior and direction of travel.

2.1.2 Large Displacement, Small Strain FE

To develop a FE model capable of reproducing the behavior of a vehicle suspension, the modeling software needs to be able to deal with large displacements with small strains. The reason for this need is that suspension systems are generally not rigid structures. As described above, the suspension must be capable of providing the vertical compliance necessary to cope with irregularities in the road surface. This vertical movement of the kinematic linkage is largely a rigid body displacement with small elastic strains and is referred to as a large displacement relative to small deformation-type displacements. Large-displacement small-strain analysis results in a nonlinear structural model which requires an incremental analysis for solution. This approach to generating representative loads in the suspension components necessitates the use of software capable of handling this behavior. Abaqus is developed for this type of analysis.

Displacement-Based Finite Element Theory is based on the stiffness of a member being multiplied by the relative displacement between two points (or nodes) to obtain the internal forces between those two nodes. If the displacement of a node is due to factors that have large contributions due to rigid body movement (such as a kinematic linkage), the values determined for the displacement of the member must remove this component of movement such that the only displacement being used to calculate internal elastic force is from the deflection of the member (the strain). The nature of the suspension is that nodes in the structure will be permitted to move a large amount from the kinematics of the design. This movement is much greater than the comparatively small amount of deflection from strain that occurs in the members under load. While there is the potential for member failure in the model, the suspension members are generally designed based on compliance considerations rather than on the need for strength. This is further discussed in Chapter Chapter 4, which covers the development of the FE model.

2.1.3 Abaqus Elements including Connectors

One of the primary objectives of this model is to determine if the loads in each of the suspension members include bending moments or if the assumption that each member only “sees” axial load is valid. To accomplish this, different types of elements will need to be used. The element to be used in the early stages of FE modeling is the truss element. From the Abaqus Analysis User’s Manual, this element is a simple two or three node member that transmits only axial force [8]. A truss is not capable of transmitting moments or shear forces. A truss element is meant to represent long slender parts of a structure. The three node element is used for parts that represent curved cables or pipes and can also be used for 1D continuum problems. It is important to note that the linear

truss element has no provisions for buckling mechanics. The three node version of the truss will not need to be used in this research. For this suspension analysis, the two node linear version of these elements will suffice. Truss elements require the definition of section properties in which the cross-sectional area is specified. Since there is no bending and the displacement field as well as the axial strain and stress distribution are assumed to be uniform (constant) and do not vary across the cross-section of the element, it is unnecessary to specify the shape of the cross-section profile of the member.

The next type of element of interest for this research is the beam element. This element is similar to a truss in that it typically connects two nodes by a straight line and is used to represent long slender structural pieces which carry bending loads. As stated in the Abaqus Analysis User's Manual, the cubic beam elements are based on one-dimensional beam theory where the assumption is made that "the member's deformation can be estimated entirely from variables that are functions of position along the beam axis only." [8]. Beam elements have section properties which require a defined cross-sectional area and the profile of the cross-section defined such that the moment of inertia can be determined. Beam elements are capable of transmitting not only axial loads but bending moments, torques and shear forces. The beam element was developed to represent structural elements where the dominant mechanics is associated with bending to determine if there is a significant magnitude of bending moment present in the design. The bending mechanics in the beam element are necessary for the analysis of buckling loads.

The last element utilized in this research is the connector element. A connector is a type of element that provides kinematic degrees of freedom between two structural nodes in the model. Connector elements are unique in that there are several different types of connectors that can be created. Connectors can be of the basic or complex type [8]. Basic type connectors include simple constrained motion like a hinge. Complex connector elements would include items like velocity dependent connections. Connectors also have the capability of having a variety of internal physical properties defined by the user. These properties include friction, stops or limits on movement, spring forces, damping, and clearances/slop to name a few. For the purposes of this research, these connector properties will not be used. Further investigation into the behavior of spherical bearings would be necessary to properly model these connections in the suspension. This information is unavailable at this time and is unnecessary to determining the objectives of this research.

2.2 Suspension Loading and Dynamics

2.2.1 Tire Loads at the Contact Patch (Tire Consortium Data)

A typical vehicle has four points of contact with the road surface. These contact points are roughly rectangular in shape depending on the tire used and the vertical load being supported by the tire. The total area of these contact patches is only a few square inches, but they provide the only means of creating forces that can propel and maneuver the vehicle. The mechanics that occur at the contact patch of a tire when generating lateral

and longitudinal forces are complex. The material and structure of tires are inherently non-linear and somewhat difficult to model. The best method available to a Formula SAE Team, short of gaining access to proprietary tire analysis programs, is to purchase the tire data from an independent testing lab. Known as the FSAE Test Tire Consortium (FSAE TTC), this collection of data files represents the best source available for determining the loading at the contact patch.

The FSAE TTC data allows the user to input several parameters, most importantly, the vertical load on the tire and the camber angle, to generate graphs and data tables that display how the tire will behave over a sweep of other variables, like the slip angle. All of this data has been generated by running the tested tires on a testing machine designed to load the tire on a moving road surface and measure the forces generated at various slip angles, camber angles, and vertical loads. There are several versions of a tire testing machine produced by many manufacturers. One example, and the machine that produced the FSAE TTC data, is at the Calspan Corporation Tire and Research Facility (TIRF) [6, 9]. The machine at TIRF uses a large belt as the road surface onto which the tire is loaded and manipulated to generate the necessary data. Figure 2.3 shows the tire testing machine at the Calspan facility.

Figure 2.3. Calspan TIRF tire measurement machine [9]. Reprinted with permission from Calspan Corporation.

An explanation of the forces and behavior at the contact patch of the tire is necessary to understand some of the areas of research that will be covered. While not always true, the tire contact patch can be approximated by a rectangular area of the tire that is in contact

with the road surface. The tire is slightly distorted under the load of the vehicle in this area. When load is transferred to a tire, the contact patch will grow and the tire will distort an additional amount. This distortion of the tire carcass is what causes the tire to have a rolling radius that is slightly different from the radius of the tire as measured without any load.

Lateral force from a tire is generated through a slip angle. Figure 2.4 defines a slip angle as the difference between the tire heading (direction it is pointed) and the direction the tire is actually traveling. Generally, the most common method of creating a slip angle is through steering input from the driver. The driver steers the front tires, changing the tire heading. The vehicle inertia forces the vehicle to travel in a straight line. This difference between the tire heading and direction of travel when a steering input is created generates a slip angle. The slip angle in turn generates a lateral force on the front tires, causing the vehicle to yaw. The yaw moment on the vehicle causes the rear tires to change heading, yet inertia will continue to try and move the rear axle in a straight line. This produces the rear slip angle and consequently the rear lateral force which results in a turning vehicle. The slip angle on a tire will cause the contact patch to twist and the local tire carcass to move laterally compared to the tire heading. This movement causes a distortion in the carcass of the tire. Within the contact patch, each segment along the length of the footprint causes a finite amount of lateral force to be generated. The magnitude of this lateral force varies through the length of the footprint. There is also a region at the trailing edge of the contact patch that is actually slipping across the road surface. The distorted contact patch needs to return to the original position on the tire after it exits the footprint. This characteristic often occurs both in the contact patch and in the carcass just outside of the trailing edge of the footprint. The region of the footprint where this occurs is referred to as the slip, or slipping, region. Figure 2.4 shows a typical distribution of lateral force in the contact patch, where it can be seen that the net lateral force in the contact patch is behind the center point of the tire. The distance from the center of the contact patch to the location of the net lateral force acting upon it is called the pneumatic trail as seen in Figure 2.4. For the tires and loads of interest to the FSAE team, the pneumatic trail, while not zero, will be neglected in the analysis of the suspension loads. This assumption was made for two reasons. First, the consortium data includes a self-aligning torque, which accounts for a notable portion of the pneumatic trail. Second, at high slip angles, the pneumatic trail becomes significantly smaller, thus making the lateral force act at a point very close to the wheel center line [6]. A second type of trail, known as mechanical trail, creates an additional self-centering moment on the tire. The mechanical trail is the distance from the point at which the steering axis (the axis through upper and lower ball joints on the control arms) intersects the ground to the center of the contact patch. The mechanical trail will be accounted for in the FE model as the lateral load at the center of the contact patch will create a torque about the steering axis. Figure 2.4 shows a tire contact patch when subjected to a slip angle as well as the effects of pneumatic trail on the location of the lateral force.

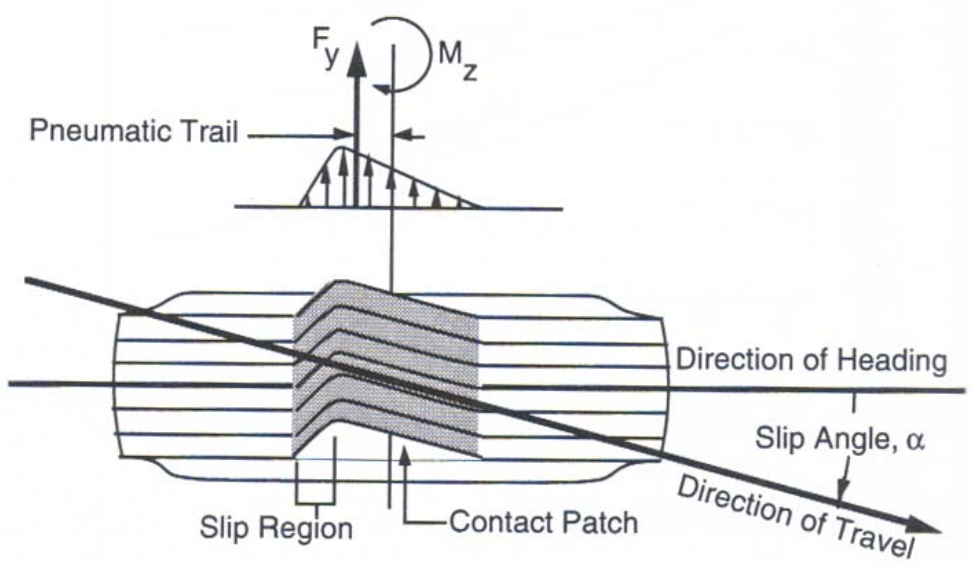

Figure 2.4. Tire contact patch under slip angle. The top section shows where the forces and moments are generated in relation to the wheel center [3]. Reprinted with permission from SAE publication *Fundamentals of Vehicle Dynamics* by Gillespie © SAE International.

An important trend to note about tire behavior is that the capacity of a tire to generate lateral force is related to the vertical load on the tire, but this is not a linear relationship. This effect results in a plot of maximum lateral force versus vertical load that has a slightly digressive curve, an example of which is shown in Figure 2.5. The general behavior shows that with increasing vertical load, there is an increasing amount of lateral force that the tire can supply; however the ratio of lateral force to vertical load decreases as vertical load increases. One objective of suspension design is to minimize the load transfer since this will minimize the losses that occur from progressing up the lateral force versus vertical load curve. Ultimately the goal is to achieve the highest lateral force possible for each tire on the vehicle in all loading scenarios.

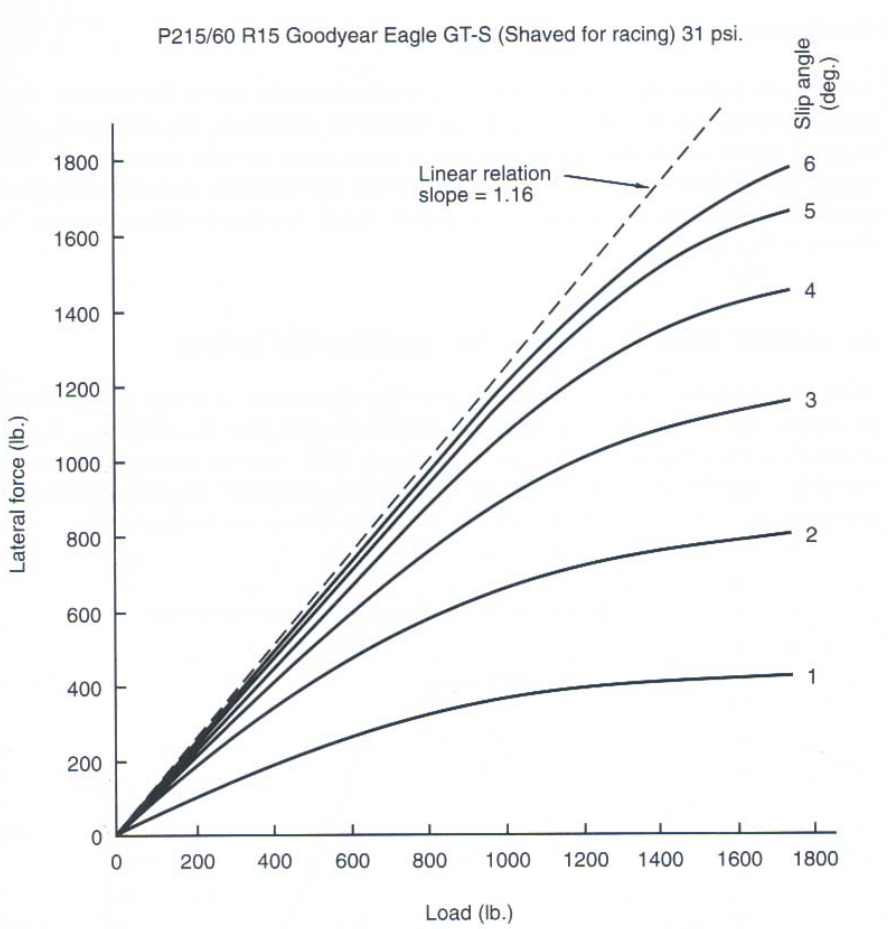

Figure 2.5. Example graph of lateral force versus vertical load across a range of slip angles [6]. Reprinted with permission from SAE publication *Race Car Vehicle Dynamics* by Milliken and Milliken © SAE International.

In order to maximize the lateral force provided by each tire, every tire has to be at the optimal slip angle. The optimal slip angle is the angle at which the maximum lateral force for a given vertical load is generated. The behavior of the maximum lateral force versus slip angle curve of the tire shows that as slip angle increases, the maximum lateral load a tire can provide increases as well, however the rate it increases at will decrease until the maximum lateral force will start decreasing with increasing slip angle as seen in Figure 2.6. At the point where the maximum lateral force starts to decrease with increasing slip angle, the driver has overextended the cornering capacity of the vehicle and the car is sliding in such a way that the tires are no longer gripping the surface. This kinetic friction will cause very rapid tire wear which degrades the performance of the tires, both by greatly increasing the heat going into the tires and by wearing the rubber off of the tread surface. A professional driver will be able to achieve the maximum lateral force possible at the ideal slip angle or slightly less, thereby maximizing tire life while still achieving the fastest possible lap times.

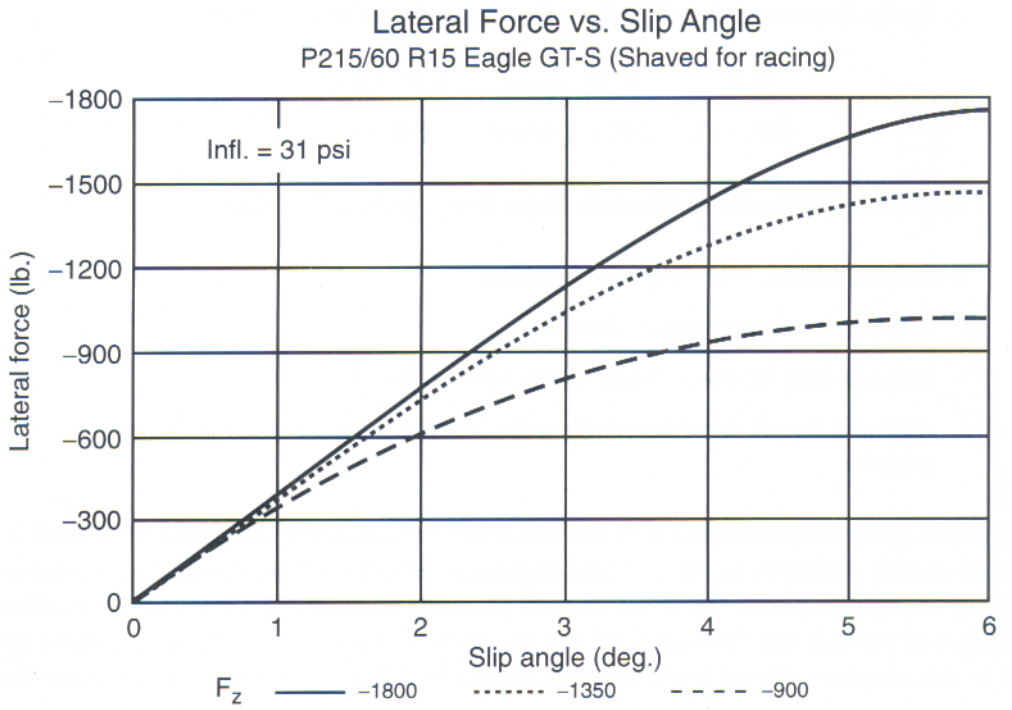

Figure 2.6. Lateral force versus slip angle for the same tire as Figure 2.5. Note that while the graph does not continue, the lateral force will decrease beyond a slip angle of 6 degrees for this specific tire [6]. Reprinted with permission from SAE publication *Race Car Vehicle Dynamics* by Milliken and Milliken © SAE International.

Another factor that needs to be determined to generate the proper loads from the FSAE TTC data is the camber angle of the tire under load. To reiterate the glossary, the camber angle is the angle by which the tire is tilted in the front view relative to a normal of the road surface. Negative camber is an angle where the top of the tire is tilted towards the chassis while positive camber is when the top of tire is tilted away from the chassis. If a tire has 0 degrees of camber, it is oriented perpendicular to the road surface. Figure 2.7 illustrates the tire orientation with camber angle.

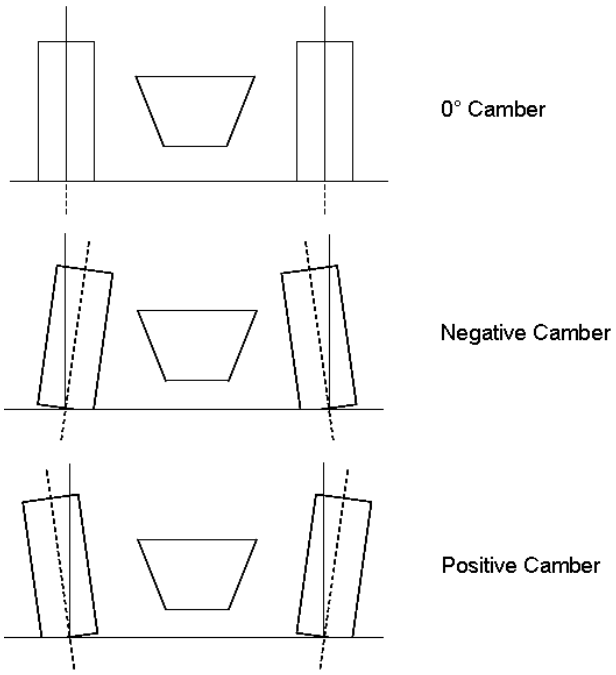

Figure 2.7. Examples of tire camber angle conventions from the front view of the vehicle.

Camber angle has a noticeable effect on contact patch loads. First, the lateral force a tire can generate will change with the camber angle. Sometimes this change is significant (a camber sensitive tire) and other times, the camber angle has little effect. The lateral force most tires can generate will drop off drastically at a certain amount of positive camber. This is due to the tire rolling over onto the sidewall. The sidewall material has very little traction capacity and it is not supported properly by the tire carcass to create lateral force. Generally tires should be oriented as vertically as possible such that the contact patch is parallel to the road surface at all times. Many tires, however, are capable of generating higher lateral forces at a slightly negative camber angle due to camber thrust [6].

Camber thrust is the phenomenon that occurs when the tire creates a lateral force by having a non-zero camber angle. This can be seen in motorcycles where the front tire is not steered a significant amount, but the bike still turns by leaning at a significant angle into the corner. Camber thrust from a typical road-car tire will fall off with increasing slip angle; however it is still present at maximum lateral force. In the pursuit of the fastest lap times, every bit of lateral force needs to be generated to maximize cornering speeds. Figure 2.8 shows how a camber angle changes the amount of lateral force generated at various slip angles.

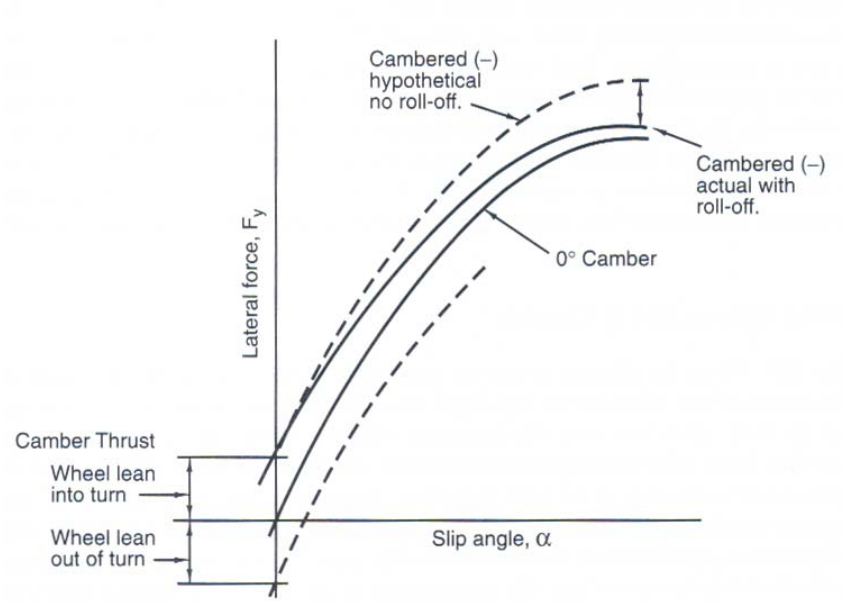

Figure 2.8. Lateral force versus slip angle with various camber angles applied to the tire [6]. Reprinted with permission from SAE publication *Race Car Vehicle Dynamics* by Milliken and Milliken © SAE International.

Under the assumption that the FSAE car has the potential to be driven by a proficient driver, the suspension must be designed to accommodate operation at the maximum possible lateral force that can be present with the normal force in each loading scenario. For this reason, in modeling the forces on the suspension, the vertical load and lateral force need to be used to calculate the corresponding slip angle that the tire will be operating at under the given conditions, including calculated camber angle. This is an important piece of information when putting the forces into the model because at each vertical load, the slip angle and maximum lateral force will be different. In addition, the combined cornering and braking scenario will have a relatively small slip angle compared to the pure cornering because the lateral force will not be maximized for the vertical load. Only a portion of total tire grip will be used for cornering, while the remaining capacity will be used for braking traction. The FSAE TTC data calculates these values by taking the information input by the user and curve fitting the user defined points to the data tables generated from the tire measuring machine. The suspension designer can ask for any combination of conditions on a curve and the MATLAB code provided with the FSAE TTC data will output the requested data either directly if available or linearly interpolated between available points. The forces that can be generated by a tire as well as their orientation to the tire are shown in Figure 2.9.

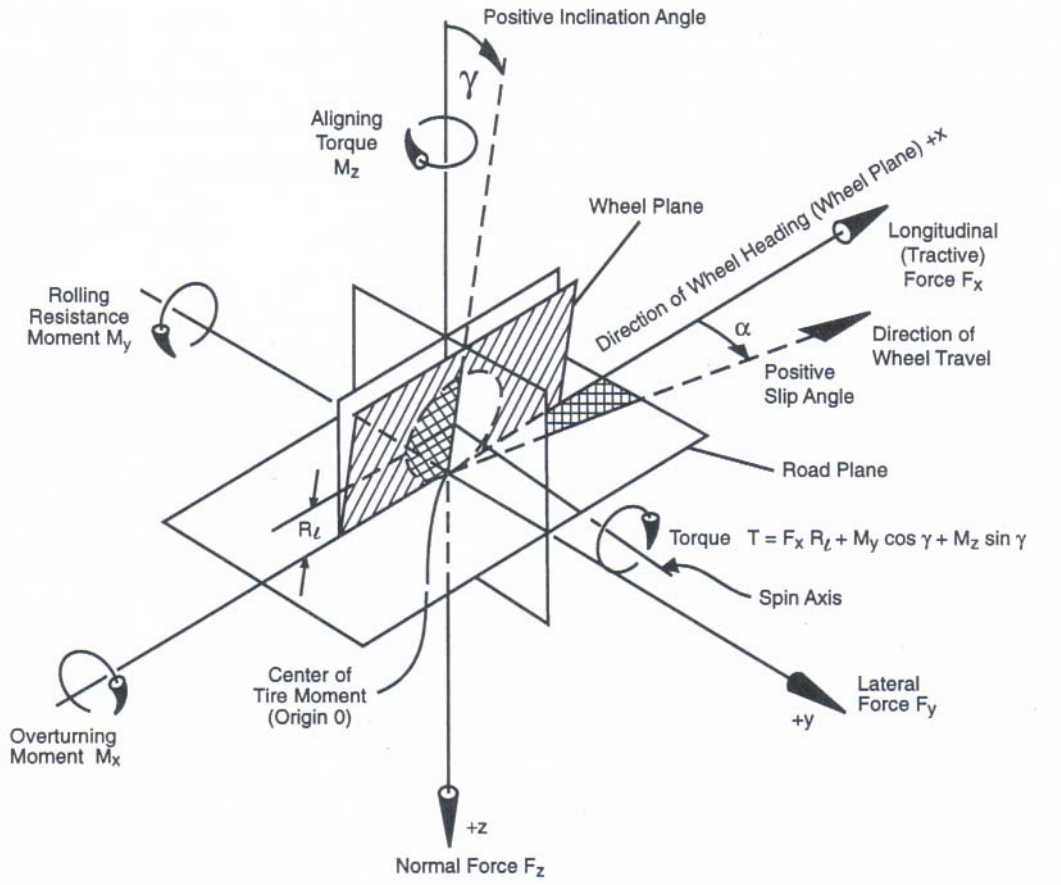

Figure 2.9. Diagram of forces and moments on a tire in the SAE standard system [6]. Reprinted with permission from SAE publication *Race Car Vehicle Dynamics* by Milliken and Milliken © SAE International.

The specific loads that are provided by the FSAE TTC data and used in the FE model are F_x, F_y, and M_z. These three loads are found by using the inputs of vertical load (F_z) and camber angle to query the FSAE TTC data tables to determine the curve representing lateral force (F_y) with varying slip angle and longitudinal force (F_x) available. The overturning moment (M_x) is created by the lateral force (F_y) creating a moment about the wheel center. The rolling resistance moment (M_y), which can also represent a braking or accelerating torque is a given value based on the estimated longitudinal acceleration of the vehicle under the specified loading scenario.

2.2.2 Forces in the Suspension

The forces at the contact patch will react to the chassis through the suspension members. The lateral and longitudinal forces in the horizontal plane are carried primarily through the control arms. The tie rod will counter the moment resulting from the lateral force at the contact patch and the pull rod will carry any vertical component of load from the tire. This arrangement of components with constrained kinematic degrees of freedom results is a structure of six long slender members connecting the chassis to the upright in which the internal member forces need to be determined. These six members are shown in

Figure 2.10 as a Unigraphics model of the front right suspension of the 2009 VT-FSAE car.

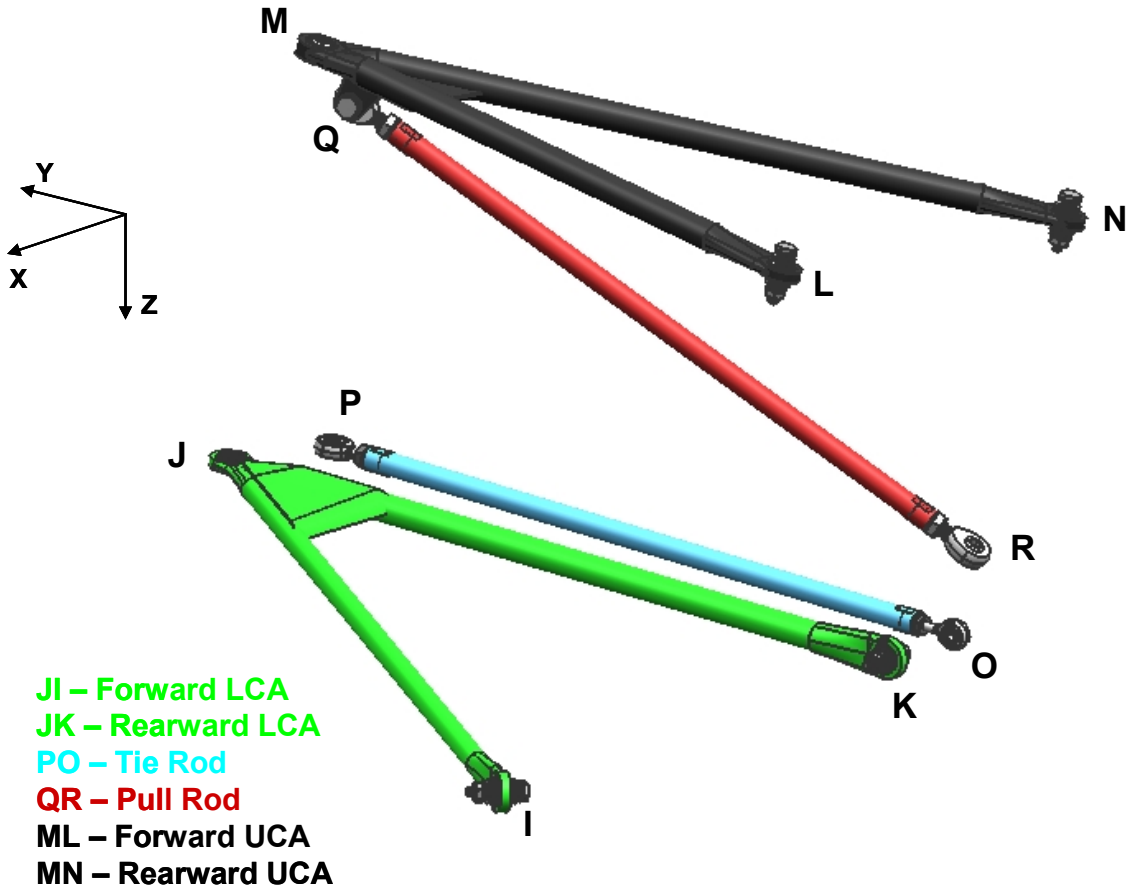

Figure 2.10. View of front right suspension from the front middle of the vehicle.

The suspension structure is very similar to the space truss in statics. A space truss is defined as a three-dimensional version of a plane truss in which rigid links are connected with revolute joints [1]. The space truss differs from the suspension in a notable way in terms of the method used at joints at the ends of each member. In the space truss, the assumption is made that each member is a two-force member and the members are connected to each other with a three-dimensional revolute joint; a spherical bearing or ball and socket joint. While this type of joint exists in the suspension, not every member is connected to the others in this way. Some members are welded to each other and therefore share all degrees of freedom at that connected end. Despite this difference, space trusses are beneficial in that there are two relatively simple methods that can be used to solve for the internal forces; the method of joints and the method of sections [1].

The method of sections involves cutting a section in the structure and then finding the forces and moments that result in equilibrium in one section. This allows the internal forces in any cut member to be calculated directly from the analysis. The analysis consists of simply summing the forces and moments on the structure section to find what internal forces result in the equilibrium of the structure [1]. By making the necessary

assumptions to use this method of calculating loads, it is simple to find the internal member loads necessary to design the suspension. The details of this method as well as the assumptions used are covered in detail in Section 3.3.1.

The primary assumptions made in the method of sections are that the members are all (1) two-force members (trusses) and (2) each member is pinned at each end. These two assumptions have been used for years at VT-FSAE and at this time, any existing explanation of the validity of using them in this particular application has been lost. Later sections in this research will investigate the applicability of these assumptions and discuss how effective they are in modeling suspension loads.

With the two above assumptions made, the member loads can be easily calculated by hand. Using the hand calculated member loads, the typical design cycle next moves to a buckling analysis of the members that see large compressive forces. Since it has been assumed that the members are pinned-pinned members, Equation (2.6) shows the Euler column calculation for the critical load in buckling as

$$P_{cr} = \frac{\pi^2 EI}{l^2}, \tag{2.6}$$

where P_{cr} is the critical compressive force to cause buckling, E is the modulus of elasticity of the material, I is the smallest area moment of inertia of the designed cross-section of the member, and l is the length of the member [10]. Note that Equation (2.6) assumes that there is only an axial force acting directly on and parallel to the centerline of the member. If the load is slightly offset from the centerline of the member or there is a moment in the member, the total stress and tendency to buckling has the potential to increase by a great deal. Equation (2.6) also assumes that each end of the member is constrained such that they are free to rotate, but there is not displacement of the end points other than along the axis of the undeformed member. Historically, these assumptions have been accounted for on the VT-FSAE team by imposing a large factor of safety against buckling. When the critical design characteristic of a member is compliance rather than resistance to buckling, adding a large factor of safety against buckling is often unnecessary. However, when the member needs to be designed for strength, this large factor of safety adds unnecessary weight to the vehicle, specifically to the unsprung mass. Reducing total weight, and unsprung weight especially, is vital to achieving the highest levels of performance in a racing vehicle. A method of calculating buckling resistance that is more thorough than this method will be developed in this research to aid in determining the use of large factors of safety.

The Euler column buckling calculation in Equation (2.6) assumes that each member is a pinned-pinned member. While this is consistent with the assumptions made for the hand calculations, the actual suspension has both pinned-pinned members (the pull rod and tie rod) as well as fixed-pinned members (each control arm member). The equation for the critical load in the case of a fixed-pinned member gets modified based on the effective length of the member. To account for this different end constraint, an end-condition constant, C, has been developed as a multiplier on the standard critical load given in

Equation (2.6). The recommend the end-condition constant for a fixed-pinned (or fixed-rounded as labeled in the reference) is $C = 1.2$ [10]. Using this constant, the critical load for a fixed-pinned member, given by Equation (2.7), becomes

$$P_{cr} = \frac{C\pi^2 EI}{l^2} = \frac{1.2\pi^2 EI}{l^2}, \tag{2.7}$$

where C is the end-condition constant and the fixed-pinned value of 1.2 has been substituted into Equation (2.7). This calculation is what has been used by the VT-FSAE team to calculate critical loads for buckling for each of the suspension members in the control arms.

Equation (2.6) and Equation (2.7) both assume that the member in question is operating in the range of an Euler beam. An Euler beam is considered a long slender member. A beam is considered long and slender if the slenderness ratio is greater than a set number. The slenderness ratio is defined by Equation (2.8)

$$\frac{l}{k}, \tag{2.8}$$

where l is the length of the beam and k is the radius of gyration. Equation (2.9) shows that the radius of gyration can be calculated from

$$I = Ak^2, \tag{2.9}$$

where I is the moment of inertia of the beam section and A is the cross-sectional area of the cross section. The limit of slenderness ratio that defines an Euler beam is often defined in Equation (2.10) as

$$\left(\frac{l}{k}\right)_1 = \left(\frac{2\pi^2 CE}{S_y}\right)^{1/2}. \tag{2.10}$$

This limit on the slenderness ratio defines when a beam should be considered an intermediate length, or a Johnson, beam [10]. If the slenderness ratio satisfies the condition of being less than $(l/k)_1$, then the critical load for buckling is defined by Equation (2.11), such that

$$P_{cr} = S_y A - \left(\frac{S_y}{2\pi k}\right)^2 \frac{A}{CE}, \tag{2.11}$$

where all variables remain the same as for a Euler beam [10]. Equation (2.11) normally results in critical loads that are lower than predicted by the Euler beam method in Equation (2.7).

The members in the 2009 VT-FSAE suspension design generally have slenderness ratios that are very close to the transition point between the Euler and Euler-Johnson ranges of buckling analysis. When calculating critical buckling loads, the slenderness ratio of the proposed member sections must be checked to determine the method to analyze each beam. This method is acceptable for axial loads only with no bending moments and no eccentric loads.

One of the early stages of the FE model development will involve the inclusion of internal bending moments. Should internal bending moments exist; the Euler-Johnson method of calculating bending resistance will not longer be valid. A more complex method that accounts for bending moments along with axial loads is the Secant column formula [10]. The Secant column formula is defined in Equation (2.12) as

$$P = \frac{S_y A}{1 + \frac{ec}{k^2} \sec\left[\frac{l}{2k}\sqrt{\frac{P}{AE}}\right]}, \tag{2.12}$$

where e is the eccentricity of the applied load that creates the internal bending moment. It can be seen that P cannot be solved for explicitly, however Abaqus has the capability to perform a buckling analysis of each element in the model. This feature will be used to solve Equation (2.12) once bending moments, if any exist, have been determined.

2.2.3 Suspension Movement and Articulation

When the suspension is subjected to loading through the tire contact patch, the kinematics of the linkage will come into play and the suspension will articulate vertically. In the case of adding a steer angle, the upright, wheel, and tire will rotate in the horizontal plane with the outward movement of the tie rod. These two types of movement often combine in the various loading scenarios commonly encountered by a vehicle.

The tire and wheel assembly rotates under steering due to movement of the tie rod. This member is attached to the steering rack, which is fixed to the chassis of the vehicle as in Figure 2.11. Turning the steering wheel results in the lateral movement of the steering rack ends and pushes or pulls the inboard point of the tie rod along a path parallel to the vehicle Y-axis. This in turn forces the upright to rotate about the steering axis, causing the tires to steer. The joints on either end of the tie rod as well as the joints of each a-arm to the upright have a spherical bearing that allows rotation in all degrees of freedom but forces the two members involved at a joint with a spherical bearing to translate in unison. These spherical bearings, or revolute joints, force the two members at each connection to share a common point in space while allowing the orientation (or angle) between the two members to change freely. Good spherical bearings will not have any internal friction as this would add coulomb damping to the system that could cause increased member loads and less predictable vehicle handling characteristics.

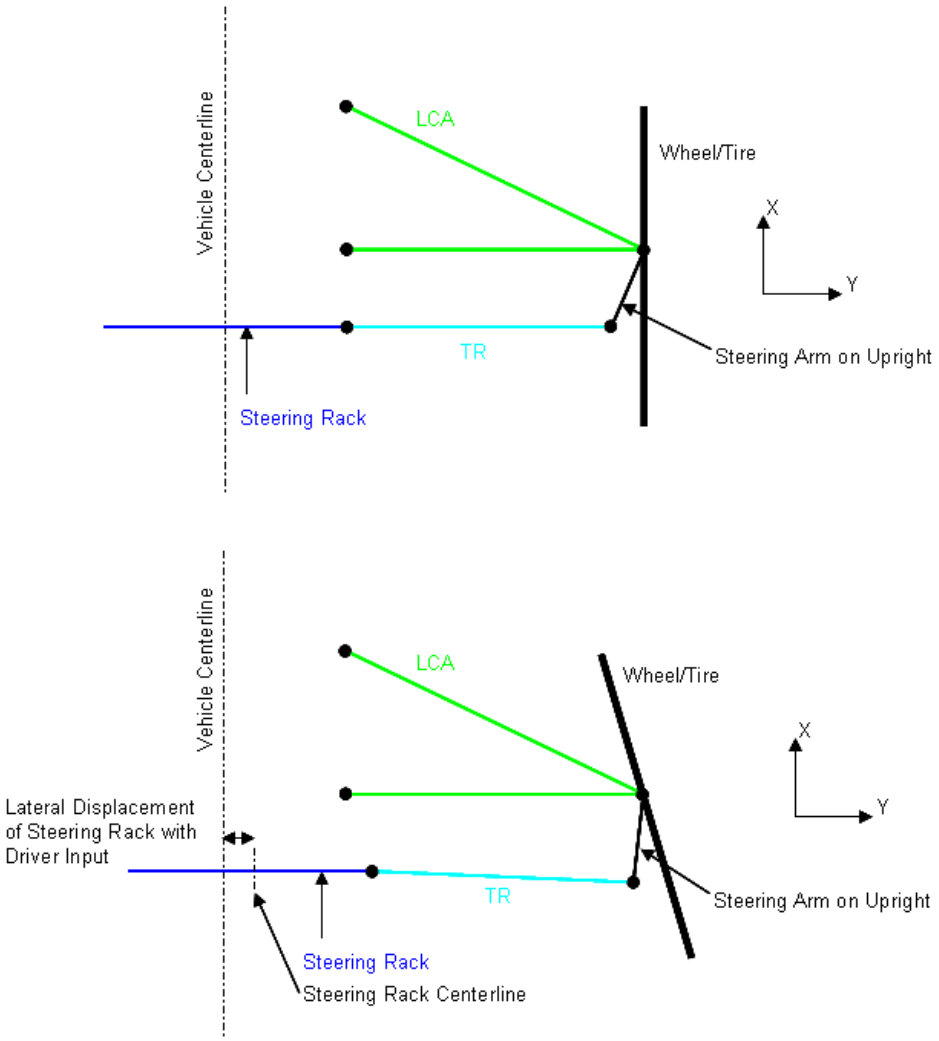

Figure 2.11. Diagram of steering linkage movement to driver inputs.

The suspension is forced up or down to articulate vertically by the combination of loading at the contact patch and the spring and ARB acting on the suspension. An increased vertical load from the static resting position will cause the spring to compress to counter the additional vertical force. This takes place because the suspension is allowed to move vertically and is only countered by the spring acting on the suspension members. The spherical bearings at the chassis mounts of each member allow rotation of the suspension about the instant center of the linkage. Figure 2.12 shows the free body diagram of the upright. The forces acting on the upright are the tire forces from the contact patch translated to the wheel center. The reacting forces are the individual suspension member reactions.

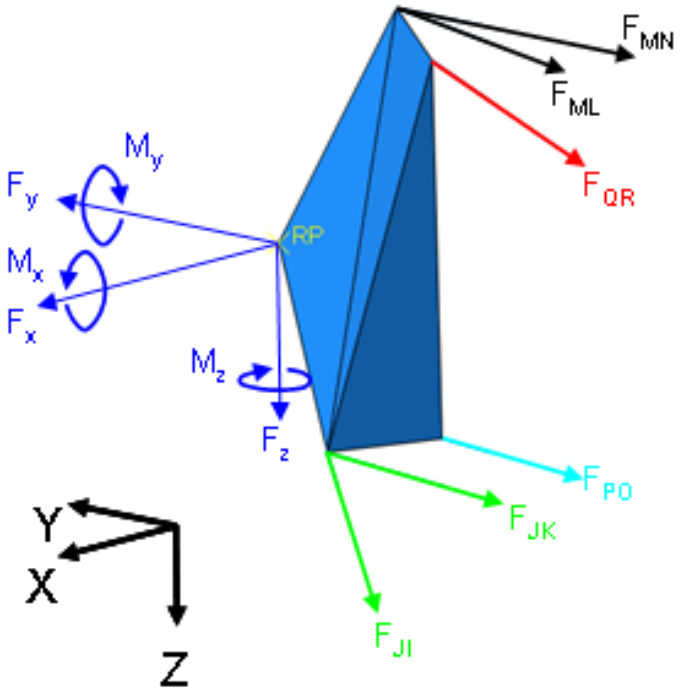

Figure 2.12. FBD of the upright.

The movement of the suspension under load can be calculated using kinematic equations for linkages. The movement can also be modeled in any type of software that is capable of modeling linkages and rigid body movement. It is not necessary to have a thorough analysis of the motion of the suspension, specifically the wheel center. The reason for this is that the suspension design (which is covered in the next chapter) is created to control the movement of the suspension in a very specific way. A desired movement of the suspension is decided upon and kinematic equations are used to solve for the necessary linkage lengths and positions to create that movement. The structural design of the suspension revolves around determining what member dimensions will allow the desired kinematic geometry to withstand the required loading.

The joint mechanics involved in suspension movement are complicated; however they are typically simplified for suspension analysis which will continue to be the approach taken in this thesis. Each joint is free to rotate in all three rotational degrees of freedom, but the two end points of connected members are constrained to move in space together. Using an idealized joint, this connection is simply a boundary condition constraint on the components in a model. It may be small, but there is some friction in the joint itself and there can also be some play in the joint. On new, high quality spherical bearings and rod ends, joint friction and play is small enough such that it can be neglected. Once the bearings start to wear out due to dirt contamination and wear, the friction may increase and a greater amount of play can be created. Analysis of these elements in the suspension could be an entire thesis in itself. For that reason, each joint will be considered to be an ideal spherical bearing in this research.

2.2.4 Examples of Finite Elements in Suspension Design

Finite elements have been used to analyze suspension members by the automotive industry as well as racing teams. One example of this is in the Abaqus example problems [11]. This example consists of analyzing a 1994 Chevrolet C1500 full size pick-up truck. This model was developed by the National Crash Analysis Center (NCAC) at George Washington University. The purpose of this research was to use computer analysis through finite elements to determine the crashworthiness of the vehicle. The NCAC performs extensive modeling of a variety of vehicles and accident situations that supersedes the need to perform numerous live crash tests [12]. The finite element modeling developments made by the NCAC reduce the costs of designing crashworthy vehicles and impact barriers by allowing for only end-stage live testing. For this type of strategy to be effective, the finite element models of vehicles must behave in as similar a manner as possible to the actual vehicle. This behavior must include the suspension articulation, chassis flex, and body structure rigidity.

The example of the NCAC FE model included in the Abaqus examples is indicative of many of the FE models developed for crash testing. These simulations consist of a fully detailed vehicle model from which the internal loads and component strains of the suspension and the vehicle body due to road inputs can be examined. The individual suspension components under a variety of loading scenarios can be examined for stress concentrations. Using an inertia relief analysis, the reaction of all modeled vehicle components, including suspension parts, to a braking load can be examined. While this research is not looking at the effects of a collision on the racing vehicle, the same approach will be used to examine the member loads under various handling maneuvers.

In Race Car Vehicle Dynamics, the authors make reference to the structural analysis of suspension components as it pertains to the design process of race car development [6]. The structural analysis of suspension components is not covered in detail, but what is mentioned is that at the time of publishing, the authors are aware of several teams that "are using advanced structural models (i.e., finite element), especially where there are rules on vehicle crush (crash testing)" [6]. The authors go on to state that simple stress analysis is a minimum in race car design, particularly to teams that have little or no prior experience from which to estimate loads. Finally, it is important to note the mention of stiffness constraining the design of a part as opposed to the strength of the part. This topic will be discussed in this research as it pertains to the critical internal member loads of a formula car suspension.

It is difficult to find specific examples regarding the development of suspension analysis methods in the world of racing. The deficiency of published information is due to the lack of time, the proprietary nature of the sport, and the desire for profit of any of the engineers who do take the time to write [13]. This fact was summarized very nicely by Carroll Smith in his compilation of SAE articles on suspension design and analysis [13]. Despite the rarity, one example of finite elements being used to analyze the suspension components of a race car was republished by Carroll Smith in the same publication [13].

This example article was written by two of the developers of a Mazda IMSA GTP race car [13]. IMSA stands for the International Motor Sports Association which is a sanctioning body for several race series including the renowned endurance race, the 24 Hours of Le Mans. The Grand Touring Prototype (GTP) series raced prototype cars, which are full-bodied purpose build racing vehicles, similar to formula cars with fenders. The article covers a collection of parts analyzed using finite elements including the engine compartment, the roll over structure, and the anti-roll bars.

Looking specifically at the anti-roll bars, the analysis performed for the Mazda GTP car found that several components connected to each anti-roll bar resulted in increased compliances and therefore, an unexpected amount of roll stiffness provided by the bars. This phenomenon occurred on the rear bar due to the mounting brackets attaching the anti-roll bar to the chassis. Using finite elements, the engineers were able to stiffen these brackets with a new design for the existing steel parts. The engineers then analyzed aluminum replacement components and were able to achieve nearly identical stiffness with a significant weight reduction. The results of the researched performed for the Mazda are similar to the goals of this research. A finite element model for both of these design projects exposes the areas of high load and stress and gives the designers more information from which to create suspension component designs that will provide sufficient stiffness while preventing failure due to excessive stress or fatigue.

Chapter 3
Suspension System and Load Calculations

3.1 Suspension Design

Any structural analysis of a suspension must begin by understanding the suspension system being used. There are many variations in types of suspensions. The VT-FSAE vehicle, like most race cars, uses a Short Long Arm (SLA) suspension. A background on this type of suspension is given prior to discussing the various components in the suspension. A free body diagram (FBD) for the upright and the degrees of freedom are discussed, followed by the conventions used in this research. Lastly, a detailed description and explanation of the current hand calculations is presented as a basis for comparison to the development of the FE model in Chapter 4.

3.1.1 Background on Short Long Arm (SLA) Suspension

The traditional suspension used in race vehicle design for many years has been the SLA, or Short-Long-Arm suspension. This design incorporates a long lower control arm with a shorter upper control arm. Often the two suspension arms are not parallel but this is not a requirement of SLA suspension design. A primary reason for using this type of layout is that it allows for a wide range of camber curves to be designed into the suspension. The camber curve of a suspension is the amount of camber gain or loss plotted against a range of vertical displacement of the wheel. It is also easy to manipulate the design of other suspension characteristics with the SLA design. These characteristic include the roll center height, the roll center migration characteristics, anti-squat, and anti-dive. In terms of a single seat race car like the Formula SAE vehicle, this layout is also extremely easy to package with the rules mandated aspects of the chassis design. This is why the short-long-arm suspension is used for the FSAE vehicle design. An example SLA suspension is shown in Figure 3.1.

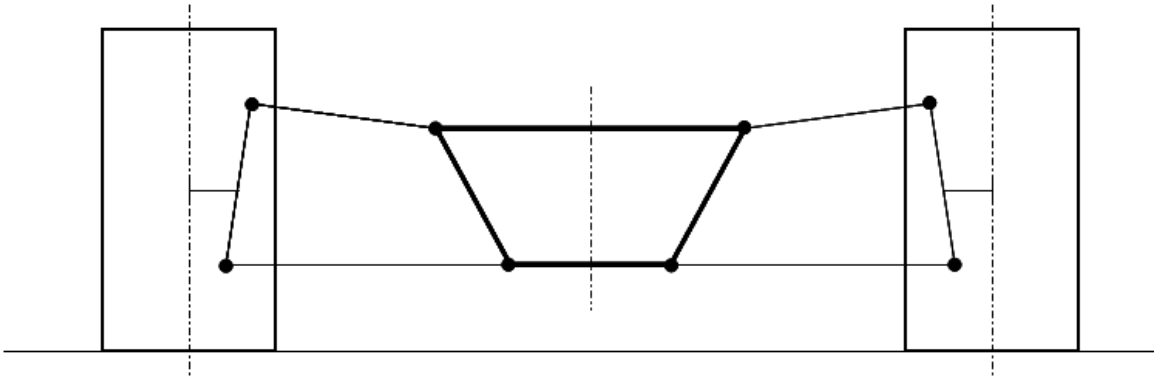

Figure 3.1. SLA suspension in the front view.

The design of the suspension begins with a series of decisions made by the suspension designer. With help from other team members, the overall dimensions of the car are defined. These dimensions are the track width in the front, the track width in the rear, and the wheelbase. Next, the roll center height for the front and rear are chosen by the

suspension designer, thus defining the roll center axis, or the neutral roll axis. To reiterate Section 2.1.1, the neutral roll axis is the axis about which the car will rotate under lateral load. Subsequently, the lower control arm length will be selected. This length is usually based on the chassis width at the front, as the chassis must be wide enough to fit the driver's feet and the pedals. At the rear, the chassis width must accommodate the engine and differential.

Working with members of the suspension team, the suspension designer will determine the needed camber curve for the system. This curve must account for the roll of the vehicle to keep the tire in its ideal orientation to the road surface. This is often vertical or at a slight negative camber and is partially determined by the tire data. In addition, the camber curve must account for the compliance of the suspension components as these will deflect under load in such a way that the tire typically gains camber. The camber curve must not be so aggressive such that the tires gain excessive negative camber under pitch (typically brake dive in the front and squat under acceleration in the rear) as this limits the longitudinal traction capacity of the tires.

The final factor to determine is the outboard ball joints, which define the steering axis. There are numerous considerations that go into these points in the front view, packaging being a key element. In the front, the wheel must house the brake rotor and caliper, in addition to the front upright and control arm ends. The control arms must be situated in such a way as to provide the desired caster and king-pin inclination angles, as well as the designed scrub radius and mechanical trail. These suspension parameters are shown in Figure 3.2. All of these suspension geometry considerations need to be balanced with reasonable operating clearances for the braking components, as well as allowing the control arms to clear the wheel, upright, and brakes under steering and vertical articulation of the suspension.

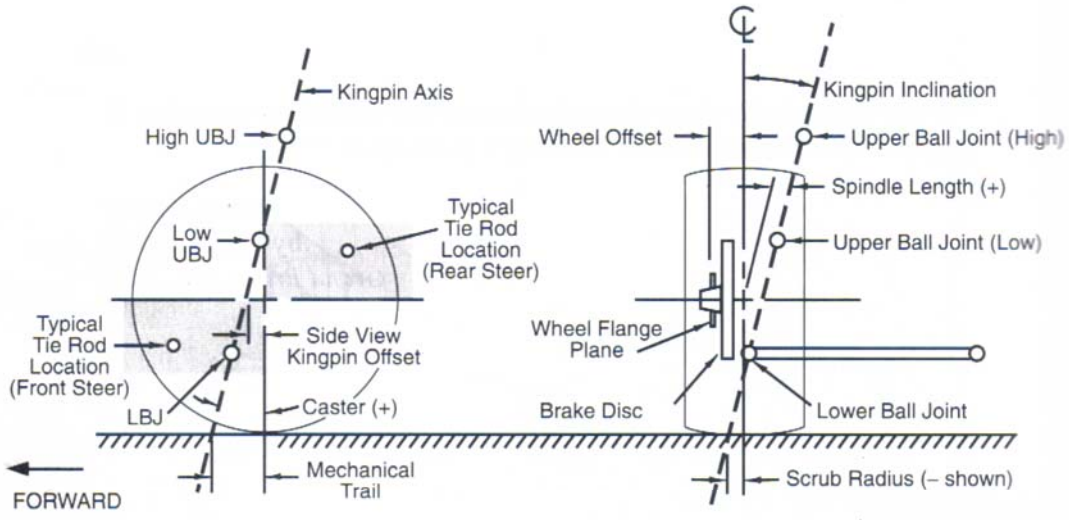

Figure 3.2. Kingpin geometry [6]. Reprinted with permission from SAE publication *Race Car Vehicle Dynamics* by Milliken and Milliken © SAE International.

The goal of the suspension design is to maximize the tire contact with the road surface while giving the driver a vehicle that is predicable and easy to drive. Traditionally, compromising slightly on tire orientation to make the vehicle easier to drive will result in faster lap times as the driver is able to drive the car closer to the limit of the tires for a longer period of time. To maximize the predictability of the suspension, the roll centers should not move in any vehicle conditions including roll, pitch, jounce/rebound, or any combination of thereof. Thus, a set of kinematic equations is used to determine link lengths and positions such that the roll centers do not migrate under suspension movement. These equations were put into a MATLAB program originally designed by the 2006 VT-FSAE suspension team. The principals have remained the same but each team has developed their own program in order for each suspension team to learn the methods involved. This program is then used to determine the inboard mounting points for the lower control arm (LCA) and upper control arm (UCA), and in doing so, define the length of the UCA and orientation of both control members.

This process is repeated (typically with different LCA lengths and outboard points) to create several sets of suspension points that meet all of the required geometric and kinematic requirements. The suspension designer and chassis designer will work together to determine which set of points gives the suspension the longest members while still allowing for acceptable chassis dimensions. Longer suspension members are desirable because they reduce the magnitude of suspension member rotation. This condition allows the suspension to operate in a more linear range while still achieving the necessary vertical wheel movement required in vehicle operation.

Once the final suspension points have been determined, the rest of the vehicle is designed around these points. Occasionally, the suspension points are designed to be adjustable on the vehicle to test various geometry set ups, however with the method used by VT-FSAE to design a suspension with little to no roll center migration, this is typically unnecessary. The current method of defining roll center migration as zero and solving for member lengths and orientations that possess the desired suspension characteristics has proven to be extremely accurate. Optimum K and Adams/Car have both been used in the past to analyze the calculated points and both programs have revealed extremely small levels of roll center migration. The roll center migration is not zero according to these programs, however through the range of interest, the migration is extremely close to zero, therefore the minute amount of movement can be neglected and the roll center migration assumed to be zero.

3.1.2 Components of Suspension (Members, Springs, Damper, Tire, etc.)

Many components make up the suspension of a racing vehicle. For the version of the SLA design used by VT-FSAE, the following components are shown in Figure 3.3 on the current 2009 VT FSAE design:

- Lower Control Arm (LCA)
- Upper Control Arm (UCA)
- Upright

- Push or Pull Rod (PR)
- Tie Rod (TR)
- Rocker Arm (or Bellcrank)
- Spring
- Damper
- Anti-Roll Bar (ARB)

The 2009 VT-FSAE vehicle uses a pull rod in the front suspension as shown in Figure 3.3. Other components that should be included in the suspension but are also part of the wheel assembly are also shown in Figure 3.3:

- Top hat (or wheel hub)
- Wheel
- Tire

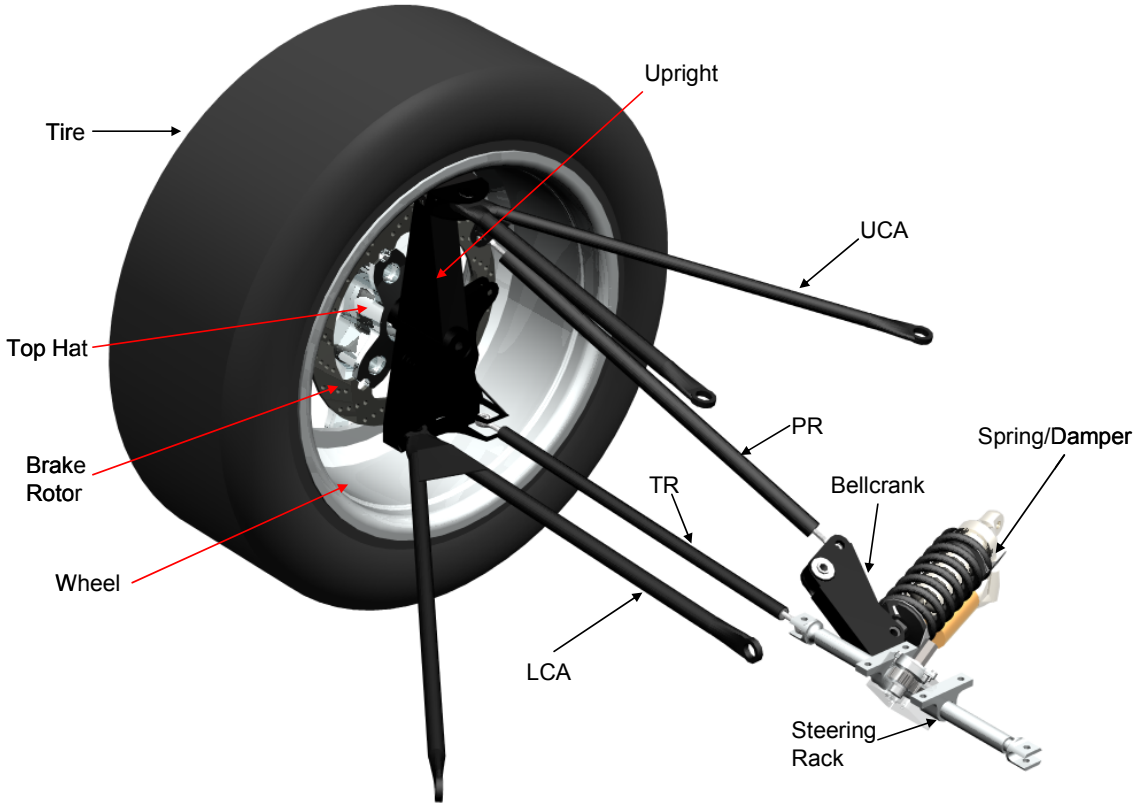

Figure 3.3. Corner suspension assembly with all components labeled.

Each component has a specific purpose for which it must be designed. The most important point on any race car is the contact patch of the tire. As stated earlier, this is the small area of the tire that is in contact with the ground. Loads are generated at the contact patches that allow the vehicle to maneuver. These loads are transmitted through the tire to the wheel.

The wheel needs to seal with the tire to hold air, transfer the loads from the tire to the top hat, provide enough stiffness to prevent undesirable camber gain, and sometimes provide effective air movement to cool the brakes in the front. The wheel is both unsprung and rotating mass, making the wheel one component that must be as light as possible. The weight of the wheel must be balanced with the need for a wheel that is stiff enough to not cause undesirable camber effects when loaded. The wheel loads on the upright and the suspension member reaction forces are shown in Figure 2.12 which is reproduced here as Figure 3.4.

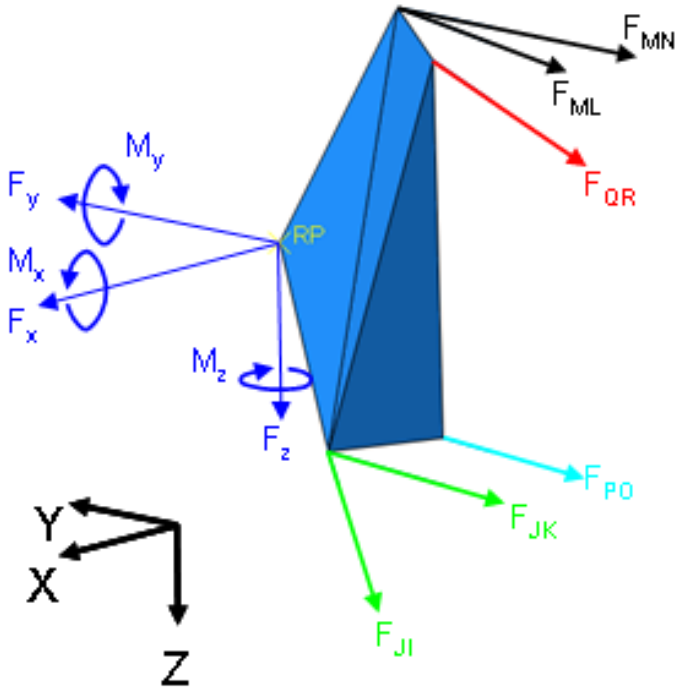

Figure 3.4. FBD of the front upright showing wheel center forces and suspension reaction forces.

The top hat (or hub) is the component the wheel bolts to. The top hat also contains the wheel bearings. The brake rotor is often connected to the top hat in many designs. Mounting the brake rotor on the top hat requires the top hat to withstand all of the braking torque that is generated in this design. The proximity to the brakes and the heat generated when stopping means this part must be capable of withstanding loads at elevated temperatures. The wheel bearing seals are often housed in this part.

The upright is the non-rotating portion of the suspension on which the wheel bearings are installed. Loads are transferred from the top hat, through the wheel bearings, to the spindle on the upright. On option for the spindle, as on the 2009 VT-FSAE car, is a dead spindle mounted on or part of the upright. A dead spindle does not rotate with the wheel. In prior years, the VT-FSAE car has had a live spindle, which rotates with the wheel and is typically a part of the top hat. If this design is used, the upright consists of a large bearing housing into which the outer wheel bearing races are installed. The upright

transfers the wheel forces from the top hat and wheel bearings to the suspension members.

The control arms connect the upright to the chassis and determine the movement of the wheel through the design of the suspension points. The LCA connects the chassis to the lower ball joint of the upright. The UCA connects the chassis to the upper ball joint on the upright. These A-Arms typically have two mounts on the chassis and one mount on the upright; however less common designs have one mount on the chassis and two on the upright. In the more common design with two mounting points on the chassis, as on the 2009 VT-FSAE car, the a-arms have spherical bearings at each of their three points and rotate about the axis between the two inboard chassis mounts.

The suspension loads are transferred from the control arms to the chassis; however two control arms do not constrain the upright in all of its degrees of freedom. The additional two members needed for this are the tie rod and the pull (or push) rod. Figure 3.5 shows the six degrees of freedom of the upright. The tie rod connects the steering arm on the upright to the steering rack in the front suspension. The tie rod in the rear suspension connects directly to the chassis, often sharing an inboard suspension point with one of the rear control arms. The tie rod is the member that imposes steering movement to the front suspension and resists rotation about the vertical Z-axis.

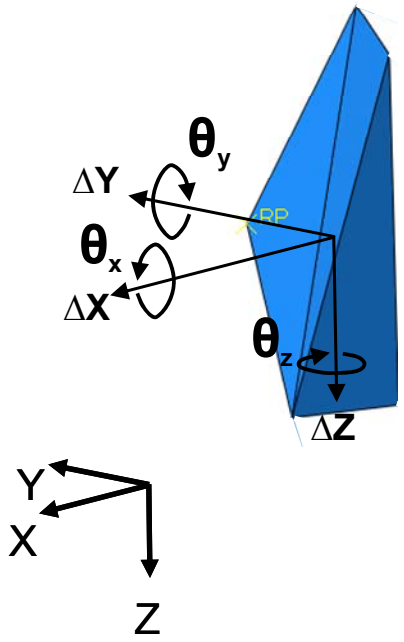

Figure 3.5. Degrees of freedom on the suspension upright.

The pull rod used in the design of the 2009 VT-FSAE car connects the upright and wheel assembly to the spring and damper unit. The more traditional suspension design calls for a push rod instead of the less common pull rod. On the 2009 VT-FSAE car, a pull rod is used at the front while a push rod is used for the rear suspension. The advantage of a pull rod over a push rod is that it is always in tension where a push rod is always in

compression. A pull rod also allows the spring and damper to be mounted lower on the car, lowering the overall vehicle CG. The pull rod attaches to the UCA (other designs may use the upright) at the outboard end and to the rocker arm at the inboard end.

The bellcrank is a lever that pivots in one plane and connects the spring/damper to the pull rod. The ratio of the connection points can be used to tailor the constant spring rate to a rising or falling rate at the wheel. The bell crank is often required to aid in packaging the spring and damper assembly in the tight confines of a single seat race car.

The spring and damper assembly controls the suspension movement when the vehicle is under load. The spring is designed to carry all the vertical loads which provide resistance to vertical displacement of the suspension in all situations. The spring acts whenever the wheel it is connected to moves vertically, regardless of any movement in the other wheels.

The damper prevents excessive oscillation of the vehicle body and wheel/tire assembly. The damper only functions while the suspension is moving, however it has a great effect on the handling characteristics of the vehicle. Desirable damping characteristics allow the vehicle to be predictable when driving and help maintain tire contact with the road surface.

The anti-roll bar (ARB) is the last piece used to control the wheel movement of the vehicle. The ARB is design to transfer roll loads and only adds resistance in roll conditions. This means if one axle experiences a condition in which one wheel moves upward relative to the chassis and the other wheel on that axle moves downwards, the ARB will add resistance, or roll rate, to this movement. If both wheels on an axle move vertically relative to the chassis in the same direction, the ARB will not add any resistance to the movement.

This spring and damper system with an ARB is a very common type of independent suspension design. There are other more complex designs that decouple certain vehicle rates and allow the race engineers more freedom in tuning suspension behavior. These designs can offer some advantages at the cost of complexity in both design and tuning. The 2009 VT-FSAE vehicle will not use these more complex systems as they are more difficult to tune and the complexity raises durability concerns for finishing the endurance event.

3.1.3 Major Areas of Concern with Loading

Internal loads must be analyzed in all suspension parts in order to design a suspension that will give favorable vehicle handling. The simplest parts to analyze are the pull rod and tie rod. These parts have spherical bearings in rod ends on both ends that allow them to be represented as simple two-force members. The most complex part to analyze is the upright, as it is subjected to large bending stresses from the suspension members and wheel bearing loads, while also needing to handle the braking forces created by the brake caliper which is mounted to the upright. There are numerous areas with unique loading

concerns that must be analyzed; however the scope of this research is limited to the suspension members.

The term "suspension members" refers to the LCA, UCA, TR, and PR. The first area of concern is that these members are typically modeled as two-force members or truss elements. This is not accurate as the LCA and UCA have two members that are fixed to each other in all degrees of freedom at the outboard end. There is often a gusset plate welded in place at this connection, designed to decrease the effective free length of these members to address buckling concerns. This type of connection will induce some bending in the members under load. At this time, it is unknown how great this bending moment is and it therefore cannot be neglected until proven insignificant.

The next area of concern is the mounting of the pull rod. This member acts on the UCA via a bracket welded to the gusset connecting the two UCA members. This creates a bending load on the UCA members due to the pull of the spring acting through the pull rod.

All suspension members will exhibit large displacements with small strains during suspension movement. This means that the geometry of these members and the direction of loading will change as the vehicle is subjected to different loading conditions. This geometry change may create differences in the loads within the members. It is also possible that some of the loading scenarios may move the suspension to the bump stops. Hitting a bump stop will greatly increase the load within the pull rod and will load the rest of the suspension members appropriately. This scenario is very important to analyze as it is a common occurrence on a rough race track or during an off track excursion.

3.2 Conventions Used in Thesis

3.2.1 Coordinate Systems

There are three coordinate systems that will be referenced in this research. As much as possible data, results, and models will be shown in the car coordinate system. This system is based on the SAE standard vehicle coordinate system. In the SAE system, the longitudinal axis of the car is the X-axis and is positive in the forward direction, the lateral direction is the Y-axis with positive towards the right side of the vehicle, and the vertical direction is the Z-axis with the positive direction downward as in Figure 3.6 [3]. The center of gravity (CG) of the vehicle is the origin of this system. For the VT-FSAE system, instead of the origin being at the CG like the SAE system, the origin is located at the CG projection on the road surface. The Z-axis is flipped to be positive upwards and the Y-axis is considered positive when heading away from the center line in either direction. This means all the suspension points are at a positive Z-coordinate. Also due to the convention for the Y-axis, one side of the car has a right hand coordinate system, and the other side has a left hand coordinate system. Specifically, and somewhat confusingly, the right side of the car has a left handed coordinate system and the left side of the car has a right handed coordinate system. This change in coordinate system was made since most points of interest on the car and the chassis are determined in reference

to the ground. Referencing points from the ground plane to begin with makes establishing any measurements to ground much faster. In addition, the CG height is subject to change more drastically than the location of the CG in the ground plane during the design process. To remain consistent with the calculations done by the suspension subteam, the right-side suspension will be modeled so that the team's results can be more easily compared to the research performed here. This means that a left handed coordinate system will be used for the suspension points and geometry. There is no specific reason to use the right side suspension over the left side, it is simply the convention chosen by the VT-FSAE team. To be consistent with the research performed by the team, this research will adopt the same convention.

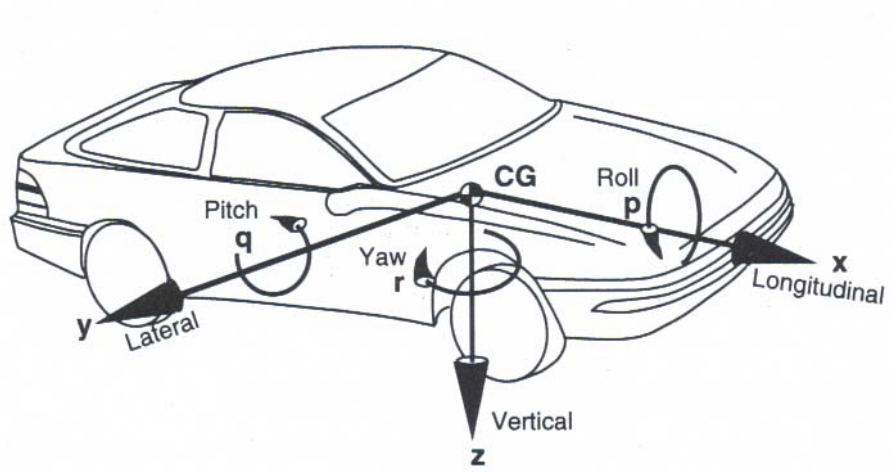

Figure 3.6. SAE Car Coordinate System [3]. Reprinted with permission from SAE publication *Fundamentals of Vehicle Dynamics* by Gillespie © SAE International.

The second coordinate system is for the load calculations, which involve matrix algebra. In order for this to work properly in MATLAB, a right hand coordinate system needs to be defined. The above VT-FSAE car coordinate system is modified by reversing the z-axis so that positive Z is downward for all of the loading calculations. This results in a coordinate system that is simply the SAE system with the origin translated from the vehicle CG to the projection of the CG on the ground.

Additionally, the Abaqus program works in a right hand coordinate system. A conversion needs to occur with the data from the team before it is used in the Abaqus model. In this case, the X-axis will remain the forward longitudinal axis on the vehicle, just as in the car coordinate system. To keep consistency with positive axes pointing in the same directions, the Y and Z axes will be swapped from the VT-FSAE car coordinate system. This makes the system in the Abaqus model follow the same X-axis forward longitudinally on the vehicle, the Y-axis positive in upward vertical movement and the Z-axis to the right laterally on the vehicle with positive outward. Figure 3.7 shows the Abaqus model coordinate system.

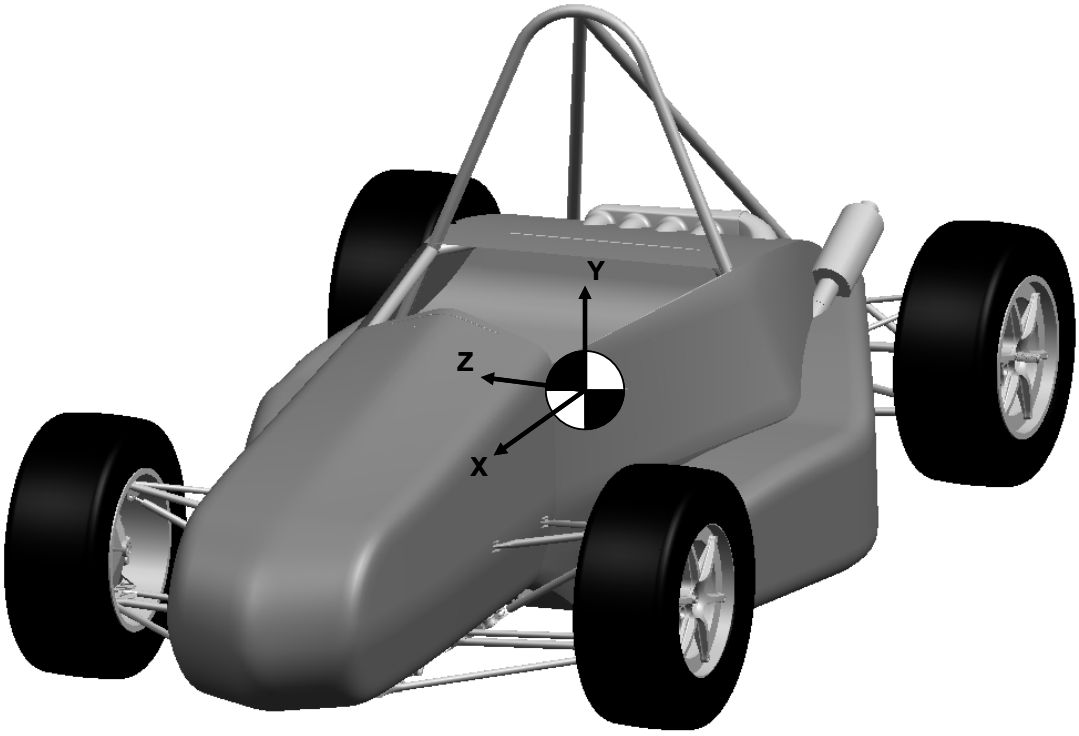

Figure 3.7. Abaqus coordinate system shown on a CAD model of the 2009 VT-FSAE vehicle. Model of car created by 2009 VT-FSAE team members.

3.2.2 Member Nomenclature

The convention on the VT-FSAE team has been to define each suspension member by the letters of the two suspension points it connects. Each suspension point has been given a letter designation in accordance with past years to make comparison of designs easier for the engineers. Since the suspension is symmetric along the centerline of the vehicle, there are 10 points for the front and 10 for the rear. The front corner is the only corner of interest in this research so only those points will be referenced. The rear suspension can be analyzed in an identical manner without the steer angle analysis. The front suspension points are designated as:

- Forward LCA Inboard – I
- Rearward LCA Inboard – K
- Outboard LCA – J
- Forward UCA Inboard – L
- Rearward UCA Inboard – N
- Outboard UCA – M
- Inboard TR – O
- Outboard TR – P
- Inboard PR – R
- Outboard PR – Q

The list for suspension members consists of the six members that make up each segment of the components of the suspension. This list includes members:

- MN – Rear UCA member
- ML – Forward UCA member
- JK – Rear LCA member
- JI – Forward LCA member
- PO – Tie Rod
- QR – Pull Rod

Figure 3.8 is a graphic representation of the suspension arrangement in the top view. Note that this figure is not to scale but is as close as possible in graphically representing the suspension point nomenclature on the current suspension layout.

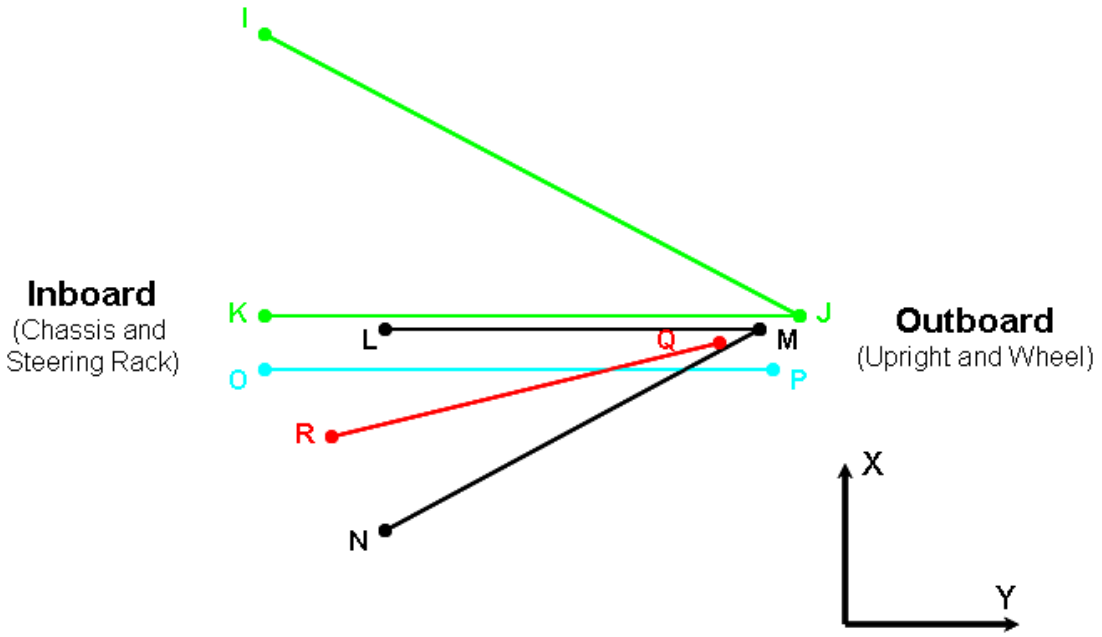

Figure 3.8. Definition of suspension point nomenclature represented graphically.

3.3 Load Calculations

3.3.1 Outline of Method (Hand Calculations)

The hand calculations used to determine suspension loading begin with the tire data obtained from the FSAE TTC data. Tire data for the Goodyear D2692 20x7.0-13 tire on a 7.0" rim is used to determine the forces and moments at the contact patch of the tire under the various loading scenarios to be analyzed. These forces are translated to the wheel center, providing the forces and moments that are applied to the wheel bearing on the upright. Since it is assumed that the suspension structure can be represented as a rigid body attached to six rigid truss members (each representing one tube in the suspension), the loads in each member can be solved for using the method of sections from statics for structures. The suspension points are used to create vectors representing each member.

Using vector geometry and statics equations, the loads at the wheel center are used to solve for each of the axial loads in each suspension member subjected to each of the loading scenarios. The process starts by taking the forces at the contact patch and solving for the equivalent system of forces and moments at the wheel center. This loading data at the wheel center was provided by the suspension designer and will be the loads used in the FE model to ensure consistency between the FE model and the hand calculations. The loading data provided by the suspension designer is located in Section 4.1.4 as is a discussion of the loading scenarios to be used.

The next step after determining the wheel center loads is to create unit vectors for the suspension members. Member JI, one of the lower control arm members, will be used as an example for the calculations in determining the member loads. Let J and I represent the corresponding suspension points as shown in Figure 3.9 and represented by Equation (3.1) and Equation (3.2) such that

$$J = \left[J_x, J_y, J_z\right], \tag{3.1}$$

$$I = \left[I_x, I_y, I_z\right], \tag{3.2}$$

where J_x is the X-coordinate of suspension point J, J_y is the Y-coordinate of suspension point J, and J_z is the Z-coordinate of suspension point J. This naming convention is used for each of the suspension points. Figure 2.10 is reproduced here as Figure 3.9 to reiterate the labeling convention of the suspension points.

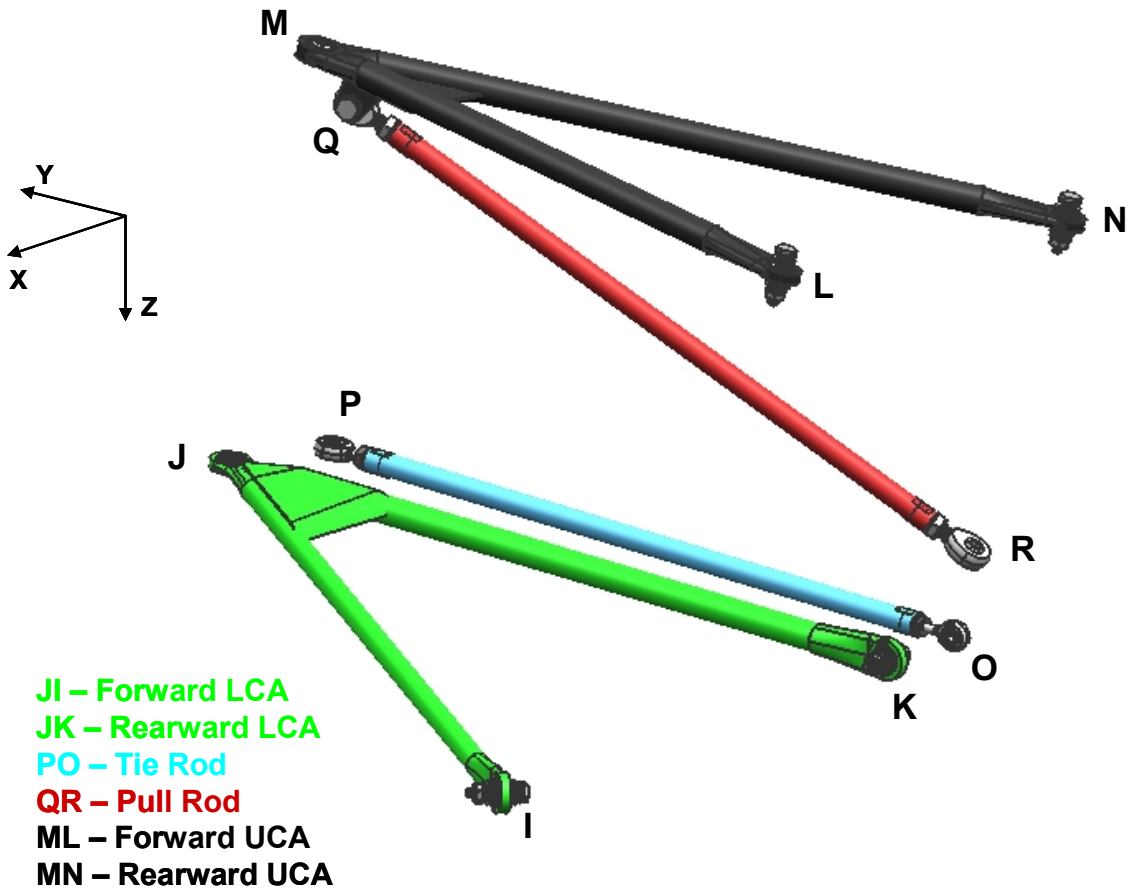

Figure 3.9. Suspension point labeling convention.

JI in Equation (3.3) will represent the vector connecting from point *J* to point *I* in the suspension and *ji* in Equation (3.4) will be the magnitude of that vector such that

$$JI = \left[J_x - I_x, J_y - I_y, J_z - I_z\right], \tag{3.3}$$

$$ji = \sqrt{\left(J_x - I_x\right)^2 + \left(J_y - I_y\right)^2 + \left(J_z - I_z\right)^2}\,, \tag{3.4}$$

which allows the unit vector in Equation (3.5) to be calculated as

$$\eta_{JI} = \left[\frac{JI_x}{ji}, \frac{JI_y}{ji}, \frac{JI_z}{ji}\right], \tag{3.5}$$

where JI_x, JI_y and JI_z are the x-, y- and z-components of the *JI* vector respectively. This same procedure is used to calculate a unit vector for each of the six suspension members resulting in the unit vectors η_{JI}, η_{JK}, η_{ML}, η_{MN}, η_{PO}, and η_{QR}. Since this is a static structure in this calculation, the sum of the forces must equal 0. Equation (3.6) expresses the summation of forces in the X-direction = 0, yields

$$\sum F_x = 0 = F_{JI}\eta_{JI_x} + F_{JK}\eta_{JK_x} + F_{ML}\eta_{ML_x} + F_{MN}\eta_{MN_x} + F_{PO}\eta_{PO_x} + F_{QR}\eta_{QR_x} + F_X, \quad (3.6)$$

where F_{JI} is the axial load in member JI, the other forces follow this nomenclature, and F_X is the X-component of force at the wheel center for the specific loading scenario in question. The same process is used for forces in the Y and Z directions.

With six unknown member loads and only three equations (ΣF_X from Equation (3.6), ΣF_Y, and ΣF_Z), the moments about a point need to be summed to create an additional three static equations. To do this, moments will be summed about the wheel center. The front wheel center point will be called T_{WC} and will have an X, Y, and Z component just as the suspension points. Using the wheel center as a starting point, vectors connecting the wheel center to each of the inboard suspension points can be created. These vectors will become the *r* vectors in the cross product of the specified *r* and *F* used to determine the moments about the wheel center. As an example, point *J* will have the *r* vector defined from point T_{WC} to point *J* as given in Equation (3.7), calculated by

$$r_J = J - T_{WC} = \lfloor r_{J_x}, r_{J_y}, r_{J_z} \rfloor. \quad (3.7)$$

This process is repeated for each of the four outboard suspension points (points *J*, *M*, *P*, and *Q*). To sum the moments about the wheel center, the *r* vectors for each point are crossed with the *F* vectors in Equation (3.8), which for the X direction is

$$\begin{aligned}\sum M_x = 0 = {} & F_{JI}\left(\eta_{JI_z} r_{J_y} - \eta_{JI_y} r_{J_z}\right) + F_{JK}\left(\eta_{JK_z} r_{J_y} - \eta_{JK_y} r_{J_z}\right) + F_{ML}\left(\eta_{ML_z} r_{M_y} - \eta_{ML_y} r_{M_z}\right) \\ & + F_{MN}\left(\eta_{MN_z} r_{M_y} - \eta_{MN_y} r_{M_z}\right) + F_{PO}\left(\eta_{PO_z} r_{O_y} - \eta_{PO_y} r_{O_z}\right) + F_{QR}\left(\eta_{QR_z} r_{Q_y} - \eta_{QR_y} r_{Q_z}\right) + M_X\end{aligned}, \quad (3.8)$$

where M_X is the moment at the wheel center from the loading scenario. This process is repeated for the moments about the Y and Z axes. With the six equations (three force equations and three moment equations) the forces in each of the six members can be calculated.

A MATLAB program has been developed that solves these equations, making different loading scenarios easy to compute in a short amount of time. The program uses matrix algebra to solve the above equations for each of the member loads. A copy of this m-file is located in Appendix A-1. This method of load calculations has been used for several years; however the accuracy of load calculations derived from this method may not eliminate major suspension failures due to overly simplifying the structure. The real reason for a lack of member failures is likely that excessively large factors of safety have been applied to prevent buckling of members in compression. These factors are sometimes as high as 10. In addition to these high factors of safety, transient loading scenarios are often modeled as static scenarios (the most prominent of which is the 5g Bump). The 5g Bump static load case results in extremely high member loads due to a sustained loading force that is better represented by a change in road surface height through a step input, rather than a sustained force. These assumptions, amongst others, are what must be investigated further to better understand the behavior of the suspension system.

The resulting overall equation for member loads is given in Equation (3.9) by

$$[A]=\begin{bmatrix} \eta_{JI_X} & \eta_{JK_X} & \eta_{ML_X} & \eta_{MN_X} & \eta_{PO_X} & \eta_{QR_X} \\ \eta_{JI_Y} & \eta_{JK_Y} & \eta_{ML_Y} & \eta_{MN_Y} & \eta_{PO_Y} & \eta_{QR_Y} \\ \eta_{JI_Z} & \eta_{JK_Z} & \eta_{ML_Z} & \eta_{MN_Z} & \eta_{PO_Z} & \eta_{QRZ} \\ \left(\eta_{JI_Z} r_{J_Y} - \eta_{JI_Y} r_{J_Z}\right) & \left(\eta_{JK_Z} r_{J_Y} - \eta_{JK_Y} r_{J_Z}\right) & \left(\eta_{ML_Z} r_{M_Y} - \eta_{ML_Y} r_{M_Z}\right) & \left(\eta_{MN_Z} r_{M_Y} - \eta_{MN_Y} r_{M_Z}\right) & \left(\eta_{PO_Z} r_{O_Y} - \eta_{PO_Y} r_{O_Z}\right) & \left(\eta_{QR_Z} r_{Q_Y} - \eta_{QR_Y} r_{Q_Z}\right) \\ \left(\eta_{JI_Z} r_{J_X} - \eta_{JI_X} r_{J_Z}\right) & \left(\eta_{JK_Z} r_{J_X} - \eta_{JK_X} r_{J_Z}\right) & \left(\eta_{ML_Z} r_{M_X} - \eta_{ML_X} r_{M_Z}\right) & \left(\eta_{MN_Z} r_{M_X} - \eta_{MN_X} r_{M_Z}\right) & \left(\eta_{PO_Z} r_{O_X} - \eta_{PO_X} r_{O_Z}\right) & \left(\eta_{QR_Z} r_{Q_X} - \eta_{QR_X} r_{Q_Z}\right) \\ \left(\eta_{JI_Y} r_{J_X} - \eta_{JI_X} r_{J_Y}\right) & \left(\eta_{JK_Y} r_{J_X} - \eta_{JK_X} r_{J_Y}\right) & \left(\eta_{ML_Y} r_{M_X} - \eta_{ML_X} r_{M_Y}\right) & \left(\eta_{MN_Y} r_{M_X} - \eta_{MN_X} r_{M_Y}\right) & \left(\eta_{PO_Y} r_{O_X} - \eta_{PO_X} r_{O_Y}\right) & \left(\eta_{QR_Y} r_{Q_X} - \eta_{QR_X} r_{Q_Y}\right) \end{bmatrix}$$

$$\{x\}=\begin{Bmatrix} F_{JI} \\ F_{JK} \\ F_{ML} \\ F_{MN} \\ F_{PO} \\ F_{QR} \end{Bmatrix},$$

$$\{b\}=\begin{Bmatrix} F_X \\ F_Y \\ F_Z \\ M_X \\ M_Y \\ M_Z \end{Bmatrix}, \tag{3.9}$$

where the format for these variables is defined by Equation (3.10) such that

$$[A]\{x\}=\{b\}. \tag{3.10}$$

3.3.2 Results of the Hand Calculations

The final results of these hand calculations will form the baseline for the internal member forces that will be the basis of comparison for the FE models later in this research. These calculations were performed using the finalized suspension points for the 2009 VT-FSAE car. The suspension points for the front right suspension are given in Table 3.1.

Table 3.1. Suspension points for the front right corner of the 2009 VT-FSAE car.

All units mm		Start			End		
Member		**X**	**Y**	**Z**	**X**	**Y**	**Z**
FLCA	J-I	940.5	571.5	-149.9	1282.7	133.4	0.0
	J-K	940.5	571.5	-149.9	940.5	133.4	0.0
FUCA	M-L	914.5	539.4	-378.5	914.5	230.7	-317.6
	M-N	914.5	539.4	-378.5	661.7	230.7	-292.1
FTR	P-O	880.8	548.3	-149.9	880.8	133.4	-127.8
FPR	Q-R	908.9	520.4	-352.9	790.1	191.7	-143.4
Wheel Center		935.4	609.6	-254.0			

The member load calculations were determined using seven loading scenarios used by VT-FSAE to determine maximum member loads on the front suspension. These loads are shown in Table 3.2. These seven loading scenarios represent common loading conditions that a FSAE vehicle will experience in a competition. The scenarios include pure cornering, pure cornering with full load transfer to the outside tires, pure braking, pure braking will full load transfer to the front of the vehicle, combined cornering and

braking (which generally occurs during corner entry), a 5g Bump, and a full vehicle skid (which occurs when a driver loses control).

Table 3.2. Wheel center loading for the front right corner of the suspension.

LOADING AT WHEEL CENTER FOR RIGHT FRONT								
Car Cood Sys	Loading Scenario:	Left Hand Corner at 1.4g	Left Hand Corner - Full Load Transfer	Braking at 1.4g	Braking with Full Load Transfer	Corner and Braking Combined	5g Bump	1.5g Vehcile Skid
	Forces (N)							
	X	0	0	-1585	-2236	-1443	0	0
	Y	-1802	-1891	0	0	-1343	0	-933
	Z	-1135	-1204	-935	-1334	-1214	-3009	-602
	Moments (N-m)							
	Mz	-12.7	-14.3	-12.9	-15.4	30.6	0.0	-27.6
	My	0.0	0.0	-402.6	-567.9	-366.5	0.0	0.0
	Mx	457.8	480.4	0.0	0.0	341.1	0.0	237.0

Each of these loading scenarios is calculated from the tire data using the estimated load transfer and desired vehicle performance. These loads form the basis for the structural analysis of the suspension members. The maximum internal loads for each member that occur in all of these loading scenarios are determined and these loads become the critical design loads for the suspension components. Each member is then designed to withstand the maximum load it will see from these loading scenarios with a large factor of safety to account for any unknown amount of internal bending moment. Depending on the loading scenario in question, the members may be designed for compliance rather than ultimate strength; however this is not an either or condition, the member must be capable of withstanding the critical load while also providing the necessary compliance. The critical design loads for each of the suspension members as determined by the hand calculations are given in Table 3.3. The full results of all of these loading scenarios as determined by the hand calculations can be found in Appendix B-1.

Table 3.3. Critical member loads for each suspension member for the seven loading scenarios as determined by the hand calculations.

Max Member Loads		
Hand Calcs		
Tension		
FUCA (MN)	527.821	N
FUCA (ML)	-267.745	N
FLCA (JK)	259.124	N
FLCA (JI)	5949.970	N
FTR (PO)	325.612	N
FPF (QR)	9477.440	N
Compression		
FUCA (MN)	-4603.396	N
FUCA (ML)	-4725.675	N
FLCA (JK)	-4225.453	N
FLCA (JI)	-140.936	N
FTR (PO)	-1291.536	N
FPF (QR)	1774.247	N

3.4 Assumptions of the Hand Calculations and where Improvement is Needed

There are three main assumptions made with the hand calculations that need to be addressed to determine the validity of the hand calculations. The first assumption to investigate is the use of trusses instead of beams. Performing a bending analysis may prove that certain members undergo substantial internal bending that can greatly decrease the buckling resistance of a member to an axial load.

The second assumption to test is the lack of steering angle for steered scenarios. A steering input will change both the geometry of some of the suspension members as well as the location and orientation of the wheel center loads. The tires used on the FSAE vehicle work best at large slip angles that may further effect the orientation of the wheel center loads under a steered condition.

Lastly, the vertical movement of the suspension should be accounted for in any analysis. When the suspension articulates vertically, the orientation of each member changes and this may result in changes to internal loads of the suspension members.

3.4.1 Members Modeled as Beams Instead of Trusses

Several assumptions are made when using this method of hand calculations. First and foremost, each of the suspension members is assumed to be an individual pinned-pinned truss member. This may be true for the pull rod and tie rod but both of the control arms have two members welded together at their outboard ends. This will likely create bending loads in the members of the control arms that may make them more prone to buckling. The bending loads, if significant enough, may cause large amounts of

deflection that will cause the suspension to camber out excessively, causing an undesirable drop in the lateral capacity of the vehicle.

Since the suspension members are represented by pinned-pinned trusses in the hand calculations, a very large factor of safety is applied to account for any unknown bending and buckling stresses. This may be a method that works, as evidenced by a lack of suspension failures due to buckling; however it is not the appropriate way to design a suspension. A thorough understanding of the bending loads in each of the members will result in better knowledge of the suspension loads and thus a more appropriate design can be created.

The bending loads will be most prevalent in the upper control arm due to the pull rod attachment to this member. While the 2009 VT FSAE suspension design uses a pull rod attached to the upper control arm, the same principles apply to a push rod mounted on the lower control arm. Every effort is made in the control arm design to minimize the bending loads the control arm is subjected to by the pull rod. Despite these efforts, it is impossible to mount the pull rod outboard bearing to the exact same point in space as the upper ball joint. This compromise results in the potential for bending loads in the upper control arm when vertical movement causes the angle between the pull rod and UCA to change.

Bending will also be present due to the gussets and welded joints at the outboard end of the two suspension members in each control arm. The two members in each control arm are attached such that they are not free to independently rotate at the outboard end. The gussets are added specifically to reduce the bending stresses at the welded joint as well as to reduce the effective free length of each of the members to reduce the chances of buckling. This element of the design reveals that past knowledge believes that bending loads are present in the suspension, even if no analysis has been done to determine the exact values. Often, these stresses have been determined by an axial load in each of the two control arm members in a finite element model of a single control arm. While this may give the designer the illusion that they are accounting for bending at the welded joint, the actual bending loads may be more complex than the simple interaction of two axial forces.

Related to the assumption of all pinned-pinned truss members, these calculations assume that each member acts on a rigid body, the upright, at the outboard end of the suspension. While it is assumed that the upright is a rigid body, it is actually a deformable structure, however this assumption that will not be examined in this thesis. Were the pull rod attached directly to the upright, this assumption may have less merit, however due to packaging and other design constraints, the pull rod acts on the UCA. This geometry results in forces from the spring and damper being transmitted through the UCA instead of directly to the upright, and thus increasing the bending loads on the UCA. The decision to attach the pull rod to the UCA also changes the load that goes through the pull rod, changing the amount that the spring will allow the suspension to move. This configuration can potentially have adverse effects on the vertical movement of the suspension, especially when hitting a bump stop.

3.4.2 Forces and Members Rotated with Steered Tire

The suspension loads using the hand calculations are determined with the suspension points at static ride height. This may be fine for calculating the loads in the members as the vehicle sits in the shop or when the vehicle is traveling at a constant speed over a very smooth road, but these are not typical conditions for a race car. Generally, a vehicle needs to have a suspension (usually, but not always the front) that can rotate the wheel/tire in the top view to create a steering input. Steering inputs will change the orientation of the tie rod member associated with steering rotation of the wheel/tire and therefore the forces acting on the tire, in space. Maximum steering angles on this type of vehicle are generally in the 20-25 degree range. This is a significant amount of rotation in the loading forces and is likely to have a measurable impact on member loads.

Similarly to steering inputs, the hand calculations also do not account for any slip angle generation in the tire. Slip angle and lateral force go hand in hand; a properly designed and built tire will not have one without the other. The slip angle is the difference between the direction the tire is traveling and the direction the tire is pointed. In bias ply tires like those used on the FSAE car this angle can approach 15 degrees. As with steering angle, this is a large amount of rotation, which will impact the member orientations and the direction of travel under steered loading scenarios.

Large steering angles are very common in competition due to the tight turning radii typical of a FSAE course. The rotated wheel and tire will result in forces that are also rotated in relation to the suspension geometry. In 2006, the author created a MATLAB code that analyzed what the member loads would be if the forces were rotated about the wheel center. This program would sweep steering angle for each loading scenario and would plot a graph of how the load in each member would change with steering angle. The results revealed that while some changes were insignificant, some resulted in 25% increases in compressive loads in members where this compressive load is the limiting design factor.

While somewhat effective, this program did not take into account all of the considerations needed to properly analyze changes in member loads with steering angle. Firstly, the model still used the fixed suspension points at static ride height. In order to generate a steering angle, the suspension needs to articulate, specifically the tie rod needs to translate outward (Y direction) to force the upright to rotate. This movement changes the geometry of the suspension as a whole, which may change the loading of the suspension members. In addition to the different orientation of the suspension members, the upright and therefore the wheel center have rotated/translated in space. This moves where the point of force application in space, further adding to the potential change in the suspension loading.

Finally, while the forces rotate with the steering angle subjected to the suspension by the tie rod, the direction of travel of the vehicle will be oriented with the slip angles. In scenarios where a steer angle is present, the generation of lateral load will be

accompanied by a slip angle. This angle reduces the amount that the wheel changes direction during a corner, but it does not reduce the amount that the suspension members rotate. Adding to the complexity, the slip angle is dependent upon the lateral force, vertical load, and camber angle of the tire. Using the tire data from the FSAE TTC, the lateral force and vertical load for each scenario are used with an estimated camber angle to determine what slip angle is appropriate for each situation. There are some assumptions made here; first, the camber angle is assumed based on calculations of the amount of roll (which will vary with changes in spring rate and ARB stiffness) and the designed camber curve of the suspension. It is also assumed that the driver is capable of maneuvering the vehicle into corners at the ideal slip angle on each of the outer tires. In reality the driver will either be at a lower slip angle to reduce tire wear, but may also be at a higher angle to heat the tires or due to overdriving the vehicle.

This research will focus on the idealized cornering scenario with the tire at the optimal slip angle for maximum lateral force generation at the calculated vertical load. Since the lateral force will be maximized, the suspension will be at the most heavily loaded point of a cornering maneuver. Should the driver push beyond the limits of the tires, the lateral forces will decrease as the optimal slip angle is exceeded. The orientation of the forces at the wheel center will change but these forces will also decrease in magnitude substantially. Therefore, all steered scenarios will be performed at the optimal slip angle for the vertical load and expected lateral force. The slip angle data is available from the FSAE TTC data.

3.4.3 Suspension Articulates Vertically with Load Transfer

The last assumption to be examined in this research is the vertical, or sprung, aspect of the static suspension analysis. Like steering, the suspension being fixed at ride height does not account for geometry changes due to the vertical movement of the suspension relative to the car body. The orientation of the forces will not be changing as greatly as with steering, but no analysis has been done to date on whether there are measurable changes in member loads due to vertical wheel displacement.

The suspension model should also account for vertical movement of the suspension under load. The reasons for this are similar to the steering angle assumptions. While it is likely that vertical displacement of the suspension will result in a less significant effect than effects accounting for the steering angle, the change in vertical movement of the suspension may result in significant changes in the member loads.

With a bellcrank added to the model, the spring and ARB can also be added, introducing a very important element to the analysis; the element of vertical suspension displacement. While it is known that the suspension moves vertically under load, without costly data acquisition equipment, it is often difficult to determine how much the suspension moves under different loading scenarios. The primary point of interest here is whether the spring and damper assembly is reaching the maximum or minimum stroke. This condition results in contact with the bump stop, causing a rapid increase in the wheel rate at that corner of the car. A large, rapid change in a wheel rate is one of the causes of an

ill-handling vehicle, which commonly occurs when the suspension engages a bump stop at the limit of the compressive travel; however it can also include lifting a wheel off of the road surface. An accurate model of the vertical movement of the suspension will allow the suspension tuner to determine if a softer spring or ARB might cause the suspension to bottom out in certain loading scenarios. Having this capability creates the possibility to shed some light on potential handling problems during the testing process of preparing the vehicle for competition.

In addition to the vertical displacement analysis, the motion ratio of the bellcrank can be tested in the model. The motion ratio is the ratio of spring movement to wheel movement. Due to the nature of the lever arm bellcrank design, the movement of the spring and the wheel is going to be non-linear. It is desirable to have as close to a linear rate as possible and the bellcrank is designed accordingly. Using a working FE model, the movement of the wheel compared to the spring, and ARB, can be determined to see if the movement is too far from linear or if the design results in a falling-rate geometry. A falling-rate is defined as a wheel rate that decreases with increasing vertical movement; that is as the wheel moves vertically, the effective spring rate at the tire decreases. A falling rate is undesirable as it results in an unpredictable car and excessive roll in maneuvers with high lateral acceleration. A rising rate occurs when the wheel rate increases with vertical displacement. A rising rate allows for a slightly softer suspension in small ride movements, but stiffens as the suspension moves through larger suspension movements. A slight rising rate is often desirable as large wheel movements often require increasingly stiff roll or ride rates to counter the large forces involved. A rising rate suspension provides this while remaining soft at lower amount of movement, thus increasing the mechanical grip of the vehicle at these smaller vertical displacements.

Chapter 4
Development of FE Model

4.1 Truss Model Design

The development of the FE model begins with determining the type of software necessary to provide the needs of the problem, mainly the need for a solve capable of small strain and large displacement problems. The development process proceeds to a comparison of the hand calculations with an equivalent FE model. This comparison forms the basis for all future model development. The FE model is then modified in stages to determine how each change affects the internal member loads.

The four stages to be examined in this research begin with the Truss Model which represents the conditions of the hand calculations and will be used to validate the decisions made in the creation of the initial FE model. The second stage is the Beam Model in which the truss elements from the Truss Model are converted to beam elements to determine if forces other than axial forces are a significant design factor in any member. The third stage is the Steered Model. The Steered Model articulates to simulate the geometry change due to a steering input. The Steered Model also includes loading forces that have been rotated to account for the tire slip angle and the steered angle. The last stage is the Sprung Model. This model articulates for steering in the cases that need that condition, and also articulates vertically through the designed bellcrank, spring, and ARB. Changes of internal member loads with vertical movement are examined as well as the amount of vertical movement at the wheel center. Analyzing the vertical movement at the wheel center can be used to validate the model as well as give the suspension designer and tuner information about what the vehicle may need to exhibit the proper handling characteristics.

4.1.1 Explanation of the Need for a Large Displacement/Small Strain Model

The FE model must be created using software that is capable of performing the analyses in a specified manner. Specifically, the software must be able to represent the suspension members as elastic pieces that are part of a kinematic linkage. This feature will allow the model to show any changes in internal loads due to member compliance. The software must also be capable of performing finite element analyses on not just the simple first stage model, but also have the capabilities to model suspension movement with springs and possibly dampers. The primary need is for a program capable of large displacement and small strain analysis. This need arises from the articulation of the suspension to be used in the Sprung Model as well as future research. As the suspension moves vertically, each element and node will be translating and rotating by large displacements relative to the small deformations on the members. However the suspension members, while elastic, will be subjected to a small strain relative to that movement. Traditional analysis of static structures does not need to account for large displacements as any deflection or movement of an element is due to the stresses within the structure. Since the suspension

is a kinematic linkage, it is very important that the software have a capability to deal with movement of elements due to factors other than internal stress/load. Abaqus is an excellent finite element solver that has all of the necessary capabilities.

Adams (and Adams/Car) is a program that is often used in suspension analysis. This program allows the user to enter suspension points into a user defined or pre-existing template and run kinematic simulations on the suspension design. Common outputs include camber versus jounce movement, toe versus jounce movement, and camber versus degrees of body roll. This data is of great interest to the suspension designer in determining the best kinematic design for the suspension. This program does have some drawbacks when it comes to analyzing the suspension in terms of the goals of this research. The primary purpose of this research is to study the structural behavior of the suspension members. This includes the internal forces and moments within the members as well as the compliance these loads cause under load. While Adams can calculate the member loads for various conditions, the program does not handle the actual stress and strain of the members as each member is modeled as a rigid part. Informational material suggests taking the loads calculated in Adams and using them as a loading condition in a proper FE program such as Nastran (or in the case of this research Abaqus). Since one of the goals of this study is to develop a model that can be used for structural analysis of future teams, it is desirable to have a program that is fundamentally FE based and capable of modeling compliances in addition to kinematic movements.

4.1.2 Pin-Pin Six Member Truss Model

As previously outlined, the hand calculations assume that there are six independent pinned-pinned two force members that make up the suspension. To represent this in Abaqus, truss elements will be used. The length between each suspension point of all members is calculated and a part is made in Abaqus consisting of a line the length of the member to be modeled. Each part is represented as a truss element with two nodes, one node at each end of the line. The specifications of the truss elements used are shown in Table 4.1. This is consistent with the assumption made in the hand calculations that each member is an independent two-force member. Each member is added to an assembly representing the right-front corner of the vehicle. All six suspension members are modeled as elastic deformable bodies since the component deflection will be necessary to look at the suspension compliance in the future. For simplicity, each member is represented in the model as a round bar with a unit area cross section. Once all the members are oriented properly, displacement constraints and externally applied loads need to be added to the model. Figure 4.1 shows an overall view of the truss model.

Table 4.1. Truss element specifications for the Truss Model.

Truss Model Element Specifications	
Specification	**Value**
Element Name	T3D2
Element Library	Static
Geometric Order	Linear
Family	Truss
Scaling Factors	1
Hybrid Formulation	unchecked

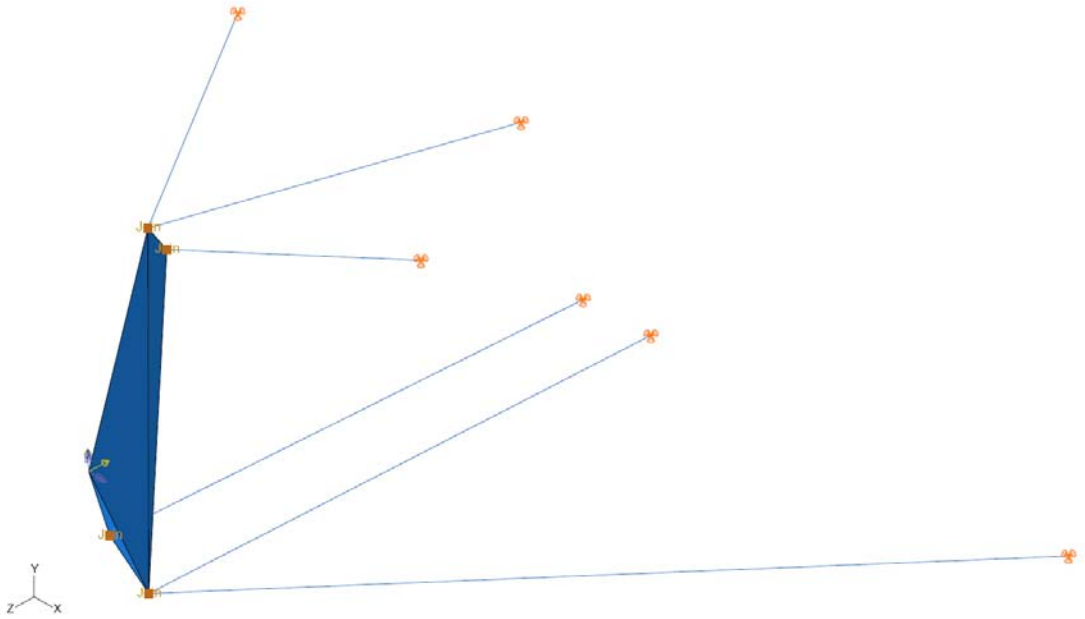

Figure 4.1. Truss element FE model as viewed from the right front view of the vehicle looking towards the left rear showing boundary conditions and loads for a left hand cornering scenario.

Each truss element is fixed at the chassis (inboard points) in all directions for translation; however each is free to rotate about all axes. The actual chassis is not modeled and is simply represented by the fixed translational degrees of freedom on the inboard side of the suspension. This is done based on the assumption that the chassis is significantly stiff such that it can be treated as a rigid body. One of the design considerations of the chassis designer is to create chassis mounts that have small enough compliance that the suspension behaves as if they are rigid mounts. In reality these mounts are not perfectly rigid due to the excessive vehicle weight that would create. Since this research is limited to the effects of compliance and loading on the suspension members only, the chassis is assumed to be rigid. This assumption keeps with the current assumptions used in the hand calculations, which will aid in the comparison of different models to these calculations. Future research should be performed to examine what, if any, effect the rigidity of the chassis mounts has on the suspension loading and potentially expand this corner assembly model to a model of the entire vehicle for a more thorough chassis analysis.

At the outboard side of the suspension, each member is attached to a rigid body representing the upright. Figure 4.1 shows this in the completed truss model assembly. No member is attached to any other member; each member attaches to the upright at the outboard suspension point specified by the suspension designer. It is important to note that each member attaching to the upright is a significant difference from the actual geometry when looking at the pull rod mount. This member attaches to the upper control arm through a bracket welded at the gusset attaching each member on the actual suspension. Since the hand calculations assume each member is attached to the upright, a rigid body shaped to accommodate this type of mounting is used to model the upright in this first stage FE model. Table 4.2 shows the section properties and member lengths used in the Truss Model and Beam Model. These values will later be changed to the section geometry supplied by the suspension designer. All suspension members are modeled as AISI 4130 steel, a common alloy used for suspension components. All stages of the FE model use this same material for all deformable suspension members. Table 4.3 shows the material properties used to represent this steel.

Table 4.2. Section properties for each member of the Truss Model and the Beam Model.

Truss Model - Section Properties		
	Area (mm^2)	Length (mm)
FUCA (MN)	645.16	314.6
FUCA (ML)	645.16	408.2
FLCA (JK)	645.16	556.4
FLCA (JI)	645.16	438.7
FTR (PO)	645.16	415.5
FPR (QR)	645.16	407.5

Table 4.3. Material properties of AISI 4130 steel.

Material Properties - All Models		
Property	Value	Units
Modulus of Elasticity	205	GPa
Yield Strength	460	MPa
Poisson's Ratio	0.29	

At each of these attachment points to the upright, every member is connected to the upright in a similar manner to the chassis mounts. The difference is that the translational degrees of freedom are not connected to ground; they are defined as a relative displacement restriction between the upright and the outboard end of the member. In this manner, the outboard end of each member may rotate freely where it is attached to the upright, but the outboard end of each member at the corresponding point on the upright must move in unison. To represent these joints in Abaqus, connector elements will be used. These are discussed in the next section. Table 4.4 summarizes the constraints on the Truss Model.

Table 4.4. Constraints on the Truss Model.

Truss Model Boundary Conditions			
Points	**Translation**	**Rotation**	**Type**
Inboard Suspension	Fixed	Free	Geometric BC
Outboard Suspension	Shared with Upright	Free	*Join Connector

4.1.3 Discussion of Connector Elements (*Join)

All the suspension members are connected to other components with spherical bearings at each end. A spherical (or 3-D revolute) bearing consists of an inner ball or sphere with a through hole. Figure 4.2 shows a cross section of a spherical bearing as well as a photo of a typical spherical bearing. This ball fits tightly inside a ring like cup that fully surrounds the ball. The contact surfaces on the ball and the cup are designed with low friction coatings such that the ball is free to rotate within the cup. In an ideal world, there would be no friction at all and the clearance between the cup and the ball would be zero. The high quality spherical bearings used today in the aerospace and racing industries are able to provide a reasonable service life while also providing near zero friction and clearance between the ball and cup. For these reasons, as well as to keep this stage of the model simple, it is assumed that an ideal spherical bearing will consist of the same translational and rotational degrees of freedom as a real spherical bearing with the idealized conditions of no friction and no clearance/slop in the bearing. Bearing internal friction is discussed in Section 6.3.4 as it pertains to future research.

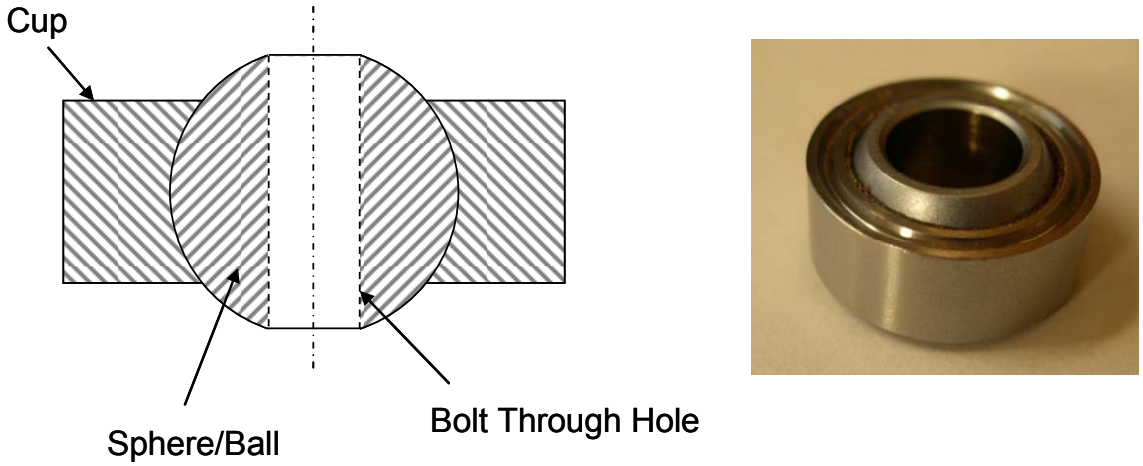

Figure 4.2. The cross-section and photo of a typical spherical bearing.

To represent an ideal spherical bearing, the connector elements in Abaqus will be used. As mentioned earlier, a connector is a type of element that constrained kinematic degrees of freedom between two nodes. For the idealized spherical bearing used in this model, none of the additional internal physical properties available to connector elements will be used. This represents the assumption that these spherical bearings are idealized and have no internal friction or kinematic limits on rotation degrees of freedom. Having the capability to add these properties in later research is a desirable trait as past research has

shown that there is potential for the internal friction in these bearings to be high if not properly installed and maintained.

A basic type of connector element will be used for the ideal spherical bearings. The Abaqus *Join connector element restricts the translational degrees of freedom of two nodes to be equal, while allowing all rotational degrees of freedom of each node to remain independent. This is the behavior that the model must have to simulate the required suspension performance.

To create an Abaqus connector element, a wire is created that connects the outboard end node of the suspension member to the appropriate point (node) on the upright. Once the wire element is created, it is assigned a connector type, in this case a "*Join" connection to represent the ideal spherical bearing. This operation is performed on all connections in the model between suspension members and rigid bodies. Abaqus does not require that the two nodes connected by a connector element be coincident, however in this model, all instances of a *Join connection of members are coincident at the appropriate suspension point.

An important aspect of the Abaqus *Join connectors used here is that they have the capability to transmit forces, but not moments from one member to another. In the case of the *Join connector used for the spherical bearings, the element can only transfer translational forces from the node at one end to the node at the other. The unconstrained rotational degrees of freedom in the element prevent any bending moment or torque from being transmitted from one member to another.

4.1.4 Calculations of Forces at the Contact Patch for Loading Scenarios

Loads are applied to the suspension at the wheel center. This was done to simulate the same procedure used with the hand calculations. It also simplifies the modeling as there is no need to represent the wheel assembly including the top hat and bearings.

The loads at the wheel center for the test scenarios are provided by the suspension designer. These loads were determined by first obtaining the loads at the contact patch. The loads at the contact patch are derived from data sourced from the FSAE Tire Test Consortium (FSAE TTC). Milliken Research Associates, Inc. (MRA) provides website space and organizes the finances of FSAE TTC but is otherwise unaffiliated with FSAE TCC. MRA coordinates the tire testing with the Calspan Tire and Research Facility (TIRF) [14]. TIRF uses tire testing machines with load cells to measure the forces produced by a tire under a variety of normal loads, camber angles, and slip angles. The data is provided in a digital format in which the user inputs tire type, tire load, camber angle, and other inputs to generate tables and graphs of the desired data. These tables and graphs specify what the loads at the contact patch will be under the different scenarios used for suspension loading.

The vertical tire load mentioned above is determined by the suspension designer using the track width, center of gravity height, and expected lateral acceleration as discussed in

Section 2.1.1. The lateral acceleration is estimated based on past year's vehicles and information provided by Goodyear tire engineers. Past experience has shown that the Goodyear D2692 20x7.0-13 racing tires on a 7.0" rim are capable of producing 1.4g acceleration (both lateral and longitudinal) on a vehicle the size and weight of a typical FSAE car. While an iterative process could be used to determine the expected conditions as precisely as possible, the tire data has shown that there is a certain amount of insensitivity to small changes in load and larger changes in camber angle below 0 degrees. In addition, experience has shown that the competition drivers are typically only capable of achieving 1.4g lateral acceleration, regardless of vehicle design. For these reasons, it is has been decided that an iterative process is unnecessary to determine contact patch loads. With contact patch loads determined based on the FSAE TTC data; it is a simple matter of vector geometry and statics to transfer these loads to the wheel center, located 254 mm (tire radius) above the contact patch.

To transfer these forces from the contact patch to the wheel center, the three forces (F_x, F_y, and F_z) are translated vertically 254 mm from the contact patch to the wheel center. The measurement 254 mm is the radius, r_T, of the Goodyear D2692 tire being utilized. The aligning torque, (M_z) is also translated vertically to the wheel center. This moment is created within the tire itself by the pneumatic trail as discussed in Section 2.2.1. Since the forces at the contact patch in the ground plane (F_x and F_y) do not point through the wheel center, these forces will create moments about the wheel center. Equation and Equation define these moments as

$$M_X = F_Y r_T , \tag{4.1}$$

and

$$M_Y = F_X r_T , \tag{4.2}$$

where r_T is the radius of the tire. This process yields equivalent wheel center loads that represent the contact patch loading. This process is performed for each of the desired loading scenarios. There are seven loading scenarios typically investigated. These scenarios are:

- Left Hand Corner with Expected Load Transfer
- Left Hand Corner with Full Load Transfer
- Left Hand Corner with Braking
- Straight Line Braking with Expected Load Transfer
- Straight Line Braking with Full Load Transfer
- A 1.5g Full Vehicle Skid
- A 5g Bump Subjected to One Corner

Table 4.5 shows the contact patch loads for each of the above loading scenarios which are transferred to the wheel center by the above process to create the wheel center loads used in all the FE models as shown in Table 4.6.

Table 4.5. Contact patch loads for each loading scenario as given by the FSAE TTC data for the Goodyear D2692 20x7.0-13 tire.

LOADING AT CONTACT PATCH FOR RIGHT FRONT								
Car Cood Sys	Loading Scenario:	Left Hand Corner at 1.4g	Left Hand Corner - Full Load Transfer	Braking at 1.4g	Braking with Full Load Transfer	Corner and Braking Combined	5g Bump	1.5g Vehcile Skid
	Forces (N)							
	X	0	0	-1585	-2236	-1443	0	0
	Y	-1802	-1891	0	0	-1343	0	-933
	Z	-1135	-1204	-935	-1334	-1214	-3009	-602
	Moments (N-m)							
	Mz	-12.7	-14.3	-12.9	-15.4	30.6	0.0	-27.6
	My	0.0	0.0	0.0	0.0	0.0	0.0	0.0
	Mx	0.0	0.0	0.0	0.0	0.0	0.0	0.0

Table 4.6. Wheel center loads for each loading scenario in the car coordinate system.

LOADING AT WHEEL CENTER FOR RIGHT FRONT								
Car Cood Sys	Loading Scenario:	Left Hand Corner at 1.4g	Left Hand Corner - Full Load Transfer	Braking at 1.4g	Braking with Full Load Transfer	Corner and Braking Combined	5g Bump	1.5g Vehcile Skid
	Forces (N)							
	X	0	0	-1585	-2236	-1443	0	0
	Y	-1802	-1891	0	0	-1343	0	-933
	Z	-1135	-1204	-935	-1334	-1214	-3009	-602
	Moments (N-m)							
	Mz	-12.7	-14.3	-12.9	-15.4	30.6	0.0	-27.6
	My	0.0	0.0	-402.6	-567.9	-366.5	0.0	0.0
	Mx	457.8	480.4	0.0	0.0	341.1	0.0	237.0

After each set of forces corresponding to a loading scenario is transfer from the contact patch to the wheel center, these wheel center forces and moments are applied in the FE model at the point on the rigid upright body that represents the wheel center. Figure 4.3 is a reproduction of Figure 2.12 and shows the FBD of the upright where the wheel center loads are given by F_x, F_y, F_z, M_x, M_y, and M_z.

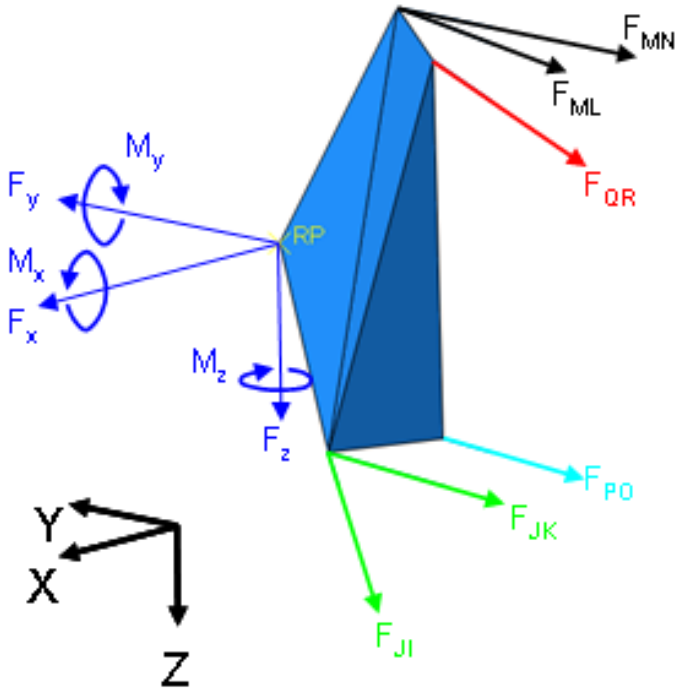

Figure 4.3. FBD of upright showing wheel center forces as they are applied to the upright.

A case labeled as expected load transfer occurs where the suspension designer has used the expected center of gravity height, the track width, wheelbase, and the expected lateral and longitudinal accelerations to determine the amount of vertical load on a tire for the given scenario. Each tire is modeled with the calculated load transfer that is expected given the vehicle characteristics and handling conditions. These include cornering with pure lateral acceleration, braking with pure longitudinal acceleration, and combined braking and cornering.

A case with full load transfer is defined as a loading condition in which the entire weight of the vehicle is transferred to the end of the car that is loaded. In a left hand corner, the right side of the vehicle carries a higher amount of load. In a full load transfer cornering scenario, the right side of the vehicle would carry the entire vehicle load, leaving the left side completely unloaded (zero vertical load). Under braking, the front of the vehicle carries the entire vehicle load in a full load transfer scenario. While these are not situations typically seen under normal operating conditions, full load transfer scenarios are not uncommon on bumpy racing circuits or tracks with major elevation changes.

A full vehicle skid is a condition where the driver has lost control of the vehicle and has spun. The specific condition modeled here is where the vehicle has rotated to the point where the direction of travel is perpendicular to the vehicle center line. This is a condition that can often occur where the vehicle is still on the racing line where there is a large amount of traction. Once the vehicle rotates past this point, it has often traveled far enough in a straight line that it is off track (in grass, dirt, or gravel) or in the marbles

(stones and bits of tire rubber thrown from the racing line to the outside of a corner by passing vehicles) where traction is reduced.

The final scenario of interest is a 5g bump to the suspension. This is an industry accepted value for the acceleration on the unsprung mass due to an impact with a road surface disturbance, such as a crack in the pavement [15]. Often if the dynamic competition portion of the FSAE event is held on a smooth course, the practice areas used before competition are not smooth. In addition, even on a smooth course, an impact like this can occur due to an unavoidable piece of debris from another vehicle falling on to the racing line. While this is a truly dynamic loading scenario, the hand calculations are performed on a vertical force equal to five times the static load on the tire. This is a relatively large assumption as the damping of the shock absorber will be a significant force which is currently unaccounted for in the model. The force on the suspension will also not be a sustained force as represented by the hand calculations.

4.1.5 Results of Truss Model for Key Loading Scenarios

Results for the Truss Model and the hand calculations are compared in Table 4.7. It is clear that the maximum loads seen within each member for all the loading scenarios of interest are virtually identical between the model and the hand calculations. Full details of each loading case can be seen in Appendix B-1. These numbers confirm that for every individual case, the loading in each member determined by the hand calculations is nearly the same as it is for the member loads determined by the model. The maximum percentage difference is 0.11%, which equates to 0.133 N for that specific scenario. This small difference is well within acceptable limits for design tolerances and represents a successful model that accurately emulates the hand calculations. The small differences that do occur are likely due to the nature of the Abaqus solver. Finite element analysis is based on the compliance and deformation of elastic parts and changing the relative stiffnesses of these parts will result in different internal loads. The hand calculations assume rigid bodies for all of the suspension members. Each member in the Truss Model has a unit section area which is significantly greater than the actual parts. This makes the members nearly rigid for the loads in question, however they are still elastic parts as shown by the small differences between the Truss Model and the hand calculations.

Table 4.7. Comparison of maximum member loads from hand calculations and truss model.

Member Loads						Percent Difference
Hand Calcs			Truss Model			
Tension			**Tension**			**Tension**
FUCA (MN)	527.821	N	FUCA (MN)	527.999	N	0.03%
FUCA (ML)	-267.745	N	FUCA (ML)	-267.693	N	-0.02%
FLCA (JK)	259.124	N	FLCA (JK)	259.208	N	0.03%
FLCA (JI)	5949.970	N	FLCA (JI)	5949.941	N	0.00%
FTR (PO)	325.612	N	FTR (PO)	325.537	N	-0.02%
FPR (QR)	9477.440	N	FPR (QR)	9476.536	N	-0.01%
Compression			**Compression**			**Compression**
FUCA (MN)	-4603.396	N	FUCA (MN)	-4602.931	N	-0.01%
FUCA (ML)	-4725.675	N	FUCA (ML)	-4725.257	N	-0.01%
FLCA (JK)	-4225.453	N	FLCA (JK)	-4225.415	N	0.00%
FLCA (JI)	-140.936	N	FLCA (JI)	-140.953	N	0.01%
FTR (PO)	-1291.536	N	FTR (PO)	-1291.546	N	0.00%
FPR (QR)	1774.247	N	FPR (QR)	1774.142	N	-0.01%

A point of note is that in the 5g bump scenario, every member has either a maximum compressive or tensile load. Please note that tensile loads have a positive value and compressive loads have a negative value. Entering a negative force in the tension columns of the table indicates that the member never sees a tensile load and the value represents the minimum compressive value the member experiences instead. The same holds true for positive values in the compression section of the table.

With a successful first stage linear truss finite element model accurately reproducing the member forces determined from the hand calculations, methods of improving the model can begin. This model is represented entirely by pinned-pinned truss elements in the place of each suspension member with the pull rod attached to the upright. The next stage will move to representing the correct geometry and extend the structural representation using beam elements.

4.2 Beam Model Development

Before the Truss Model can be reconfigured to accept steering angle inputs, the truss elements must be replaced with beam elements. This intermediate Beam Model state will investigate the existence of bending moments and other non-axial forces within each of the members. The pull rod attachment must be modeled more accurately in order to properly represent the geometry changes that occur with steering. This process requires the use of beam elements and will therefore be implemented in the Beam Model stage.

4.2.1 Trusses Converted to Beams/Explanation of Geometry Changes

While the Truss Model accurately reproduces the conditions and results of the hand calculations, several of the key assumptions made with the hand calculations still need to be addressed. These assumptions include using truss elements to represent suspension

members, attaching the pull rod to the upright instead of the upper control arm, and fixing the suspension at static ride height in the straight ahead position for all scenarios. The next stage of modeling investigates these assumptions and how creating a better representation of the suspension may lead to changes in member loads.

The first aspect of the Beam Model is the change in the geometry around the pull rod outboard attachment point. Figure 4.4 compares a photograph of the pull rod mounting on the 2009 VT-FSAE car to the representation used in the Truss Model. Clearly seen in Figure 4.4, the pull rod attaches to a bracket on the upper control arm and not to the upright as currently defined in the hand calculations and the Truss Model. This means that all of the forces in the pull rod caused by compressing the spring and moving the damper must act through the upper control arm and the upper ball joint at the outboard end of the upper control arm.

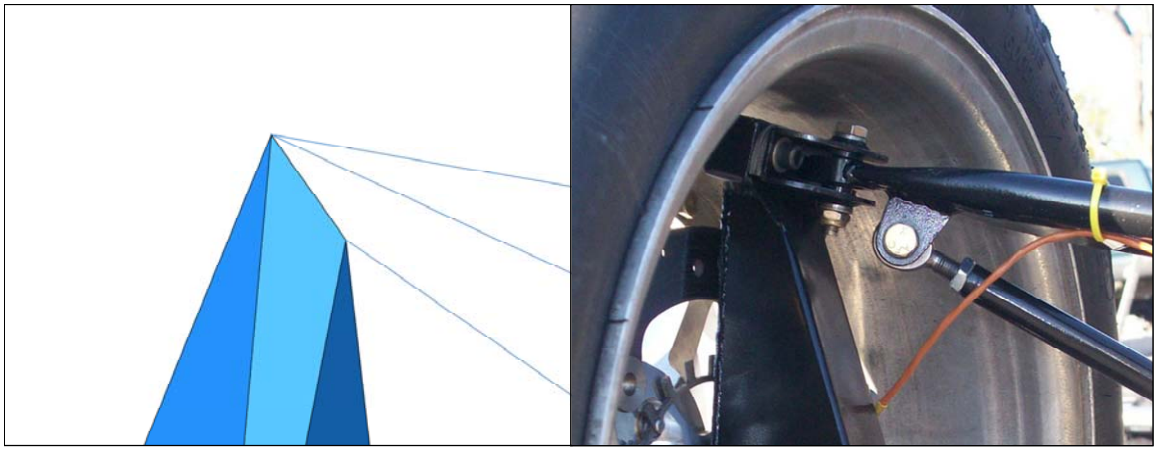

Figure 4.4. View comparing the pull rod mount in the Truss Model to a photograph of the same area from the completed 2009 VT-FSAE car.

An extension to the upper control arm must be made that extends downward and inward to meet the pull rod at the appropriate suspension point for the pull-rod mount. The pull rod mount, must remain at a fixed angle to the upper control arm members; the point where the pull rod mounts must rotate about the same axis on the chassis as the control arm itself.

There are many ways to accomplish this geometric constraint. A large solid object similar to the upright can be used to model the entire control arm and mount assembly, however this method adds material and therefore load carrying capacity in areas that do exist on the real suspension. Abaqus connectors could be used to create a "*Link" element. An Abaqus link element constrains two nodes by fixing the distance between them to be constant, while allowing any rotation and displacement so long as the fixed distance between the nodes remains. These members were tested in a trial model, however the results were unsuccessful. The kinematics behaved correctly in this model, but the *Link elements would carry a significant amount of the control arm loads, thus rendering the results of the model for member loads unacceptable. The ideal situation would be to model the bracket itself as a solid object. While this modeling approach would likely result in an accurate representation of the suspension, it would not eliminate

the complex behavior and stress concentrations in the area of the pull rod mount. Investigating the detailed behavior in this area is beyond the scope of this research and therefore, these stress concentrations should be removed from the model to better understand the basic behavior of the system as a whole. Figure 4.5 shows the modified model design for mounting the pull rod to the upper control arm.

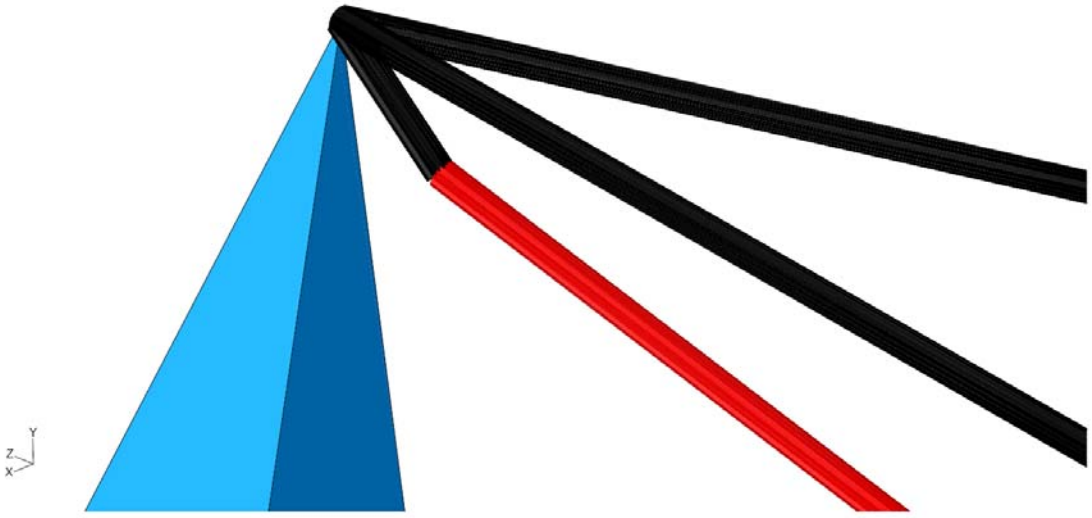

Figure 4.5. Beam element FE model showing the modified pull rod mount area to accurately represent the load path of the pull rod through the upper control arm.

The approach chosen to model the pull rod mount involves adding a simple beam extension in the form of a line from the upper ball joint to the point in space where the pull rod must mount. In attempting to create this assembly, it quickly becomes apparent that the elements in this area must be capable of modeling members that carry shear forces and bending moments. The truss elements in the Truss Model do not fit this requirement, thus each truss element in the model is replaced with a beam element. Like the Truss Model, each element of the Beam Model has a unit area, and a solid circular cross section. This was done to ensure that there are not too many changes taking place at once in the model. Converting the unit area cross-sections to the proper designed sections is covered in Section 4.2.2 later in this research.

The beam model was originally created with one beam element per member. This formed the starting point for the mesh convergence. The axial force remained the same regardless of the number of elements per member. The bending moment and shear force however increased to nearly double the original value as the mesh was converged. At 20 elements per member, the model had converged to within 1% for stresses, displacements, internal forces, and buckling eigenvalues. For the remainder of this research, all models (with the exception of the Truss Model) are run with 20 elements per member. The specifications of the beam elements used in the Beam Model and all subsequent models are shown in Table 4.8.

Table 4.8. Beam element specifications for the Beam Model and all subsequent stages of the FE Model.

Beam Model Element Specifications	
Specification	**Value**
Element Name	B31
Element Library	Static
Geometric Order	Linear
Family	Beam
Scaling Factors	1
Beam Type	Shear-Flexible
Hybrid Formulation	unchecked
Open Section	unchecked

A point to note at this time is that changing the Truss Model's truss elements to beam elements with the same cross-section geometry, material and end conditions would not result in different member loads. The reason for this is that in the basic model, each suspension member is attached only to the ground or to the upright. At each of these points the member is free to rotate about all axes. This eliminates the creation of shear forces and bending moments in the suspension members. As a result, substituting beam elements in this configuration would result in the same axial forces as the truss model and there would not be any internal bending moments or shear forces. By changing the geometry and connecting the control arm members to each other with a connection similar to a weld at the outboard points, moments and shear forces can be transmitted across the joint from one member to another. The completed Beam Model is shown in Figure 4.6 and Figure 4.7. Table 4.9 shows the constraints used in the Beam Model.

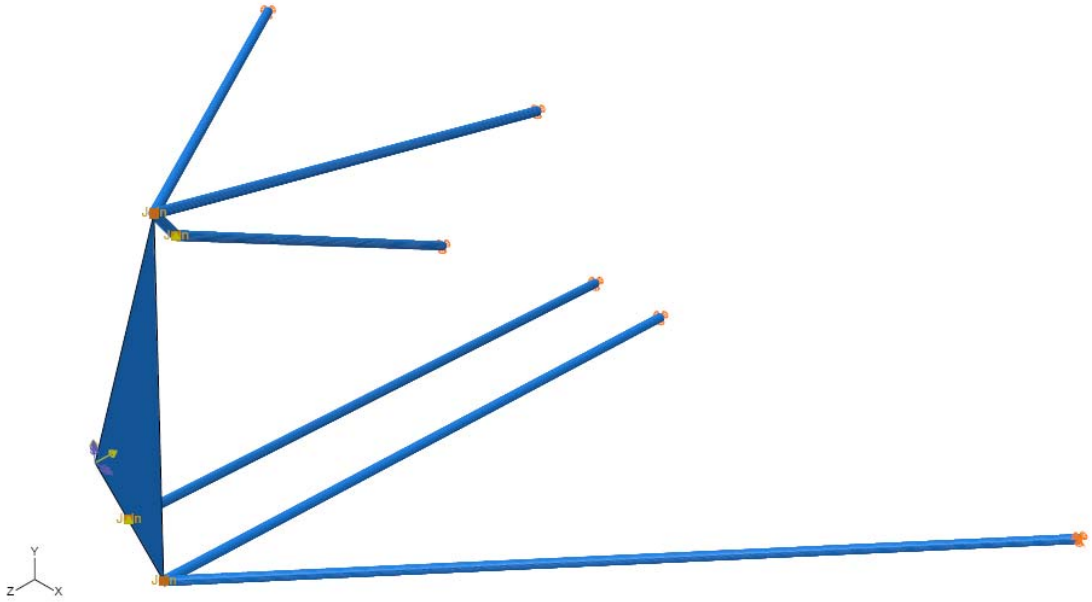

Figure 4.6. Beam element FE model with modified pull-rod mount as viewed from the front right with chassis mount boundary conditions and loading for a left hand corner.

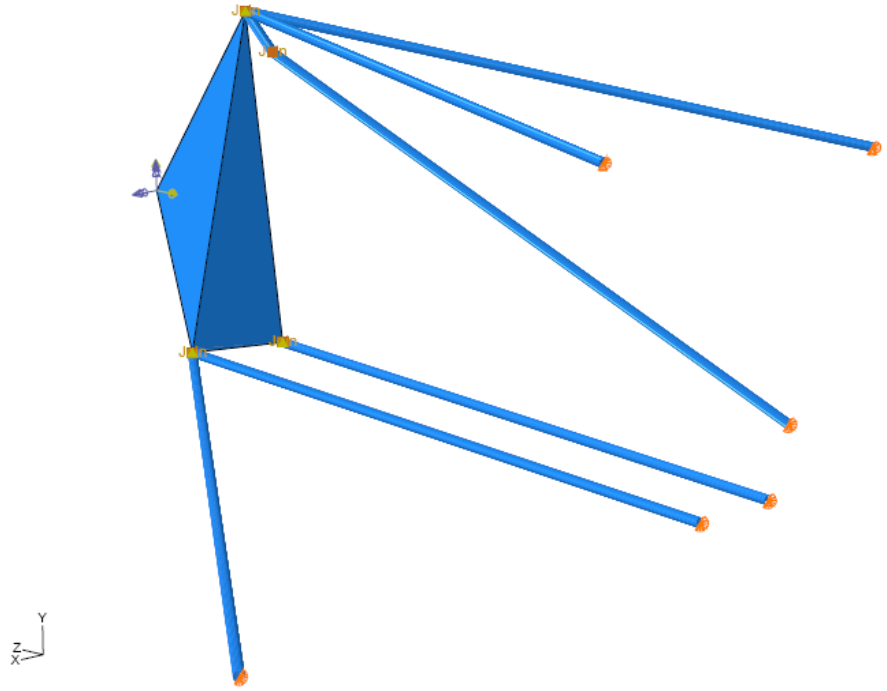

Figure 4.7. Beam element FE model with modified pull-rod mount as viewed from the front middle of the vehicle with chassis mount boundary conditions and loading for a left hand corner.

Table 4.9. Boundary conditions on the Beam Model.

Beam Model Boundary Conditions			
Points	**Translation**	**Rotation**	**Type**
Inboard Suspension	Fixed	Free	Geometric BC
Outboard Suspension	Shared with Upright	Free	*Join Connector

4.2.2 Comparison of Truss Model to Beam Model

With the pull-rod mount change in geometry and the switch to beam elements, the same seven loading scenarios were run and the results were recorded. Table 4.10 compares the results for axial load of the hand calculations, the Truss Model, and the Beam Model. While the loads are still very similar, the beam element model has notable differences in the maximum compressive and tensile loads, and in many cases these loads are less than that of the truss model or hand calculations. Complete results for all loading scenarios using the Beam Model can be found in Appendix B-2.

Table 4.10. Comparison of maximum compressive and tensile loads with hand calculations, truss elements, and beam elements.

Member Loads - Axial Force								
Hand Calcs			**Truss Model**			**Beam Model**		
Tension			**Tension**			**Tension**		
FUCA (MN)	527.821	N	FUCA (MN)	527.999	N	FUCA (MN)	569.875	N
FUCA (ML)	-267.745	N	FUCA (ML)	-267.693	N	FUCA (ML)	-250.695	N
FLCA (JK)	259.124	N	FLCA (JK)	259.208	N	FLCA (JK)	1016.396	N
FLCA (JI)	5949.970	N	FLCA (JI)	5949.941	N	FLCA (JI)	5828.549	N
FTR (PO)	325.612	N	FTR (PO)	325.537	N	FTR (PO)	254.403	N
FPR (QR)	9477.440	N	FPR (QR)	9476.536	N	FPR (QR)	8779.588	N
Compression			**Compression**			**Compression**		
FUCA (MN)	-4603.396	N	FUCA (MN)	-4602.931	N	FUCA (MN)	-4495.284	N
FUCA (ML)	-4725.675	N	FUCA (ML)	-4725.257	N	FUCA (ML)	-4634.469	N
FLCA (JK)	-4225.453	N	FLCA (JK)	-4225.415	N	FLCA (JK)	-3924.871	N
FLCA (JI)	-140.936	N	FLCA (JI)	-140.953	N	FLCA (JI)	-444.261	N
FTR (PO)	-1291.536	N	FTR (PO)	-1291.546	N	FTR (PO)	-1316.825	N
FPR (QR)	1774.247	N	FPR (QR)	1774.142	N	FPR (QR)	1643.658	N

While Table 4.10 indicates that there are noticeable differences in axial load, many of the loads are not a significant amount greater than the hand calculations, with the one exception of the compressive load on the JI member of the lower control arm. In fact, many of the members are experiencing less axial load. When the design criteria is collected to size each member, the critical design load in every case is smaller with the Beam Model than with the hand calculations, however this data does not represent the complete picture. The switch to beam elements results in members capable of supporting bending moments and shear forces. Each member is also capable of carrying torsion loads, however in every loading scenario these loads are less than 1.13×10^{-16} N-m and can therefore be neglected from the analysis. Table 4.11 shows the maximum and minimum internal loads of each member including shear force and bending moment magnitudes as determined by the Beam Model. It is important to note that the maximum shear forces and bending moments do not necessarily occur in the same loading scenario as the maximum axial force. Appendix B-3 contains a table of the complete loading for each scenario including shear force and bending moment components.

Table 4.11. Maximum and minimum loads in each member for the beam element model.

Internal Member Loads								
Beam Model								
Tension			**Max Shear Force Magnitude**			**Max Bending Moment Magnitude**		
FUCA (MN)	569.875	N	FUCA (MN)	240.512	N	FUCA (MN)	59.180	N-m
FUCA (ML)	-250.695	N	FUCA (ML)	156.401	N	FUCA (ML)	47.979	N-m
FLCA (JK)	1016.396	N	FLCA (JK)	1.601	N	FLCA (JK)	0.486	N-m
FLCA (JI)	5828.549	N	FLCA (JI)	1.265	N	FLCA (JI)	0.685	N-m
FTR (PO)	254.403	N	FTR (PO)	0.000	N	FTR (PO)	0.000	N-m
FPR (QR)	8779.588	N	FPR (QR)	0.000	N	FPR (QR)	0.000	N-m
Compression			**Min Shear Force Magnitude**			**Min Bending Moment Magnitude**		
FUCA (MN)	-4495.284	N	FUCA (MN)	27.838	N	FUCA (MN)	11.079	N-m
FUCA (ML)	-4634.469	N	FUCA (ML)	29.282	N	FUCA (ML)	8.938	N-m
FLCA (JK)	-3924.871	N	FLCA (JK)	0.029	N	FLCA (JK)	0.012	N-m
FLCA (JI)	-444.261	N	FLCA (JI)	0.023	N	FLCA (JI)	0.012	N-m
FTR (PO)	-1316.825	N	FTR (PO)	0.000	N	FTR (PO)	0.000	N-m
FPR (QR)	1643.658	N	FPR (QR)	0.000	N	FPR (QR)	0.000	N-m

The shear forces and bending moments are small in several scenarios, indicating that the overriding design consideration appears at first to remain the axial loads. The maximum shear forces and bending moments in the upper control arm (both members MN and ML) occur when those member are experiencing the maximum axial compressive forces seen in Table 4.11. While the shear forces and bending moments are relatively insignificant compared to the axial forces in the members, the axial force in these situations is compressive and therefore prone to buckling. The addition of a bending moment and shear force in these members is likely to increase the tendency of these members to buckle. When designing the member sizes (wall thickness and outer diameter), a buckling analysis with all the internal loads should be performed to ensure that the size of the member will allow it to withstand these forces without significant deflection.

The final aspect of the Beam Model that is examined is the effect of including the proper section profiles on each of the members. Unit sections have been used through this point of the FE model development. Replacing the unit sections as given in Table 4.2 with the appropriate section profile as specified in Table 4.12, reveals very similar internal forces. The results of this modification are shown in Table 4.13. While the changes are small, they do exist. This difference is due to the change in relative stiffness that occurs when member sections are modified, thus changing the equations used by Abaqus to calculate the internal loads. The major result of this change is in the increased stresses within each member. The member von Mises stresses are shown in Table.

Table 4.12. Suspension member sections as specified by the suspension designer for the 2009 VT-FSAE car. Note that all profiles are circular.

Designed Section Properties					
	Diameter (mm)	Wall Thickness (mm)	Area (mm^2)	I (mm^4)	Length (mm)
FUCA (MN)	15.9	1.2	57.21	1541.66	314.6
FUCA (ML)	14.3	1.2	51.00	1094.33	408.2
FLCA (JK)	12.7	0.9	32.99	578.46	556.4
FLCA (JI)	15.9	1.2	57.21	1541.66	438.7
FTR (PO)	12.7	0.9	32.99	578.46	415.5
FPR (QR)	14.3	0.9	37.42	843.41	407.5

Table 4.13. Comparison of internal axial forces for the Beam Model with unit sections and Beam Model with proper sections.

Member Loads - Axial Force						Percent Difference
Beam Model			Designed Member Sections			
Tension			**Tension**			**Tension**
FUCA (MN)	-56.359	N	FUCA (MN)	-56.359	N	0.00%
FUCA (ML)	228.495	N	FUCA (ML)	228.495	N	0.00%
FLCA (JK)	-23.750	N	FLCA (JK)	-23.752	N	0.01%
FLCA (JI)	57.192	N	FLCA (JI)	57.192	N	0.00%
FTR (PO)	1973.730	N	FTR (PO)	1973.730	N	0.00%
FPR (QR)	0.000	N	FPR (QR)	0.000	N	0.00%
Compression			**Compression**			**Compression**
FUCA (MN)	-1041.870	N	FUCA (MN)	-1041.870	N	0.00%
FUCA (ML)	-322.173	N	FUCA (ML)	-322.173	N	0.00%
FLCA (JK)	-99.873	N	FLCA (JK)	-99.883	N	0.01%
FLCA (JI)	37.216	N	FLCA (JI)	37.216	N	0.00%
FTR (PO)	369.509	N	FTR (PO)	369.509	N	0.00%
FPR (QR)	0.000	N	FPR (QR)	0.000	N	0.00%

Table 4.14. Comparison of member stresses in the Beam Model with unit sections and with proper sections.

Beam Model, Unit Cross-sections							
Stress (MPa)	1.5g Skid	5g Bump	Braking	Braking FLT	LH_Corner_Braking 0	LH_Corner 0	LH_Corner_FLT 0
FUCA (MN)	4.26	27.84	9.77	13.93	10.40	7.98	8.49
FUCA (ML)	6.13	32.55	7.75	9.27	9.22	11.52	12.23
FLCA (JK)	2.23	1.60	4.58	6.38	5.55	3.29	3.47
FLCA (JI)	0.17	0.71	6.62	9.33	5.95	0.30	0.31
FTR (PO)	0.26	0.39	0.24	0.41	2.04	0.56	0.56
FPR (QR)	2.55	13.61	3.78	5.40	4.84	4.80	5.09

Beam Model, Proper Cross-sections							
Stress (MPa)	1.5g Skid	5g Bump	Braking	Braking FLT	LH_Corner_Braking 0	LH_Corner 0	LH_Corner_FLT 0
FUCA (MN)	47.10	309.19	108.84	155.19	115.57	88.33	93.99
FUCA (ML)	83.51	443.74	106.97	129.96	127.94	157.02	166.65
FLCA (JK)	25.08	17.77	50.34	70.15	61.44	37.02	39.06
FLCA (JI)	3.26	13.72	125.31	180.01	114.72	5.72	6.07
FTR (PO)	5.02	7.71	4.77	8.05	39.92	10.94	10.94
FPR (QR)	43.92	234.62	65.13	93.13	83.37	82.73	87.80

4.3 Steered Model

The completed Beam Model is now used to develop the Steered Model, which will incorporate the geometry changes due to steering articulation. The Steered Model will also adjust the radius of travel to account for the slip angle that exists at the contact patch under steered conditions. A sweep of steering angles will be performed in order to determine any trends that exist in individual member loads due to changes in steering angle.

4.3.1 Slip Angle vs. Steered Angle and Effect on Direction of Travel

Possibly the single largest assumption made with the hand calculation method is the decision to fix the suspension in the straight ahead position. While this assumption is similar to the lack of vertical movement, there are some factors that make it a more drastic assumption. The rotational changes with steering are significantly greater in magnitude than that of vertical articulation. Vertically, each member will rotate about its axis on the chassis. With the member lengths of the control arms and the rules mandated movement range of ± 25.4 mm, the members will operate in an angle range of less than 10° under vertical displacement. When steered however, the steering angle will rotate through a range closer to 50°. A byproduct of this high level of rotation is that the forces at the contact patch will rotate with the wheel. As the wheel is steered through the desired angle, the forces at the contact patch will rotate a similar amount, loading the front suspension members in a greatly different manner than leaving the forces stationary.

The approach to calculate these steered loads will begin with calculating the slip angle that will occur at a given load and cornering condition. This will be used to determine the actual radius of travel of the vehicle. The forces at the wheel center will then be rotated an amount equal to the amount the upright rotates in the horizontal plane due to a steering input from the driver.

In 2006, the author performed some analysis on the effects of steering angle on member loads using the hand calculations. The forces and moments at the wheel center were rotated by various angles in a sweep of possible steer angles. The MATLAB m-file used to compute the hand calculations was run in each steered case to generate a sweep of member loads with steer angle. The results of this study revealed that there were notable increases in several member forces with increasing steer angle. Specifically members JK and JI saw large increases in axial load with increasing steer angle with member JK seeing large increases in compressive loads. The analysis resulted in the modification of section properties by increasing the wall thickness or tubing diameter to increase the factor of safety of the members. Any member that saw an increase in critical load due to a steered scenario had material added to increase the factor of safety. No further investigation into this matter was performed due to time constraints.

While the forces at the contact patch and therefore at the wheel center rotate with steering angle, there is also the need to account for the slip angle that is developed when

cornering. When a vehicle is steered, the front tires are forced to be pointed in a different direction than the vehicle is traveling, resulting in a slip angle. A slip angle is the difference in the direction a tire is pointed and the direction the tire is traveling. The slip angle is the result of the distortion, or twisting, of the tire under load. When steering, the contact patch resists the induced twisting action between the steered wheel and the friction forces developed with the road surface. This causes the carcass of the tire (the body or structure of the tire supporting the tread surface) to twist. This elastic deformation, or distortion, of the tire causes the tire to "slip" or walk at an angle different from the direction it is pointed. The use of the word slip is not entirely correct as the contact patch itself is not actually slipping significantly.

Research in tire behavior has proven that the direction the tire travels is not perpendicular to the tire heading [6]. This means that under a slip angle, the direction the tire forces the vehicle to travel in is different than the direction the tires are oriented to the chassis, or the tire heading. It is this behavior that the Steered Model stage of the FE model development will account for in the load cases. In order to model this behavior, slip angles must be provided by the suspension designer. These angles were determined by first calculating the load transfer in each loading scenario of interest and then consulting the FSAE TTC tire data. From the FSAE TTC data, the slip angle that corresponds to the maximum lateral force for a given vertical load is read from the tables and can then be used in the steer angle calculations. This data was found for each loading scenario where a slip angle is of interest. These scenarios include left hand cornering with expected load transfer, left hand cornering with full load transfer, and combined left hand cornering with braking. The slip angle data as obtained from the FSAE TTC tables are shown in Table 4.15.

Table 4.15. Slip angle values for the three loading scenarios that involve cornering.

Loading Scenario	Slip Angle (deg)
LH_Corner	13.349
LH_Corner_FLT	14.099
LH_Corner_Braking	3.45

4.3.2 Outline of Steer Angle through Typical Course Radii

The FSAE competition is divided into several dynamics events in which the vehicle is to demonstrate the highest possible performance. All but one of these events involves the vehicle's cornering ability. One of these events, the Skid Pad Event, is designed such that the driver navigates in a figure eight with a center diameter of 18.25 m with an inner diameter of 15.25 m shown in Figure 4.8. The purpose of the Skid Pad event is to determine the steady state cornering capabilities of each FSAE vehicle. The Skid Pad event is very closely represented by the 1.4g Left Hand Cornering loading scenario as this event is almost exclusively an ultimate cornering steady-state situation. Using the half width of the vehicle with the inner edge of the vehicle directly on the inner edge of the circle, the desired radius of travel of the CG is 8.32 m. One of the angles in the steering angle sweep should exhibit a radius of vehicle travel as close to this value as possible so that one of the points in the steering sweep represents a scenario as close as possible to the skid pad event, allowing for an analysis of the expected loading and

compliance in this event to be performed. In the autocross and endurance events, a minimum hairpin radius of 4.5 m is specified. The constant radius turns of the autocross course range from 11.5 m to 22.5 m. In the endurance course, constant radius turns may range from 15 m to 27 m. The 4.5 m hairpin radius should be tested as this extremely tight corner will generate the most displacement of the suspension due to steering input. The hairpin radius and skid pad radius are necessary to test in all of the steered scenarios since the likelihood of each occurring is high in competition. These radii will determine the steering angles to be tested for the left hand corner with expected and full load transfer as well as the braking and turning scenario.

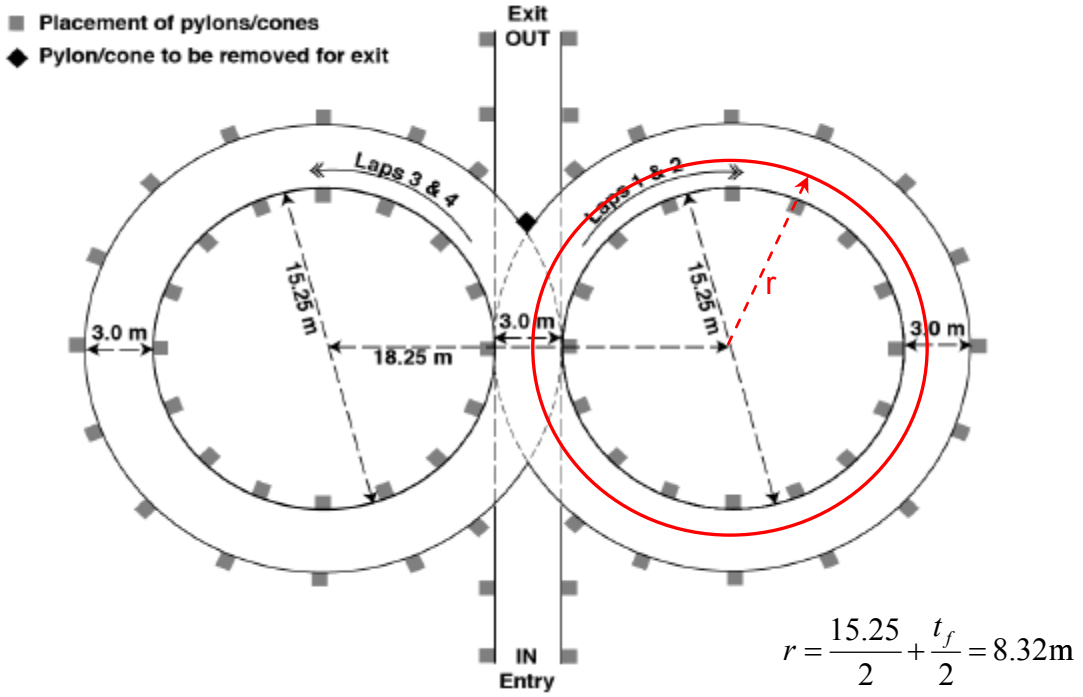

Figure 4.8. Layout and dimensions of the FSAE skid pad course modified to show the calculated path of the vehicle CG travel in red [4]. Reprinted with permission from SAE publication "2009 Formula SAE Rules" by SAE © SAE International.

To determine the radius the vehicle will travel at various steer angles, the vehicle must be looked at as a whole unit. Several assumptions need to be made to calculate the radius of travel. While it is desirable to have each tire of the vehicle perfectly angled such that the slip angles are maximized on every corner, it is not feasible within the constraints and compromises of suspension design to create this ideal case in every corner. In addition, it is highly unlikely the driver would be able to maneuver the car into this condition and keep it there for the duration of the corner. The tires that will have the greatest impact on the cornering characteristics of the vehicle will be the outer tires. Due to load transfer, the outside tires will carry a large percentage of the vehicle weight. In left-hand cornering with expected load transfer, the inside front tire of the 2009 VT-FSAE vehicle carries 7.0 kg and the inside rear tire carries 26.1 kg, for a total right-side load of 11.8% of total vehicle weight. These numbers were provided by the suspension designer as

calculated by the load transfer equations in Chapter 2 and are shown in Table 4.16. Loading scenario data for all vehicle cornering conditions can be found in Appendix C-1. These values for inside tire loads are insignificant compared to load on the outer tires. In the full load transfer scenarios, by definition, the inside tires carry no load at all. With the lack of appreciable load on the inside tires, the maximum possible lateral load is small and these tires are generally dragged across the road surface in a manner that allows the outer tires to operate at the optimum slip angles.

Table 4.16. Load transfer data for a left hand corner with expected load transfer as provided by the suspension designer.

Pure Lateral Loading - Left Hand Corner at 1.4g				
	LF	RF	LR	RR
X (kg)	0.000	0.000	0.000	0.000
Y (kg)	-12.608	-183.782	-46.007	-195.432
Z (kg)	-7.008	-115.734	-26.081	-123.332

The slip angles for each load case are applied to the outer tires of the vehicle with the rear tires fixed in direction. It is assumed that the rear tires are operating at the same slip angle as the front tires. This assumption was formed due to the nature of vehicle balance and trends in slip angle data. Specifically, the vehicle will likely be tuned to just slightly understeer in a steady state corner. This means the front tires will reach the maximum lateral load and slip angle before the rear tires. The rear tires have more load on them than the front tires due both to the rear-weight bias of the vehicle and a smaller rear track width than the front track width. Tires will generally have a larger optimal slip angle with a larger vertical load. Since the rear tires are operating just slightly below the optimal slip angle, the difference between the front and rear slip angles will be very small, therefore for these steering calculations, the two will be defined as equal. Another assumption made in the steering calculations is that there is an insignificant amount of bump steer and/or compliance steering in both the front and rear. Both of these effects should be virtually eliminated with a good suspension design.

Figure 4.9 is a diagram of the geometry involved in this process. Having applied the slip angle to the rear tire of the vehicle, a perpendicular line can be drawn to the direction of tire travel (the line normal to the slip angle). The center of the circle about which the vehicle travels will lie along this line. The slip angle is then applied to the front tire and a line drawn perpendicular to it, just as in the rear. In the case of the front tire however, there is a steer angle that can adjust the direction of tire travel. The point at which the line perpendicular to each of the tires' slip angles intersect is the center of the circle about which the vehicle is traveling. Using the vehicle width and center of gravity location, the distance from the center of the circle to the vehicle center of gravity (which lies on the center line of the vehicle) can be determined. This is the calculated radius about which the vehicle will travel at a given steer angle at maximum lateral acceleration. The derivation of the steering angle is described below. Complete results from all of the steer angle calculations can be found in Appendix D-2.

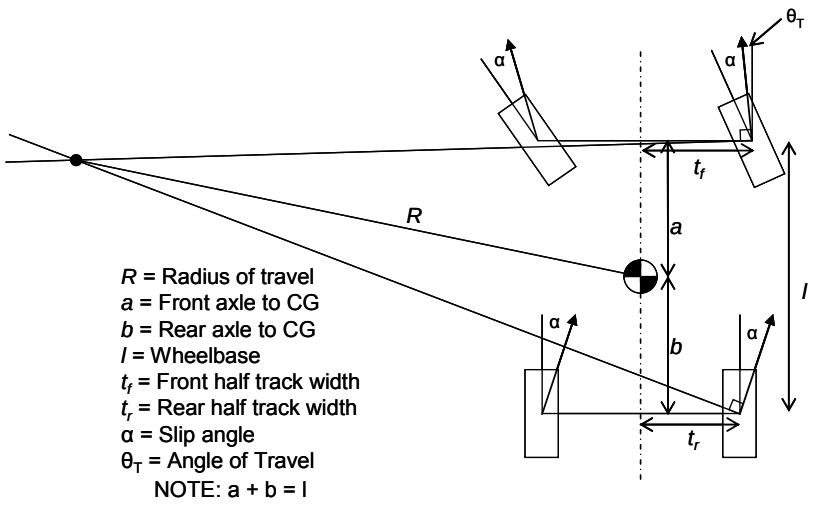

Figure 4.9. Steering diagram used to account for the effect of slip angle on the radius of vehicle travel.

Comparing the data for steer angle versus vehicle radius of travel with the specified radii of the various dynamic events, the key steer angles can be determined. A point to note is that each of the three steered scenarios results in a different slip angle for maximum lateral force. There is no way to predict the length of each corner in any of the courses or what the course will do before or after any given corner. For the sake of simplifying the analysis, the modeled steer angles will be determined from the pure left hand cornering with expected load transfer scenario. While the radius of travel will be different for the cornering with full-load transfer and the combined braking and cornering scenarios, the chances of those loads existing in a steady state condition are much smaller than for the cornering with expected load transfer. Tables comparing the radius of travel to steer angle for each of these loading scenarios are located in Appendix D-2.

Considering the case of the left hand cornering with expected load transfer scenario to determine radius of travel, a steer angle of 11° is calculated from the specified radius needed for the skid pad competition. At a steer angle of 22°, the vehicle is traveling about a radius slightly tighter than the minimum hairpin radius. To gain a better understanding of possible trends in the changes of member loads with steer angle, the sweep of steering angles is refined to twice the density of these two angles. The final sweep consists of steer angles of 0°, 5.5°, 11°, 16.5°, and 22°. A steer angle of 0° results in an infinite turning radius and could occur at the moment the vehicle completes the corner, or due to extreme side loading from cross wind loads or a cambered road surface. It is also useful to compare this scenario to the prior stage of the model which did not account for slip angles. The remaining four non-zero steer angles correspond to radii of 16.763 m, 8.478 m, 5.681 m, and 4.257 m.

Figure 4.9 forms the basis from which the steering calculations are performed. The tire slip angle as provided by the suspension designer is subtracted from the tire heading, or steer angle. This results in the angle of travel of the tire, θ_T. The assumption is made that the low levels of load on the inside tires result in the outer tires defining the overall vehicle cornering characteristics when in a steady-state corner. This loading scenario, as

shown in Figure 4.10, represents a two wheeled vehicle that is used to continue the steer angle calculations.

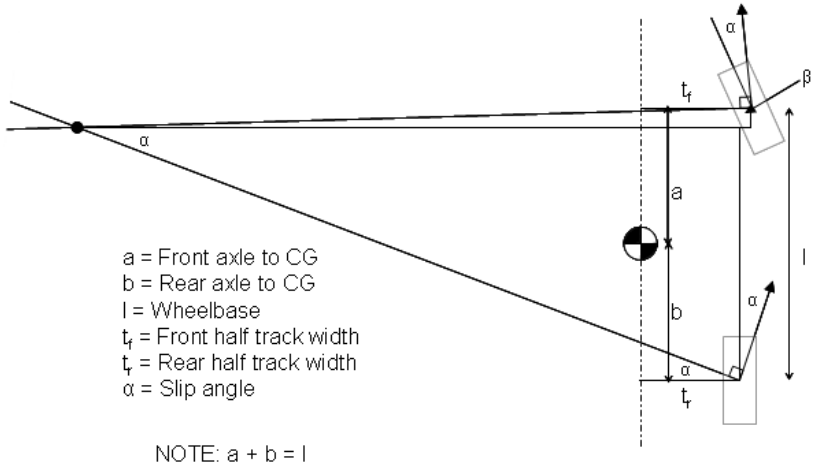

Figure 4.10. Modified two wheeled vehicle steering angle effect diagram.

The extended lines perpendicular to the individual directions of travel can be used to create the hypotenuses of two triangles. The upper triangle has an angle β which is defined as the angle of travel, θ_T, minus 90 degrees. The lower triangle has the smallest angle equal to the slip angle, α. The difference between the horizontal lengths of each of these triangles is the difference in half tracks defined in Equation (4.3) as

$$DT = t_f - t_r . \tag{4.3}$$

These two triangles are separated in Figure 4.11 to more clearly show the geometry. *L* is defined as the distance, perpendicular to the centerline of the vehicle, from the front tire to the center of the circle about which the vehicle is traveling. Variables *x* and *y* are the distances parallel to the vehicle centerline from the center of the circle traveled to the front and rear axles respectively as shown from Figure 4.11.

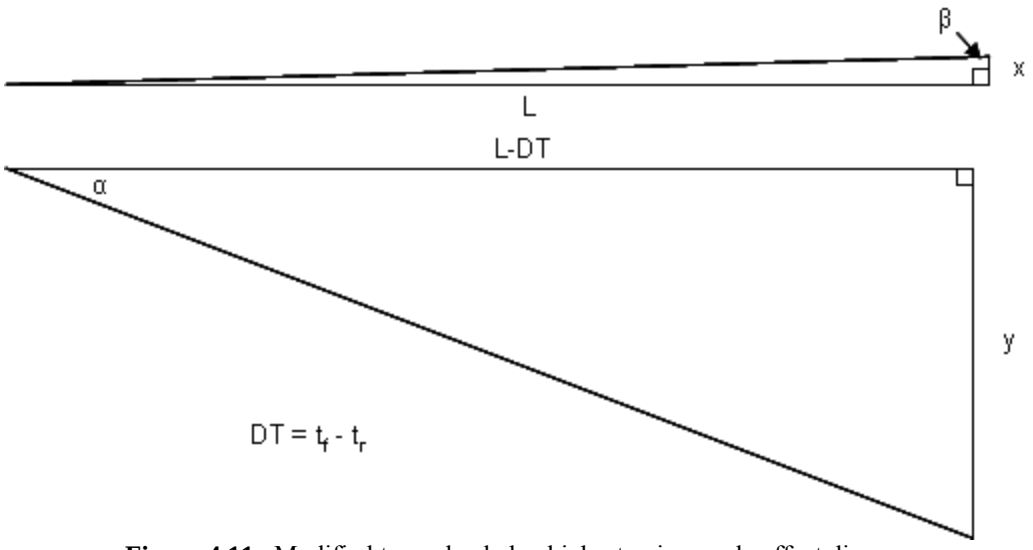

Figure 4.11. Modified two wheeled vehicle steering angle effect diagram.

Two sides and all angles of each triangle are known so the derivation proceeds easily from here starting with Equation (4.4) showing that

$$l = x + y, \tag{4.4}$$

$$\tan\beta = \frac{L}{x}, \tag{4.5}$$

$$x = \frac{L}{\tan\beta}, \tag{4.6}$$

$$\tan\alpha = \frac{y}{L - DT}, \tag{4.7}$$

$$y = \tan\alpha(L - DT). \tag{4.8}$$

Substituting Equation (4.6) for x and Equation (4.8) for y into Equation (4.4), yields

$$l = \frac{L}{\tan\beta} + \tan\alpha(L - DT), \tag{4.9}$$

$$l\tan\beta = L + \tan\alpha\tan\beta(L - DT), \tag{4.10}$$

$$l\tan\beta = L + L\tan\alpha\tan\beta - DT\tan\alpha\tan\beta, \tag{4.11}$$

$$L + L\tan\alpha\tan\beta = l\tan\beta + DT\tan\alpha\tan\beta, \tag{4.12}$$

$$L(1+\tan\alpha\tan\beta)=l\tan\beta+DT\tan\alpha\tan\beta\,, \tag{4.13}$$

$$L=\frac{l\tan\beta+DT\tan\alpha\tan\beta}{1+\tan\alpha\tan\beta}\,. \tag{4.14}$$

With the length from the front wheel to the center point, L, determined, the actual distance from the center point to the vehicle CG, can be calculated. This distance will be defined as R as shown in Figure 4.12. As shown in Figure 4.12, by creating a triangle with the horizontal line from the center point, the line from the center point to the CG, and a vertical line through the CG, the Pythagorean Theorem can be used to determine R.

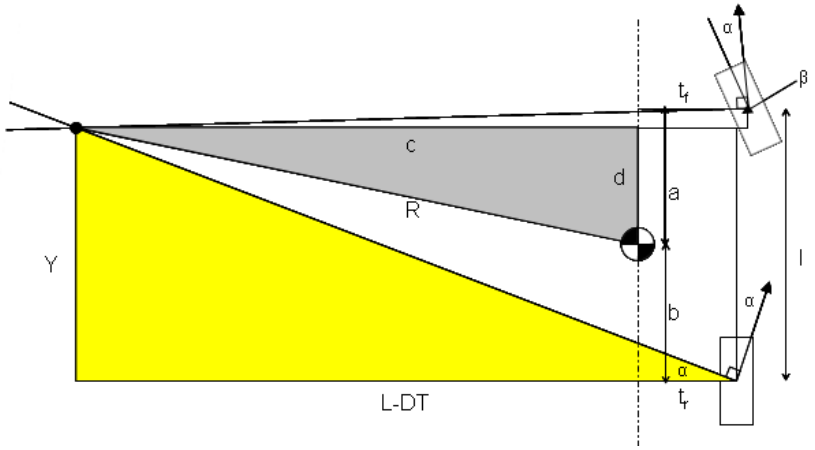

Figure 4.12. Diagram showing the triangles used to calculate the radius of travel, R.

The gray triangle is used to solve for R while the yellow triangle is used to solve for d since it is not known like distance c. Starting with Equation (4.15),

$$R^2=c^2+d^2\,, \tag{4.15}$$

and

$$c=L-t_f\,. \tag{4.16}$$

To find the distance d using the second triangle, the derivation starts with Equation (4.17), where

$$\tan\alpha=\frac{Y}{L-DT}\,, \tag{4.17}$$

$$Y=\tan\alpha(L-DT)\,, \tag{4.18}$$

$$d=Y-b\,, \tag{4.19}$$

$$d = \tan\alpha\left(L - DT\right) - b\,, \tag{4.20}$$

$$R^2 = \left(L - t_f\right)^2 + \left(\tan\alpha\left(L - DT\right)\right)^2\,, \tag{4.21}$$

$$R = \sqrt{\left(L - t_f\right)^2 + \left(\tan\alpha\left(L - DT\right)\right)^2}\,. \tag{4.22}$$

Using Equation (4.22) for *R*, the various steering angles are obtained, and the slip angle created in a specified loading scenario, the corresponding radii of travel versus steer angle can be calculated and used to determine what steering angles are the most common. The tables in Appendix D-2 contain all the calculated radii of travel for the full range of steering angles. The appropriate amount of lateral tie rod movement was applied to the inboard point of the tie rod to simulate the geometry changes due to steering. This movement necessitates a change in the constraints used when compared to the Beam Model. Table 4.17 shows the boundary conditions for the Steered Model.

Table 4.17. Boundary conditions for the Steered Model.

Steered Model Boundary Conditions			
Points	**Translation**	**Rotation**	**Type**
Inboard Suspension (except TR)	Fixed	Free	Geometric BC
Outboard Suspension	Shared with Upright	Free	*Join Connector
TR (inboard)	Fixed X, Z; specified non-zero Y	Free	Geometric BC

4.3.3 Articulate Model across a Range of Steering Angles

The appropriate amount of force rotation to account for the steered angles was put into the FE model by changing the force and moment components applied at the wheel center. The required steer angle was added by adjusting the boundary condition on the inboard end of the tie rod. Appendix D-1 shows the method used to calculate the amount of lateral movement of the inboard tie rod point with steering angle. Tables containing the steering angles and inboard tie rod point value are located in Appendix D-2. This movement represents the steering rack shifting the inboard tie rod points by a certain distance corresponding to the steering wheel input. Each of these adjustments was made in a different job within the Abaqus model and the results of each model were compiled into graphs and tables. Figure 4.13 shows the axial forces within each member for the left hand cornering scenario with expected load transfer. For this scenario, the most significant trend to note is that of member JK in the lower control arm. This member undergoes a large increase of compressive force with increasing steer angle. In fact, at full steering lock at 22°, this member is subjected to a compressive load 51.0% greater than at 0° when accounting for steer angles and is also 34.1% greater than the hand calculations. When comparing the hand calculations to the maximum loads from the steered design load scenarios, a notable difference occurs in the compressive force in the MN member of the upper control arm. This member has an axial load that decreases with increasing steer angle, an advantages trend for designing the member factor of safety. Figure 4.14 highlights member MN in the FE model. One point to note in the trends shown in Figure 4.13 is that the tie rod (PO) does not show a significant change in

loading through the range of steer angle. This is due to the loading in each scenario being equal in magnitude (at 1.4g lateral acceleration at all angles), but rotated in the top view. With this scenario the aligning torque (M_z) remains the same, thus the tie rod only changes loading due to the small angular displacement it undergoes with increasing steer angle.

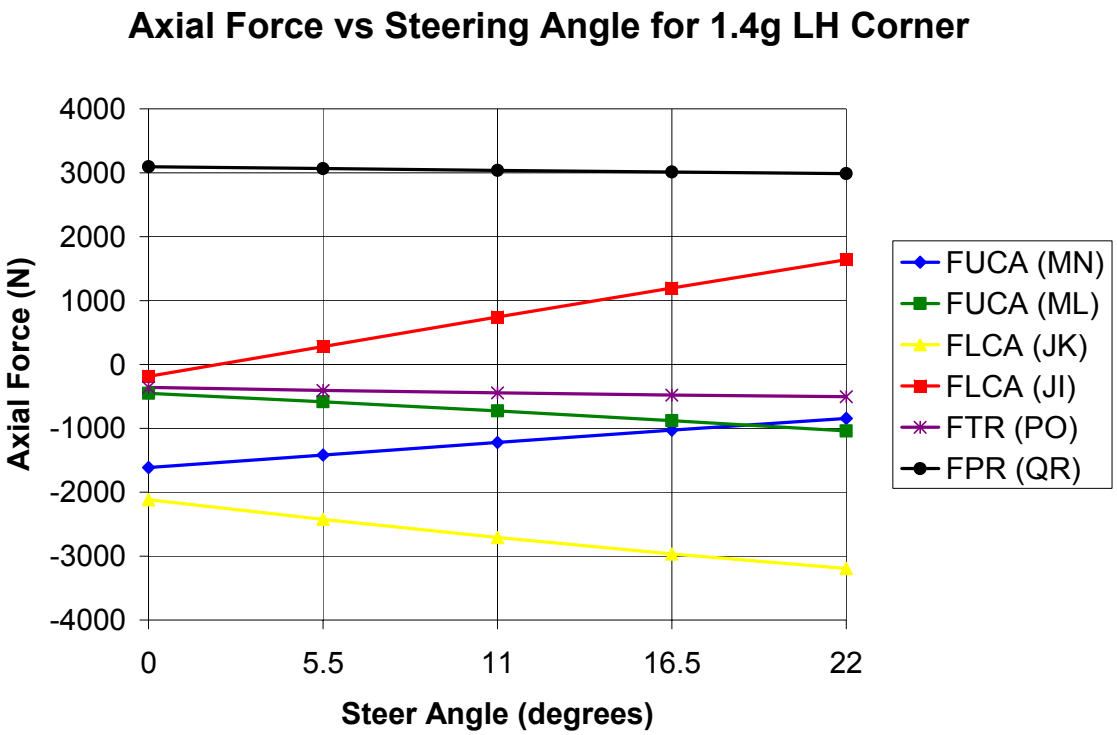

Figure 4.13. Comparison of member axial force with steering angle for left hand cornering with expected load transfer.

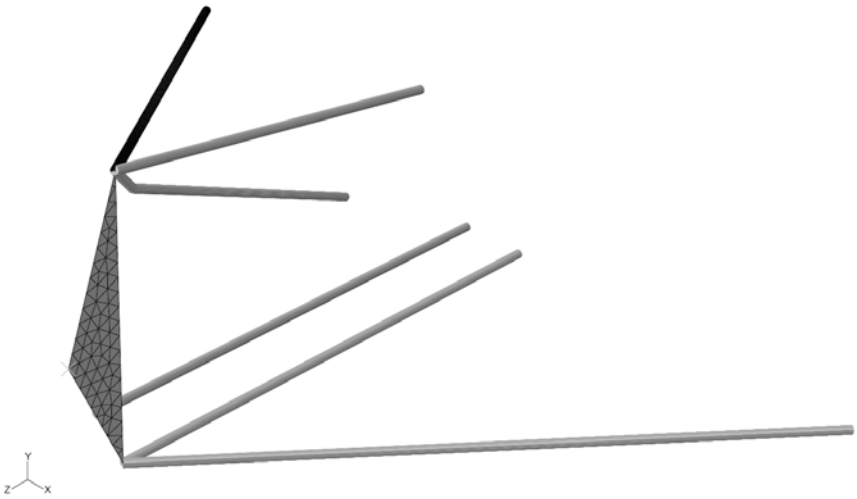

Figure 4.14. Highlighted member MN on FE model.

Table 4.18 compares the hand calculated member loads, the axial member loads from the fixed beam FE model, and the maximum and minimum axial forces from the steered FE model. This table clearly shows the increased member loads that result from steering the suspension under cornering loads. The compressive axial force in all but the pull-rod member (QR) for both pure cornering scenarios is greater in one of the steered cases than it is in the hand calculations. In some members, the increase is small while in others it is a very large increase (ex. member JI in the LCA increases in compressive force by 2194% going from slightly compressive to a high tensile load when compared to the hand calculations in the left-hand corner with expected load transfer scenario). At first glance, it may seem that the Steered Model is not working as this member has never failed in cornering despite the force being this much higher than the hand calculations used to design the part. In this case, member JI is subjected to a tensile load of 5950 N in a non-steered loading scenario and this load becomes the dominant design criteria for the section properties of this member. In Table 4.18, the critical member load in cornering is highlighted in orange. Eleven of the 18 scenarios see the critical load in cornering that occurs in the Steered Model. This reveals how adding steering angle to the FE model results in two thirds of the members needing to be stronger in cornering than determined by the hand calculations. Despite this discovery, almost all members are loaded most heavily in non-steered scenarios, even with the drastic increases in loads due to steering. The most common scenario to create the critical design load is the 5g Bump loading scenario.

Table 4.18. Axial forces in members in steered loading scenarios for each of the model stages with the critical member load in cornering highlighted in orange.

Axial Member Forces (all in N)												
Hand Calcs			**Abaqus - Beam Model**			**Abaqus - Steered Model, Max/Min**						
						Tension			**Compression**			
LH Corner Expected Load Transfer												
FUCA (MN)	-1651.46	N	FUCA (MN)	-1613.25	N	FUCA (MN)	-843.73	N	FUCA (MN)	-1415.15	N	
FUCA (ML)	-482.26	N	FUCA (ML)	-450.14	N	FUCA (ML)	-583.17	N	FUCA (ML)	-1041.06	N	
FLCA (JK)	-2382.05	N	FLCA (JK)	-2115.04	N	FLCA (JK)	-2423.10	N	FLCA (JK)	-3193.47	N	
FLCA (JI)	-78.18	N	FLCA (JI)	-185.14	N	FLCA (JI)	1637.22	N	FLCA (JI)	280.94	N	
FTR (PO)	-335.63	N	FTR (PO)	-360.74	N	FTR (PO)	-406.79	N	FTR (PO)	-504.06	N	
FPR (QR)	3341.76	N	FPR (QR)	3095.80	N	FPR (QR)	3065.26	N	FPR (QR)	2988.24	N	
LH Corner Full Load Transfer												
FUCA (MN)	-1752.76	N	FUCA (MN)	-1712.20	N	FUCA (MN)	-904.67	N	FUCA (MN)	-1504.32	N	
FUCA (ML)	-525.75	N	FUCA (ML)	-491.68	N	FUCA (ML)	-631.27	N	FUCA (ML)	-1111.77	N	
FLCA (JK)	-2514.97	N	FLCA (JK)	-2231.57	N	FLCA (JK)	-2554.85	N	FLCA (JK)	-3363.26	N	
FLCA (JI)	-83.00	N	FLCA (JI)	-196.52	N	FLCA (JI)	1715.84	N	FLCA (JI)	292.58	N	
FTR (PO)	-334.11	N	FTR (PO)	-360.76	N	FTR (PO)	-409.08	N	FTR (PO)	-511.16	N	
FPR (QR)	3546.67	N	FPR (QR)	3285.63	N	FPR (QR)	3253.58	N	FPR (QR)	3172.76	N	
LH Corner and Braking												
FUCA (MN)	-118.79	N	FUCA (MN)	-80.52	N	FUCA (MN)	346.21	N	FUCA (MN)	52.83	N	
FUCA (ML)	-2005.09	N	FUCA (ML)	-1972.70	N	FUCA (ML)	-2166.32	N	FUCA (ML)	-2724.15	N	
FLCA (JK)	-3728.04	N	FLCA (JK)	-3458.95	N	FLCA (JK)	-3381.59	N	FLCA (JK)	-3501.31	N	
FLCA (JI)	3823.03	N	FLCA (JI)	3714.91	N	FLCA (JI)	4793.23	N	FLCA (JI)	4045.27	N	
FTR (PO)	-1291.54	N	FTR (PO)	-1316.82	N	FTR (PO)	-1193.22	N	FTR (PO)	-1297.94	N	
FPR (QR)	3367.78	N	FPR (QR)	3119.86	N	FPR (QR)	3123.41	N	FPR (QR)	3113.74	N	

Inspecting the stresses in each member reveals that three members experience larger maximum stresses when accounting for steering angle. These members are MN, JK, and JI. Member MN from Figure 4.14 has an axial load that decreases with steer angle, however bending moments increase at a fast enough rate to cause the stress to increase with increasing steer angle. Table compares the stresses from the loading scenarios that

involve cornering to those produced by the Steered Model. The largest differences occur in member MN, the rearward UCA, and member JI, the forward LCA.

Table 4.19. Comparison of member stresses in cornering loading scenarios for the non-steered Beam Model and the Steered Model.

Stress (MPa)	Max Proper CS	Max Steered	Percent Increase
FUCA (MN)	115.57	128.79	11.45%
FUCA (ML)	166.65	166.65	0.00%
FLCA (JK)	61.44	62.35	1.47%
FLCA (JI)	114.72	148.02	29.03%
FTR (PO)	39.92	39.92	0.00%
FPR (QR)	87.80	87.80	0.00%

4.3.3.1 The Dubious State of the 5g Bump

At this time, a brief discussion of the 5g-bump scenario seems necessary to cover some of the nuances inherent to the methods used with these contact patch loads. While the prior example of member JI involves a critical member load from the pure braking with full load transfer loading scenario, most critical loads are generated in the 5g-bump scenario. The method used to model this specific scenario has inherent flaws that are likely to result in massively exaggerated member loads. As described earlier, this scenario is modeled (in both the hand calculations and the current FE model) by placing a vertical force at the wheel center equal to five times the load on the wheel at rest. Analyzing this as a static scenario results in an excessive amount of wheel movement which is likely the reason for the exaggerated loads. In reality, this force only exists for a short duration of time corresponding to the time for the wheel to vertically displace to the height of the road disturbance in question. A corresponding road disturbance on a relatively normal track would likely be 6.35-12.7 mm cracks in the pavement caused by wear and weather conditions. This means that the 5g acceleration would only exist for a short amount of time while the suspension traveled vertically. Once the suspension had displaced enough to rise over the disturbance, the force on the tire would reduce to zero or near zero depending on how much the chassis has displaced. For this reason, the 5g-bump scenario would be much more accurately modeled as a dynamic event rather than a quasi-static load case. Dismissing the results of the 5g bump shows an increase of the critical member loads when accounting for steer angle for the scenarios that can be modeled by a static load. Further recommendations on the 5g-bump loading scenario will be discussed in Section 6.3.3. At this time, combined loading scenarios involving cornering or braking while simultaneously undergoing a 5g bump are not calculated. For the same reasons that the 5g bump is not an acceptable method, combined loading involving a bump load will need to be performed dynamically as recommended in Section 6.3.3.

Returning to the discussion of the effect of steer angle on member loads, Table 4.20 compares the critical loads from the hand calculations, both including and excluding the 5g bump scenario, to the maximum loads resulting from steer and slip angles.

Table 4.20. Comparison of the critical loads with hand calculations, exclusion of the 5g bump scenario, and accounting for steer angle and slip angle in the steered loading scenarios.

Critical Member Loads								
Hand Calcs						Steered Model - Critical Loads for Steered Scenarios		
All Loading Scenarios			Excluding 5g Bump					
Tension			**Tension**			**Tension**		
FUCA (MN)	527.82	N	FUCA (MN)	527.82	N	FUCA (MN)	346.21	N
FUCA (ML)	-267.74	N	FUCA (ML)	-267.74	N	FUCA (ML)	-583.17	N
FLCA (JK)	259.12	N	FLCA (JK)	-1574.86	N	FLCA (JK)	-2423.10	N
FLCA (JI)	5949.97	N	FLCA (JI)	5949.97	N	FLCA (JI)	4793.23	N
FTR (PO)	325.61	N	FTR (PO)	178.87	N	FTR (PO)	-406.79	N
FPR (QR)	9477.44	N	FPR (QR)	3761.82	N	FPR (QR)	3253.58	N
Compression			**Compression**			**Compression**		
FUCA (MN)	-4603.40	N	FUCA (MN)	-1752.76	N	FUCA (MN)	-1504.32	N
FUCA (ML)	-4725.68	N	FUCA (ML)	-3732.69	N	FUCA (ML)	-2724.15	N
FLCA (JK)	-4225.45	N	FLCA (JK)	-4225.45	N	FLCA (JK)	-3501.31	N
FLCA (JI)	-140.94	N	FLCA (JI)	-83.00	N	FLCA (JI)	280.94	N
FTR (PO)	-1291.54	N	FTR (PO)	-1291.54	N	FTR (PO)	-1297.94	N
FPR (QR)	1774.25	N	FPR (QR)	1774.25	N	FPR (QR)	2988.24	N

There is only one member in which accounting for steering angle increases the critical load when including all loading scenarios. This case occurs in compression (member PO). Member PO, shown in Figure 4.15, is designed for the compressive load. The increase in member PO is only 0.49% so the factor of safety typically used by the suspension designer easily accounts for this small increase. This appears to make the addition of steering insignificant with respect to the broader vehicle loading, and this trend is continued in with the exclusion of the 5g Bump scenario. However it is important to note that six members have critical loads that decrease with the exclusion of the 5g-bump load scenario. In each of these six cases the critical load becomes much closer to the critical steered load. Note that the increased compressive loads in certain steered positions may increase the compliance of those members, thus increasing the camber compliance of the suspension as a whole. This aspect of the steered models will need to be investigated in future research to determine if the current camber curves are sufficient for the desired camber compliance of the suspension.

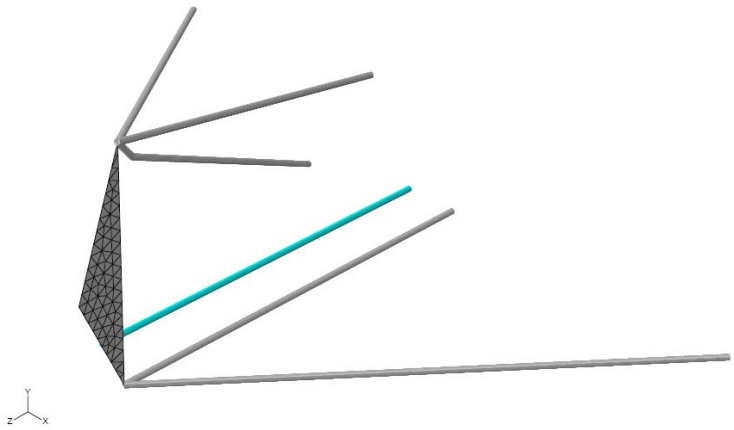

Figure 4.15. Member PO highlighted on the FE model.

Adding steer angles to the FE model greatly increases the capabilities of the Steered Model to supply meaningful member loads for a variety of loading scenarios. While most of the critical design loads in each of the members are not increased due to steering, it is clearly apparent that there is a large effect on the member loads due to steering. The implications of these changing member loads are not limited to the design of the section properties of the suspension members. The varying magnitudes of the loads will affect the design of the uprights and chassis as these components are also designed with the suspension loads determined using the hand calculations. This analysis has also shown that due to the inadequacy of the method used for the 5g-bump scenario, the suspension loads have been exaggerated to a point where there is an inherent factor of safety already applied to the critical member loads before the factor of safety added by the suspension designer. In order to further enhance the capabilities of the FE model, more of the base assumptions need to be investigated; specifically the vertical movement of the suspension to compliment the steering analysis.

4.4 Sprung Model

4.4.1 Explanation of Load Transfer and Installation Ratio

The suspension of a vehicle is designed to move vertically to absorb road irregularities and provide a smoother ride for the occupants. The suspension is also designed to provide predictable and safe handling characteristics. In the context of racing vehicles, a smooth ride is not of great concern, however keeping the tires in contact with the road surface is vital to maximizing the lateral and longitudinal traction capacities of the vehicle. To accomplish this, the suspension uses springs, dampers, and anti-roll bars to control the movement of the sprung (vehicle body) and unsprung (wheels and tires) masses of the vehicle. This requires a certain amount of vertical deflection of the suspension when subjected to road disturbances and load transfer due to driver inputs.

Like the fixed-steering assumption, the hand calculations typically used assume a fixed suspension, no vertical movement. This next stage of the FE model will account for the

vertical movement caused by the forces and loads at the contact patch. There are several goals for this step including (1) an analysis to determine if member loads will change with vertical articulation of the suspension, (2) performing a vertical articulation analysis to determine the amount the wheel and tire will displace under various loading scenarios, and (3) to aid in future analyses of suspension compliance.

First it is important to understand load transfer and its effects on suspension movement. Since the vehicle center of gravity is not at ground level, the vehicle will be subjected to a roll moment under a lateral load. This causes the vehicle to rotate about the roll axis. The amount the vehicle rolls is determined by the springs and anti-roll bars. It is a misconception that the dampers affect the amount the vehicle rolls. Dampers will only have an effect on how quickly the vehicle rolls and how much, if any, oscillation will occur in the rolling of the vehicle body.

With the need for an articulated suspension, there will be vertical movement in all loading scenarios that change the vertical load on the tire from the static load. This increase or decrease in force will cause the tire to move vertically in a corresponding manner to the wheel rate. The wheel rate is the effective spring rate at the wheel. Two versions of calculations have been performed in conjunction with the hand calculations for member loads in an attempt to determine suspension movement in each loading scenario. The first involves using the installation ratio to determine how much the spring must move to count the vertical load on the tire. This method assumes that the motion ratio is constant, which is an idealized version of reality. The second method uses the load in the pull rod to determine how much force there is on the spring, and then determines the amount of spring compression from this information. The pull rod load, as seen earlier, is substantially different in the Steered Model than in the hand calculations. Knowledge of the amount of suspension movement is critical to properly tuning the suspension and specifying the necessary spring and ARB rates.

In most racing vehicles, the suspension is controlled by a spring and damper assembly actuated through a push (or pull) rod and a rocker arm or bellcrank. This design is generally used for packaging and aerodynamic reasons, although it can also be used to create increasing or decreasing wheel rates. The wheel rate is measured in the same units as the spring rate and is equal to the change in vertical force at the wheel per unit of vertical wheel movement. The kinematics of the pull rod linkage can result in a slight non-linearity of the wheel rate. This non-linearity can lead to an unpredictable response of the car to driver inputs. It is desirable to limit this non-linearity and hence, the bellcrank is designed to account for the angle of the pull rod and spring axis and the movement of the suspension. This effect is known as the motion, or installation, ratio and is basically the multiplier by which the spring rate is multiplied to get the wheel rate. Since this value changes with suspension movement, it can sometimes be difficult to account for in the suspension design. Using the FE model to generate a kinematic analysis of the suspension movement will aid the suspension designer and tuner in determining the desired spring rate (and therefore roll rate) and to determine the possibility and extent to which the vehicle may come in contact with the bump stops. Hitting the bump stops exponentially increases the wheel rate at that corner of the car and

has the potential to create snap oversteer or understeer, usually resulting in a loss of control by the driver.

4.4.2 Adjusting Steered Model to Contain Spring/ARB Forces

Up to this point, the suspension assembly in the model has been fixed at the inboard end of the pull rod. This has prevented vertical movement of the suspension in all loading scenarios. The inboard end of the pull rod does have a spherical bearing on the actual car, however this bearing attaches to the bellcrank and not the chassis as currently modeled. The bellcrank is allowed to rotate in one plane parallel to its surface. To represent this in the model, a rigid body in the form of a sheet with four points is created and added to the assembly. Each of the points on this body represents one of the connection points on the bellcrank. The four points are the:

- Bellcrank pivot
- Pull rod attachment
- Spring/Damper attachment
- ARB attachment

Figure 4.16 shows a Unigraphics model of the bellcrank in the top view.

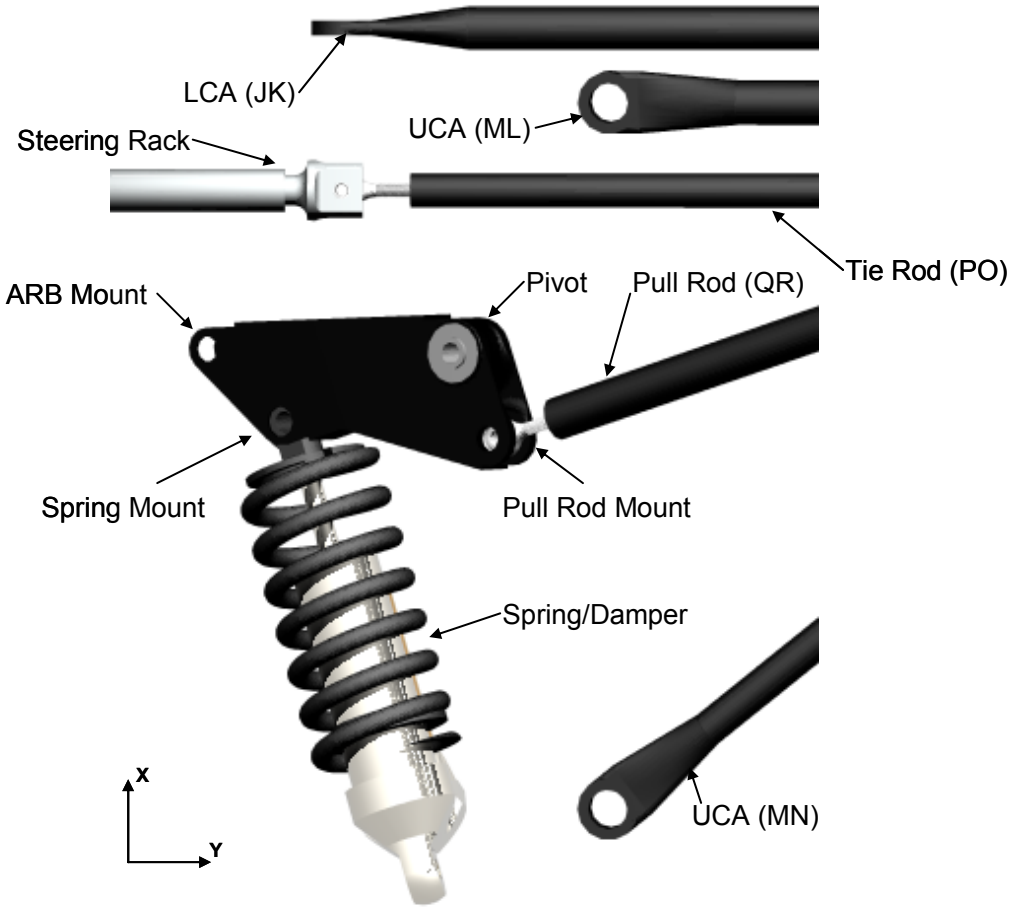

Figure 4.16. CAD model of the bellcrank with labeled connection points.

Each of the three attachment points on the bellcrank is designed to have a spherical bearing on the member that attaches there. In the FE model, this is modeled with a join connector element from the pull rod to the bellcrank. The bellcrank is then fixed in all degrees of freedom at the pivot point with the exception of rotation in the plane of the bellcrank. On the car, this is accomplished through a pair of needle or roller bearings that fix the bellcrank to rotation about the bolt that mounts it to the chassis. Figure 4.17 shows the bellcrank, spring, and ARB as added to the Sprung Model.

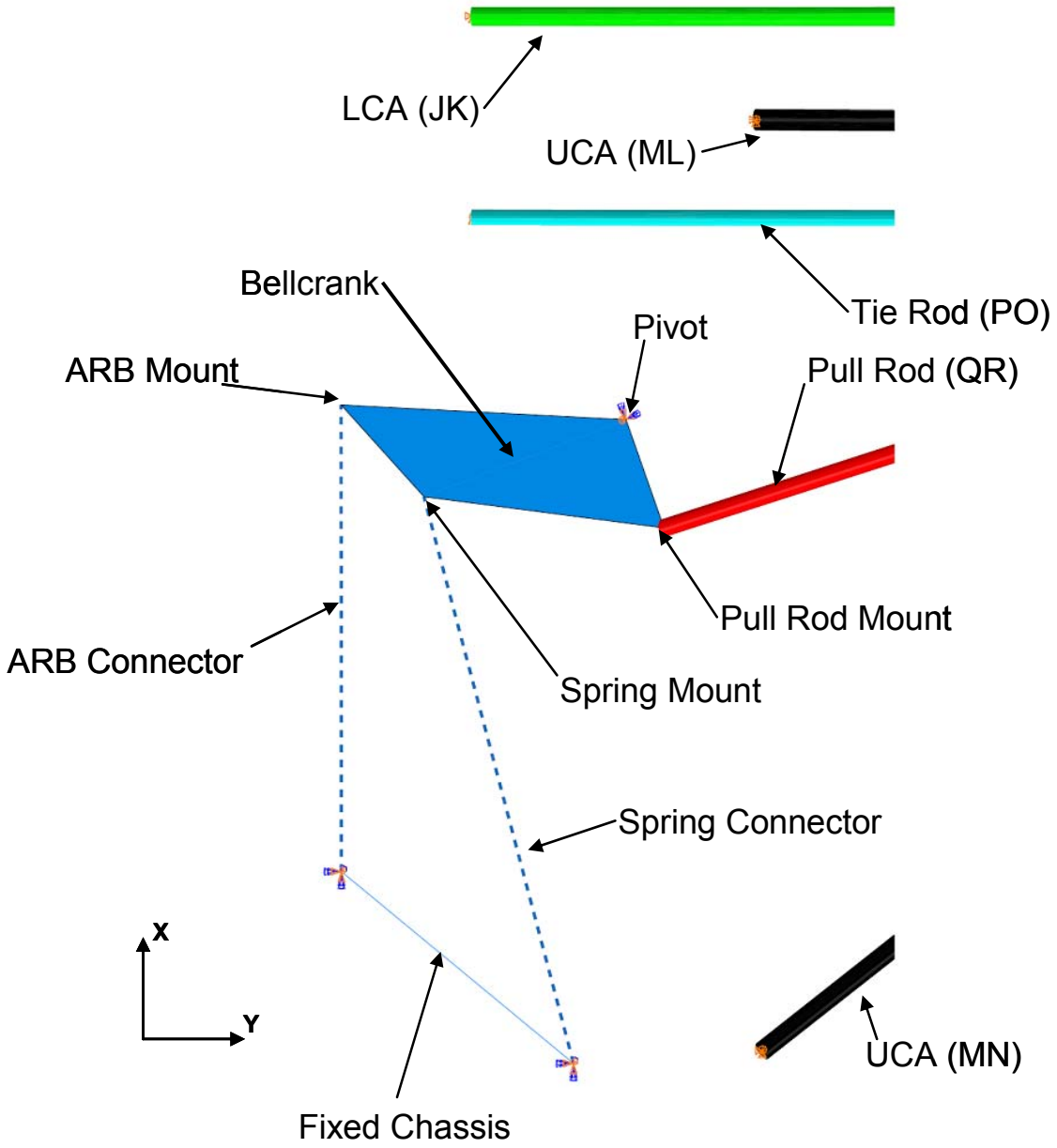

Figure 4.17. Bellcrank, spring, and ARB as added to the vertically articulated model. The spring is the top connector (shown by dashed line), and the ARB is the bottom connector.

Next, a spring and an anti-roll bar must be added. Abaqus has spring elements built into its functionality; however these elements are limited in their capability for user defined behavior. A better option is to use the proper connector elements to simulate the behavior of a spring. An Abaqus *Axial type connector acts along the line connecting two nodes. If created without user defined behavior characteristics, this connector does not have any effect on the model. By defining an elastic coefficient (spring rate) and a reference length, this connector becomes a spring. The reference length defines the free length of the spring where the internal force within the connector is zero. This allows the

connector to account for the preload that exists in the Sprung Model, which is modeled at the ride height position.

Since the ARB is a spring that is only active in roll, it is modeled by an *Axial connector as well, but is only added to the assembly for loading scenarios where a lateral load would cause body roll. Also, the ARB at ride height is not loaded and therefore does not have a reference length. Leaving the reference length blank sets this length equal to the initial distance between the two points. These connectors must be anchored to the corresponding chassis points in order to accurately reflect any changes in orientation compared to the suspension members due to the rotation of the bellcrank. A rigid wire was created that connects the two chassis mounting points of the spring and the ARB. This wire is fixed in translation and rotation to prevent any sort of movement, which represents the significant stiffness of the chassis. The chassis end of the spring and ARB connector elements are attached to the end points of this rigid chassis wire in the same manner as the bellcrank ends, allowing rotation but translating in unison. Since the rigid wire is constrained in all degrees of freedom, the ends of the connectors attached to the rigid wire do not translate but are still allowed to rotate due to the definition of the *Axial type connector. A summary of the boundary conditions for the Sprung Model are shown in Table 4.21.

Table 4.21. Boundary conditions on the Sprung Model.

Sprung Model Boundary Conditions			
Points	**Translation**	**Rotation**	**Type**
Inboard Suspension (except TR and PR)	Fixed	Free	Geometric BC
Outboard Suspension	Shared with Upright	Free	*Join Connector
Bellcrank Pivot	Fixed	Free only in plane	Geometric BC
Fixed Chassis Spring Mount	Fixed	Fixed	Geometric BC
Ride Spring	Fixed (Chassis side)/Shared with Bellcrank	Free	*Axial Connector
ARB	Fixed (Chassis side)/Shared with Bellcrank	Free	*Axial Connector
PR (inboard)	Shared with Bellcrank	Free	*Join Connector
TR (inboard)	Fixed X, Z; specified non-zero Y	Free	Geometric BC

Spring rates for both the ride spring and ARB were supplied by the suspension designer. These rates are likely to change as testing and driver feedback are provided and handling characteristics need to be changed to give the desired vehicle performance. The rates specified to start with are 61.29 N/mm (350 lbs/in) for the ride spring and 9.63 N/mm (55 lbs/in) for the ARB. The free length of the 61.29 N/mm spring as given by the suspension designer is 183.185 mm. Once the Sprung Model is completed, the spring and ARB rates can be adjusted to determine if changes in the rates will adversely affect the vertical movement of the suspension. For example, a slightly lower front spring rate might be needed to improve an understeer problem, but that might cause braking instability. If that occurs, the Sprung Model can be used to determine if the spring is so soft that the suspension is hitting the bump stops under braking, while still displacing the desired amount in roll.

It should be noted that the axial connector elements in Abaqus have the capability of adding a damping coefficient that acts along the same line of action as the spring. This is potentially an area for future research in which a dynamic analysis of suspension loading and movement could be performed. Since a vehicle damper does not exhibit the

characteristics of a constant damping coefficient, one of two things would need to occur to make this analysis valid. One option is to show that the loading scenario results in damper speeds within a linear or close to linear range of the damper curve. The other option is to find a way to model the damping coefficient as a non-constant function of velocity. This type of analysis is beyond the scope of this thesis, but is an area that should be studied further.

4.4.3 Vertical Articulation Analysis

The vertical movement of the suspension allowed the spring and ARB to react to the loads at the contact patch. The most significant result of this analysis is that there is no difference in member loads between the model with vertical articulation and the model with fixed vertical movement. Technically, there is one exception to this, member PO, the tie rod, which increases in magnitude by 0.004 N in the Sprung Model over the Steered Model; however this is not in a critical loading scenario for that member. This change is likely due to rounding within the Abaqus program itself. All other member loads from the sprung model remain identical to the fixed model using beam elements. Table 4.22 compares the maximum loads for all of the different stages of the model development.

Table 4.22. Comparison of maximum member loads for all Abaqus models and hand calculations.

Member Loads - Axial Force																	
Hand Calcs			Truss Model			Beam Model			Designed Member Sections			Vertical Movement		
Tension			Tension			Tension			Tension			Tension		
FUCA (MN)	527.821	N	FUCA (MN)	527.999	N	FUCA (MN)	569.875	N	FUCA (MN)	570.480	N	FUCA (MN)	570.480	N
FUCA (ML)	-267.745	N	FUCA (ML)	-267.693	N	FUCA (ML)	-250.695	N	FUCA (ML)	-250.697	N	FUCA (ML)	-250.697	N
FLCA (JK)	259.124	N	FLCA (JK)	259.208	N	FLCA (JK)	1016.396	N	FLCA (JK)	1016.396	N	FLCA (JK)	1016.396	N
FLCA (JI)	5949.970	N	FLCA (JI)	5949.941	N	FLCA (JI)	5828.549	N	FLCA (JI)	5829.083	N	FLCA (JI)	5829.083	N
FTR (PO)	325.612	N	FTR (PO)	325.537	N	FTR (PO)	254.403	N	FTR (PO)	254.403	N	FTR (PO)	254.403	N
FPR (QR)	9477.440	N	FPR (QR)	9476.536	N	FPR (QR)	8779.588	N	FPR (QR)	8779.588	N	FPR (QR)	8779.588	N
Compression			Compression			Compression			Compression			Compression		
FUCA (MN)	-4603.396	N	FUCA (MN)	-4602.931	N	FUCA (MN)	-4495.284	N	FUCA (MN)	-4494.883	N	FUCA (MN)	-4494.883	N
FUCA (ML)	-4725.675	N	FUCA (ML)	-4725.257	N	FUCA (ML)	-4634.469	N	FUCA (ML)	-4634.469	N	FUCA (ML)	-4634.469	N
FLCA (JK)	-4225.453	N	FLCA (JK)	-4225.415	N	FLCA (JK)	-3924.871	N	FLCA (JK)	-3924.871	N	FLCA (JK)	-3924.871	N
FLCA (JI)	-140.936	N	FLCA (JI)	-140.953	N	FLCA (JI)	-444.261	N	FLCA (JI)	-444.300	N	FLCA (JI)	-444.300	N
FTR (PO)	-1291.536	N	FTR (PO)	-1291.546	N	FTR (PO)	-1316.825	N	FTR (PO)	-1316.825	N	FTR (PO)	-1316.825	N
FPR (QR)	1774.247	N	FPR (QR)	1774.142	N	FPR (QR)	1643.658	N	FPR (QR)	1643.658	N	FPR (QR)	1643.658	N

The second result of the vertical movement analysis is a set of data points representing the vertical displacement of the wheel center and the compression of the spring under the various loading scenarios. This data can be used to determine how much suspension movement is required by the current design and if stiffer or softer springs will allow the suspension to operate in the designed range. Cornering loads are the area of most interest as suspension compression under lateral loading will have a large impact on the handling of the vehicle. In each of the loading scenarios, the component of vertical movement at the wheel center is recorded. The change in distance between the spring mounting points is also recorded as this is the amount that the spring will be compressed under load. These two measurements are shown in Figure 4.18 and Figure 4.19 over a range of steer angles. Table 4.23 shows the total vertical displacement of the wheel center for all loading scenarios as well as the amount of spring and ARB compression.

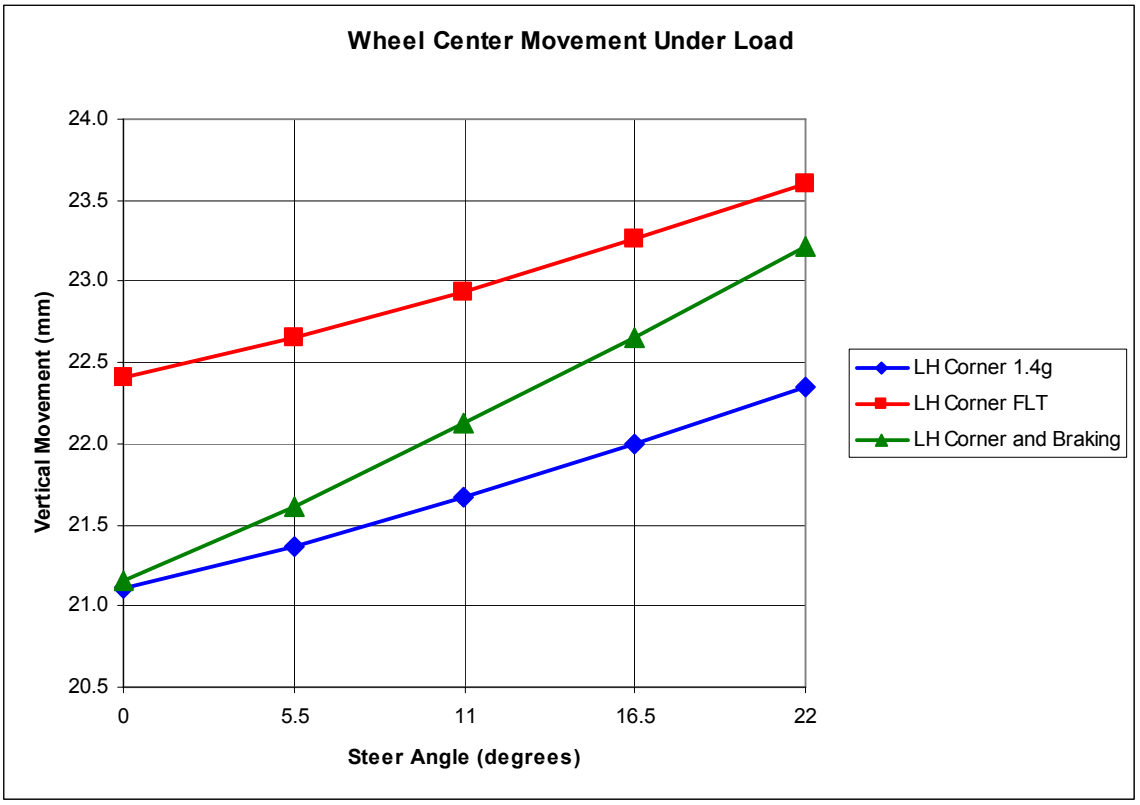

Figure 4.18. Vertical displacement at the wheel center under the steered loading scenarios over the steer angle sweep.

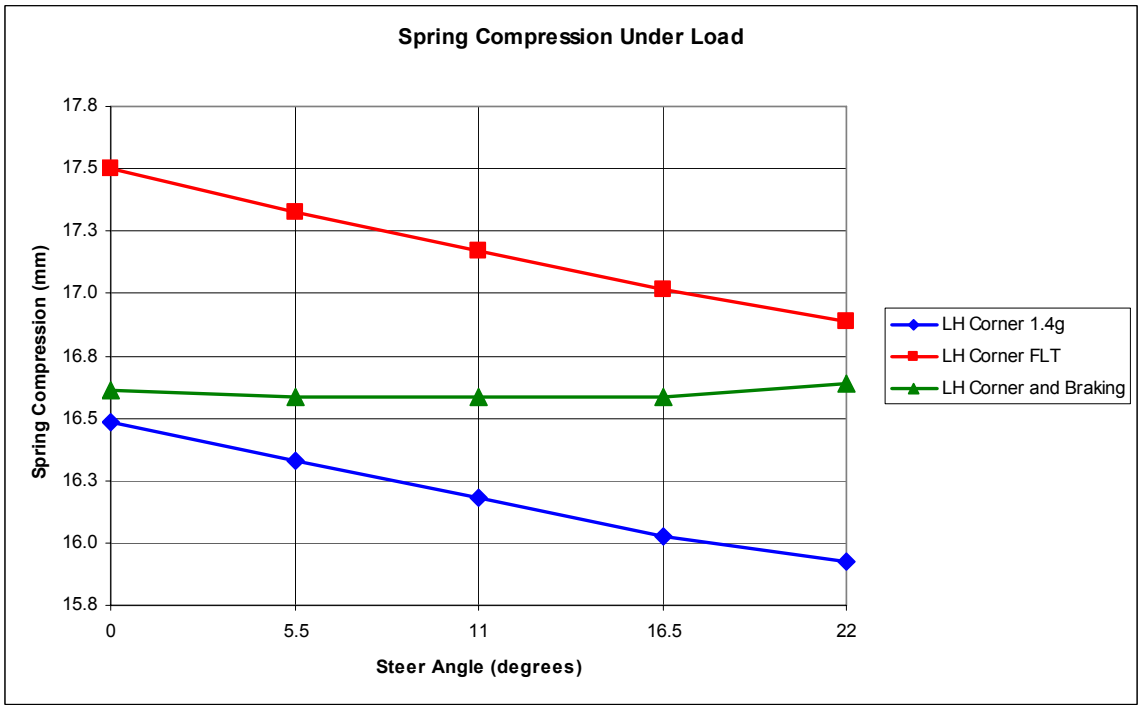

Figure 4.19. Amount of ride spring compression under the steered loading scenarios over the steer angle sweep.

Table 4.23. Vertical articulation results for all loading scenarios.

Articulation Under Load (mm)															
Scenario	**Wheel Center - Purely Vertical**					**Spring - Compression**					**ARB - Movement/Compression**				
Steer Angle (degrees)	**0**	**5.5**	**11**	**16.5**	**22**	**0**	**5.5**	**11**	**16.5**	**22**	**0**	**5.5**	**11**	**16.5**	**22**
LH Corner 1.4g	21.1	21.4	21.7	22.0	22.4	16.5	16.3	16.2	16.0	15.9	22.2	22.0	21.8	21.6	21.4
LH Corner FLT	22.4	22.7	22.9	23.3	23.6	17.5	17.3	17.2	17.0	16.9	23.5	23.3	23.1	22.9	22.7
LH Corner and Braking	21.2	21.6	22.1	22.7	23.2	16.6	16.6	16.6	16.6	16.6	22.4	22.3	22.3	22.3	22.4
5g Bump	60.0					46.8					62.9				
Pure Braking 1.4g	16.5					13.0									
Pure Braking FLT	23.6					18.6									
1.5g Skid	14.2					11.3									

An important trend can be seen in the results of the vertical analysis in the steered loading scenarios. As steer angle increases, the wheel center displaces further vertically. This behavior is due to the offset distance between the wheel center and the kingpin (steering) axis of the suspension. Since the kingpin axis is inclined slightly, the wheel center will rotate about this non-vertical axis, causing it to displace vertically with steering inputs regardless of suspension loading. This effect is shown in Figure 4.20.

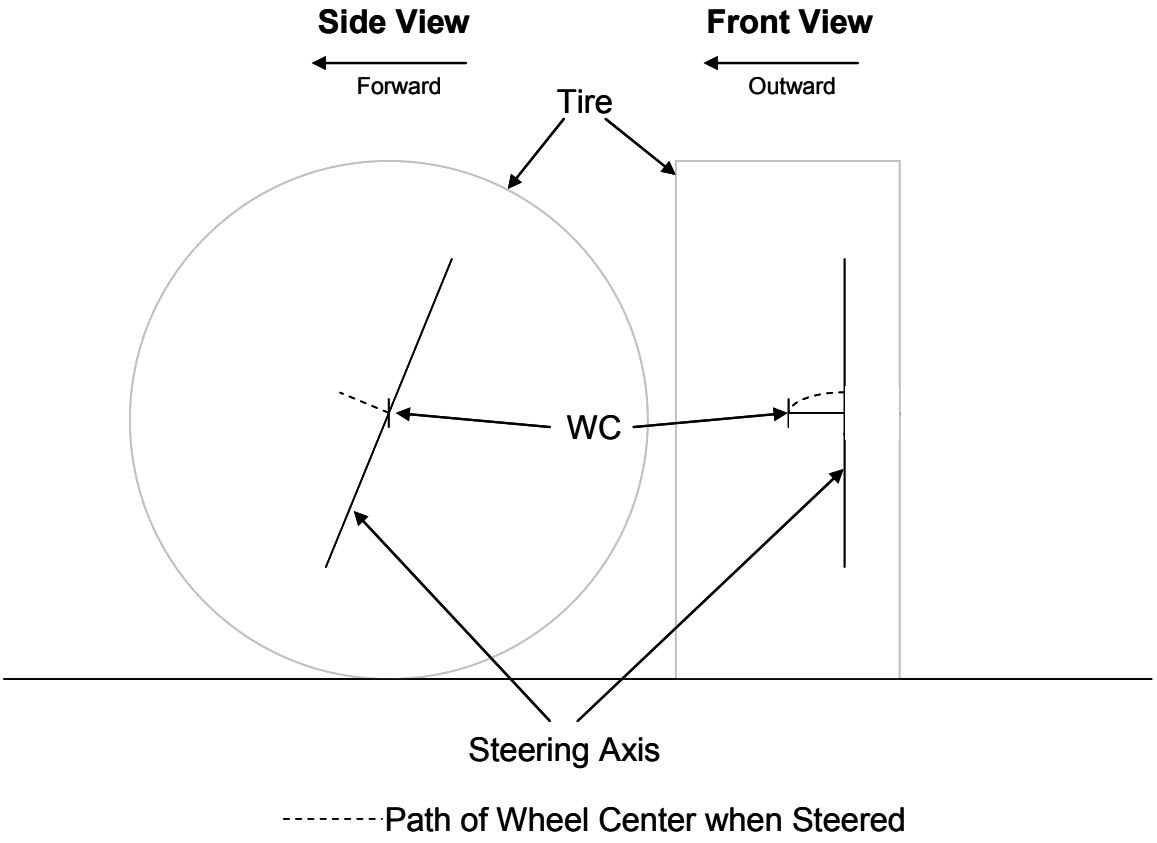

Figure 4.20. Movement of wheel center when steered.

However when comparing this data to the amount of spring compression in each loading scenario over the steer angle sweep, it becomes clear that the kingpin inclination is not the only factor for wheel center displacement. With increasing steer angle, the spring compression actually decreases in the cornering scenarios. A very small amount of

change in the amount of spring compression occurs (0.6 mm over the steer angle sweep for the left hand cornering scenario), which equates to a change in force of 36.61 N. This effect is likely due to the rotation of the overturning moment reducing the component of this moment about the vehicle X-axis. As shown in Figure 2.12 reproduced here as Figure 4.21, the value of M_x as the upright rotates decreases and the value of M_y increases. The moments relative to the upright remain the same as the upright rotates but since M_x and M_y reference the global coordinate system, rotating the upright will cause the value of these moments to change. More of this relatively significant tire load is being taken by the suspension members in a high steer angle case, thus reducing the amount of reactive force provided by the pull rod. This is an interesting trend that may have a very minor effect on the handling of the car, but given the small values of change across the steering angles, this is an effect that is insignificant enough that it can be neglected at this point in time. It may be worth looking into this aspect of the vertical movement in the future, but for now the key effect to be investigated is the vertical movement of the FE model as it pertains to handling characteristics. Further recommendations are made in Section 6.3.2.

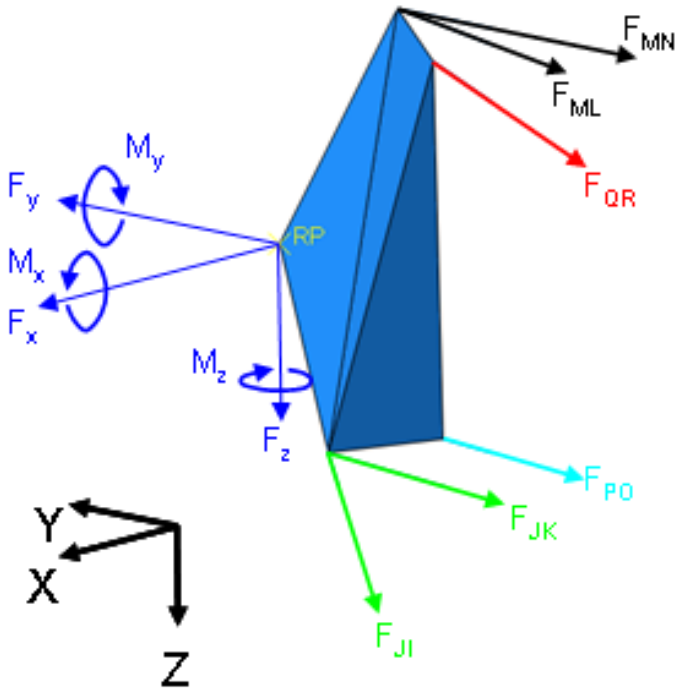

Figure 4.21. FBD of upright showing wheel center forces as they are applied to the upright.

4.5 Validation of FE Model through Vertical Movement Comparison

4.5.1 Concept of Model Validation

The FE model must be validated to measurements taken from the car it is modeling in order to be proven useful. The desired method of performing this task is to install an

array of strain gauges on the suspension members, bring the vehicle to a test facility with a suspension testing rig, such as a 7 post rig, and measure the strains each of the members experience. This is a complex process, normally only performed by high level professional racing teams as it requires a great deal of resources not available to the typical FSAE team. In order to perform some kind of analysis on the vehicle to determine if the FE model is behaving properly a simpler method of model validation has been created.

This FE model will be validated by performing a vertical load analysis. This analysis will involve taking measurement of the vehicle with various loads and determining several data points that consist of the vertical load on the right front tire and the corresponding spring displacement. The vertical load on the tire is measured using the corner scales used for suspension set up. The spring displacement is measured using potentiometers attached to the dampers such that the change in spring compression can be determined. The free length of the spring is used to determine what load is on the spring at a given amount of vertical tire load.

These spring and tire load measurements will be plotted and compared to both the theoretical calculations and the Abaqus model. If the FE model is working properly, the FE model should be very close to the theoretical model, which is calculated from the motion ration as determined by the suspension analysis program OptimumK. There will likely be small discrepancies between the measured values and theoretical values but this is common due to likely manufacturing tolerances and hysteresis in the vehicle suspension system.

4.5.2 Vertical Validation Analysis Data and Discussion

The validation data was collected from the finished 2009 VT-FSAE vehicle after a large amount of suspension tuning had taken place. The result is that the vertical load on the tire is slightly different at ride height than shown in earlier numbers. This is also due to having an actual driver in the vehicle whose weight is slightly different from the estimated amount used in prior calculations. Due to the suspension tuning sessions, the spring rate in the front had been decreased from the 61.29 N/mm used in the FE model and the original design to 35.03 N/mm. In addition to changing the spring rate in the Sprung Model, the reference length of the spring was changed to properly represent the necessary spring preload at ride height. Both of these changes were added to the Sprung Model before performing the validation analysis.

Two measurements were obtained at five data points for this analysis. First, the vertical tire load was recorded. The measurement is the load that is input to the FE model as a vertical load on the tire. The second measurement is the spring length as recorded by the linear potentiometers installed on the vehicle. This measurement is the spring length and is used with the spring rate to determine the force created by the spring. The theoretical spring force is determined by the motion ratio using Equation (4.23) such that

$$F_{TS} = mF_z, \tag{4.23}$$

where F_{TS} is the theoretical spring force, m is the motion ratio of the suspension, and F_z is the vertical load on the tire. The motion ratio of the tire was determined by the suspension designer using a suspension analysis program called OptimumK. Using this program, the motion ratio was determined to be 1.22324. The motion ratio has no units as it corresponds to amount of wheel movement per unit movement at the spring. The results of this data and the few calculations needed are given in Table 4.24. Figure 4.22 shows a plot of the theoretical, measured, and FE model tire loads compared to the force provided by the spring.

Table 4.24. Vertical validation analysis data for the theoretical, measured, and Sprung Model.

Left Front Suspension Measurements for Vertical Validation									
Spring Rate	35.025	N/mm							
Motion Ratio	1.22324	mm/mm							
Tire Load/Input Load	Spring Length - Measured	Spring Force Calculated	Theoretical Spring Force	Theoretical Spring Compression	Abaqus Change in Spring Length	Abaqus Total Spring Compression	Abaqus Spring Force	Percent Difference Abaqus-Theoretical	Percent Difference Abaqus-Measured
kg	mm	N	N	mm	mm	mm	N		
61.23	20.5	717.77	734.57	21.0	7.1	21.0	734.50	-0.00978%	2.33%
64.86	22.5	787.82	778.10	22.2	8.4	22.2	778.02	-0.00976%	-1.24%
69.40	23.5	822.84	832.51	23.8	9.9	23.8	832.43	-0.00966%	1.16%
74.84	25.5	892.89	897.81	25.6	11.8	25.6	897.72	-0.00969%	0.54%
79.38	26.5	927.92	952.22	27.2	13.3	27.2	952.13	-0.00960%	2.61%

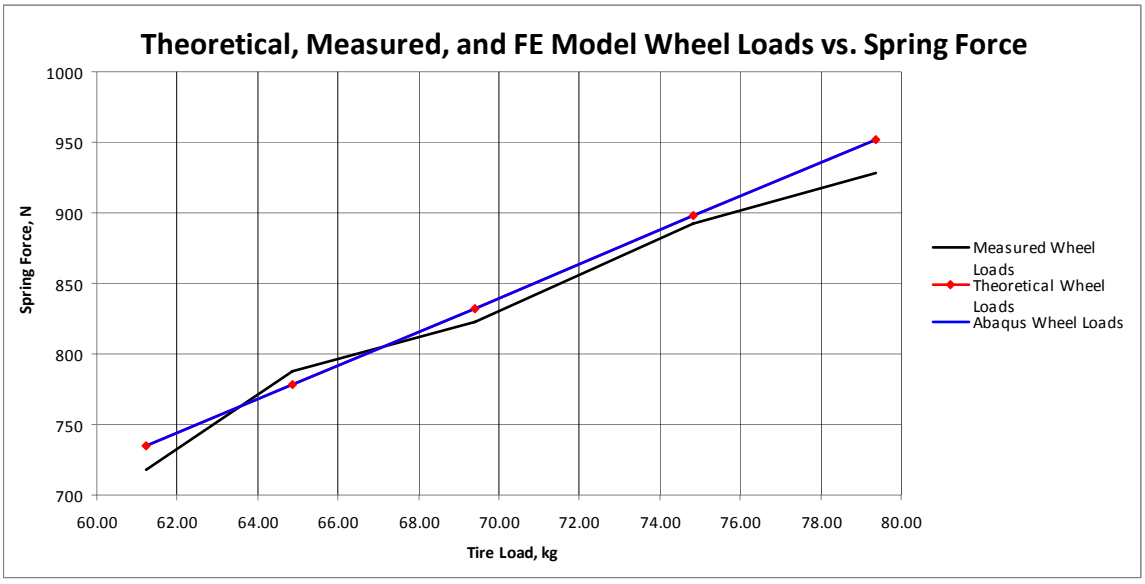

Figure 4.22. Plot of the tire load versus spring force for the theoretical, measured, and Sprung Model.

The data clearly shows that the hypothesis of this analysis holds true. The FE model is virtually identical to the theoretical numbers calculated by the motion ratio. The small difference is most certainly caused by slight differences in how Abaqus and OptimumK process calculations and potentially due to the compliance of the members in the FE model, which is absent in the OptimumK calculations. The measured data shows that there are slight differences between both the FE model and the theoretical numbers. The

trend of the data is also not as smooth as the theoretical and FE model. This behavior could be due to many things including hysteresis in the suspension bearings, hysteresis in the damper, the spring rate of the gas charge in the damper, or the load added to the vehicle while measuring being slightly offset from the CG.

Overall this experiment shows that the FE model is behaving in a very similar manner to the vehicle suspension. Since the FE model is closer to an idealized model then the actual car, it is expected that the nuances of the measured data will not be seen in the FE model. As the FE model is adapted and expanded in the future to include other effects in the suspension, the FE model will likely begin to shows effects similar to the slight discontinuities of the measured data.

Chapter 5
Final FE Model versus Calculations

5.1 Comparison of FE Model Results versus Calculations

5.1.1 Truss Model

The first stage of FE model development was to try and replicate the hand calculations and see if the using equivalent assumptions and conditions resulted in the same member loads in the Truss Model. The end result from both the hand calculations and the Truss Model are nearly identical member loads. Table 5.1 is a reproduction of Table 4.7 and shows the results summarized by the maximum load each member experiences during all of the loading scenarios. Comparing the hand calculations to the Truss Model for each loading scenario resulted in only 0.11% difference. This was seen in a member experiencing less than 133.45 N of axial force and was not a critical case for the member. Overall these results are very promising and prove that the hand calculations are valid under the assumptions used.

Table 5.1. Summary of results comparing the hand calculated member loads to the truss FE model.

Member Loads						Percent Difference
Hand Calcs			Truss Model			
Tension			**Tension**			**Tension**
FUCA (MN)	527.821	N	FUCA (MN)	527.999	N	0.03%
FUCA (ML)	-267.745	N	FUCA (ML)	-267.693	N	-0.02%
FLCA (JK)	259.124	N	FLCA (JK)	259.208	N	0.03%
FLCA (JI)	5949.970	N	FLCA (JI)	5949.941	N	0.00%
FTR (PO)	325.612	N	FTR (PO)	325.537	N	-0.02%
FPR (QR)	9477.440	N	FPR (QR)	9476.536	N	-0.01%
Compression			**Compression**			**Compression**
FUCA (MN)	-4603.396	N	FUCA (MN)	-4602.931	N	-0.01%
FUCA (ML)	-4725.675	N	FUCA (ML)	-4725.257	N	-0.01%
FLCA (JK)	-4225.453	N	FLCA (JK)	-4225.415	N	0.00%
FLCA (JI)	-140.936	N	FLCA (JI)	-140.953	N	0.01%
FTR (PO)	-1291.536	N	FTR (PO)	-1291.546	N	0.00%
FPR (QR)	1774.247	N	FPR (QR)	1774.142	N	-0.01%

The results of the Truss Model show that given the assumptions made for the hand calculations, the methods currently used are valid and produce the proper results. The correlation of these results shows that the methods used to create the Truss Model are valid and accurately portray the assumed condition of the suspension parameters. While the hand calculations produce the proper results for a suspension with six pinned-pinned truss members, this stage does not answer the question of whether the assumptions made lead to representative loads in the suspension members. The results from the Beam Model will determine if the assumptions made are valid for representing the suspension as it exists on the car.

5.1.2 Beam Model

The Beam Model required several changes to convert the suspension members of the Truss Model to beam elements. As a review of these changes, (1) the upright was redesigned to remove the existing pull rod mount, (2) the upper control was redesigned to have the pull rod mount to it via an extra beam member that represents the pull rod mounting bracket, and (3) all of the members where defined with beam elements instead of truss elements. When converting each member to beam elements, there are now additional internal forces and moments that need to be accounted for in the summary of member loads. These include the shear force and the bending moment. The beam elements used are capable of carrying torsion loads; however these loads were sufficiently small in all loading cases and all members such that they are neglected in the analysis. Table 5.2 reproduces Table 4.10 from Section 4.2.2, which summarizes the results of the beam elements including the shear force and bending moment.

Table 5.2. Summary of all internal loads from the beam element FE model.

Member Loads - Axial Force								
Hand Calcs			**Truss Model**			**Beam Model**		
Tension			**Tension**			**Tension**		
FUCA (MN)	527.821	N	FUCA (MN)	527.999	N	FUCA (MN)	569.875	N
FUCA (ML)	-267.745	N	FUCA (ML)	-267.693	N	FUCA (ML)	-250.695	N
FLCA (JK)	259.124	N	FLCA (JK)	259.208	N	FLCA (JK)	1016.396	N
FLCA (JI)	5949.970	N	FLCA (JI)	5949.941	N	FLCA (JI)	5828.549	N
FTR (PO)	325.612	N	FTR (PO)	325.537	N	FTR (PO)	254.403	N
FPR (QR)	9477.440	N	FPR (QR)	9476.536	N	FPR (QR)	8779.588	N
Compression			**Compression**			**Compression**		
FUCA (MN)	-4603.396	N	FUCA (MN)	-4602.931	N	FUCA (MN)	-4495.284	N
FUCA (ML)	-4725.675	N	FUCA (ML)	-4725.257	N	FUCA (ML)	-4634.469	N
FLCA (JK)	-4225.453	N	FLCA (JK)	-4225.415	N	FLCA (JK)	-3924.871	N
FLCA (JI)	-140.936	N	FLCA (JI)	-140.953	N	FLCA (JI)	-444.261	N
FTR (PO)	-1291.536	N	FTR (PO)	-1291.546	N	FTR (PO)	-1316.825	N
FPR (QR)	1774.247	N	FPR (QR)	1774.142	N	FPR (QR)	1643.658	N

It is important to note that the maximum shear and bending moments in each member may or may not occur during the load cases that have the maximum compressive forces in each member. When a large bending moment occurs with the maximum compressive force, a situation is created where each member in question will be more prone to buckling. While the maximum bending moment experienced is relatively small, combining any bending moment with a large compressive load has the potential to either cause the member to buckle or increase the compliance in the member by creating a large amount of deflection from bending. To determine if this amount of bending moment is of significance (and by how much), a comparison between the critical load without a bending moment to the critical load with a bending moment needs to be created.

The method used by VT-FSAE up to this point has been the Euler-Johnson method. In this method, the critical bending load from Equation (2.7) in Section 2.2.2 is used to calculate the maximum compressive load a certain member can carry safely before succumbing to buckling. This load is then compared to the maximum load that can exist

with the calculated bending moment in the member. For this example, member MN in the 5g bump scenario will be analyzed. A common material used to fabricate suspension members is AISI 4130 alloy steel. This material will be used to construct the 2009 VT-FSAE suspension. The current dimensional specification for member MN at the time of writing is 12.7 mm x 0.89 mm round tube. The critical load in this member with pure axial loading is calculated in Equation (5.1) with E = 205 GPa, I = 578.56 mm^4, and l = 461.14 mm giving

$$P_{cr} = \frac{1.2\pi^2 EI}{l^2} = \frac{1.2\pi^2 \left(2.05*10^9\right)\left(578.56\right)}{461.14^2} = 6597.05N\,, \tag{5.1}$$

which results in -6597.05 N since a compressive force is negative in the global coordinate system. To add an existing bending moment to this equation, the maximum stress that the material can withstand needs to be determined. The yield strength, σ_y, of normalized AISI 4130 is 460 MPa [16]. The derivation of the maximum axial force sustainable proceeds with the following series of equations starting with Equation (5.2) showing that the stress at mid-span for the member is equal to the axial stress plus the bending stress,

$$\sigma_y = \frac{P_{axial}}{A} - \frac{Mc}{I}\,, \tag{5.2}$$

where all values are the same as above with M as the bending moment [10]. Note that the bending moment, M, is negative for a positive amount of deflection perpendicular to the centerline of the member [10]. The derivation begins with Equation (5.2) becoming

$$\frac{P_{axial}}{A} = \sigma_y + \frac{Mc}{I}\,, \tag{5.3}$$

$$P_{axial} = \sigma_y A + \frac{McA}{I}\,. \tag{5.4}$$

Continuing the derivation above, the known variables are added for member MN to find that Equation (5.4) yields

$$P_{axial} = \left(460MPa\right)\left(32.97mm^2\right) + \frac{\left(30.35Nm\right)\left(6.35mm\right)\left(32.97mm^2\right)}{\left(578.56mm^4\right)}\,, \tag{5.5}$$

$$P_{axial} = 4180.35N\,. \tag{5.6}$$

The resulting maximum axial force becomes smaller than the critical axial force without an existing bending moment. The change in maximum supportable axial load is a 36.63% decrease from pure axial loading. This is a very significant decrease in the factor of safety of the member in buckling. The compressive load of 4495.28 N seen in this member during a 5g bump implies that this member should buckle under the expected

load. Please note that this scenario is for the 5g bump, which as discussed earlier, is flawed in the way it uses a static analysis for a dynamic event; however this example clearly illustrates the need to account for an existing bending moment in buckling calculations.

This has been the method used by VT-FSAE for many years to determine the buckling resistance of suspension members. The above method does not actually model a buckling failure mode of the suspension members; it simply determined the maximum axial load that can be supported with an existing bending moment before yielding. This is an important distinction. The critical axial load in a true buckling analysis will result in a critical load smaller than the critical load determined by this method. As discussed briefly in Section 2.2.2, the Secant column formula is an acceptable buckling failure calculation. The Secant column formula is shown in Equation (2.12), which is reproduced here as Equation (5.7)

$$P = \frac{S_y A}{1 + \frac{ec}{k^2} \sec\left[\frac{l}{2k}\sqrt{\frac{P}{AE}}\right]}, \tag{5.7}$$

which clearly shows that the critical load, P, cannot be solved for explicitly. To perform this analysis, the Abaqus buckling solver was used to determine the buckling loads of each member using the Secant column method of buckling failure.

The Abaqus buckling analysis was performed by adding a step to the solver which uses linear perturbation to determine buckling. This process returns eigenvalues for the number of modes specified by the user. These eigenvalues represent the multiple that can be applied to the load in a given member to cause failure from buckling. This process is dependent on the number of elements in the mesh. A series of mesh refinements was performed to determine the proper value for each eigenvalue. Table 5.3 shows the factor of safety for buckling in each loading scenario as well as the member in which the first failure occurs. Note that all members had negative eigenvalues for some modes, indicating that a force in the opposite direction to existing conditions would result in buckling in some cases. These values are dismissed as some members, such as the pull rod (QR) cannot experience compression in normal operation. Figure 5.1 shows the most likely buckling scenario in left hand cornering at 11 degrees of steer. This is not the most likely buckling scenario but is one of the more common loading scenarios the vehicle will experience.

Table 5.3. Factor of safety in buckling and critical member for all loading scenarios.

Loading Scenario	FS	Member
1.5g Skid	11.16	JK
5g Bump	3.54	MN
Braking	5.68	JK
Braking_FLT	4.08	JK
LH_Corner_0	7.56	JK
LH_Corner_5.5	6.60	JK
LH_Corner_11	5.91	JK
LH_Corner_16.5	5.39	JK
LH_Corner_22	5.01	JK
LH_Corner_FLT_0	7.17	JK
LH_Corner_FLT_5.5	6.26	JK
LH_Corner_FLT_11	5.61	JK
LH_Corner_FLT_16.5	5.12	JK
LH_Corner_FLT_22	4.76	JK
LH_Corner_Braking_0	4.62	JK
LH_Corner_Braking_5.5	4.57	JK
LH_Corner_Braking_11	4.57	JK
LH_Corner_Braking_16.5	4.62	JK
LH_Corner_Braking_22	4.73	JK

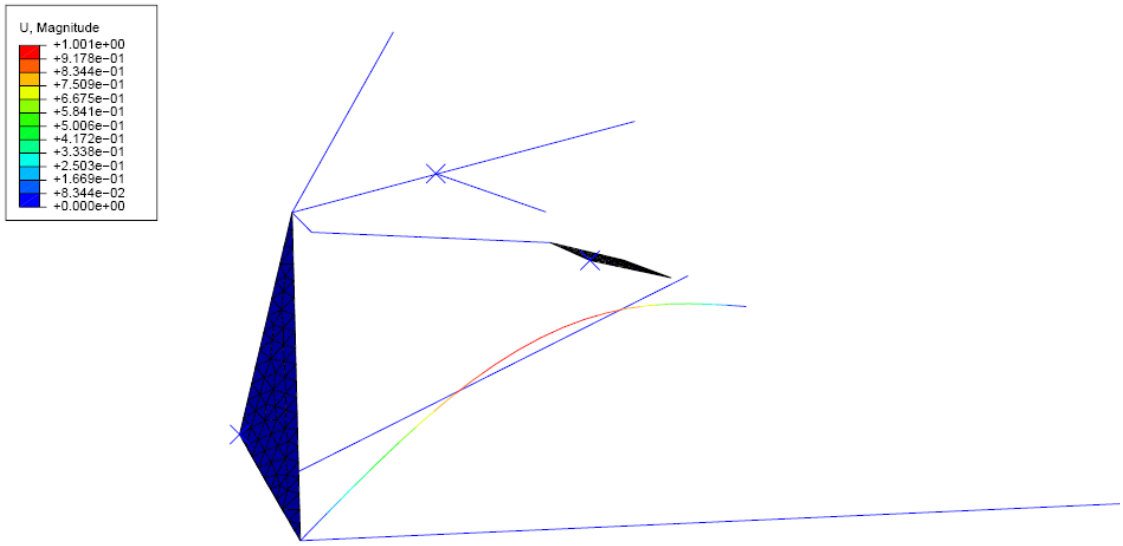

Figure 5.1. Visual representation of buckling failure in member JK in cornering at 11 degrees of steer.

The critical buckling case is in the 5g bump scenario as the Euler-Johnson method predicts. The Secant formula shows that a 5g bump is the loading scenario most likely to cause a member to buckle, however the factor of safety in buckling is 3.54 showing the structure to be relatively safe from a buckling failure. The resistance to buckling that exists in the suspension, as shown when using the Secant formula, is the result of designing suspension members for compliance, rather than strength. Table 5.4 shows a comparison of the factor of safety in buckling as determined by the appropriate hand calculation (Euler or Euler-Johnson) versus the factor of safety in buckling from Abaqus.

Table 5.4. Comparison of factors of safety in buckling between the hand calculations and Abaqus.

Buckling Factors of Safety					
Member	**Max Compressive Load (N)**	**l/k**	**Method**	**FS Hand Calcs**	**FS Abaqus**
FUCA (MN)	4603.3964	60.608	Euler-Johnson	4.72	3.54
FUCA (ML)	4725.6754	99.219	Euler-Johnson	1.71	4.34
FLCA (JK)	4225.4529	85.832	Euler-Johnson	2.65	4.08
FLCA (JI)	140.9364	88.117	Euler-Johnson	105.16	5.72
FTR (PO)	1291.5365	104.762	Euler	5.64	5.10
FPR (QR)	N/A	107.175	Euler	N/A	N/A

$(l/k)_1$	102.700

Despite the fact that the suspension is capable of preventing a buckling failure, the original intent was to design with much larger factors of safety against buckling. This buckling analysis shows that to some extent, designing in a large factor of safety in buckling was necessary; however the estimates appear to be overly conservative. The important information from this analysis is that while buckling is not the prime mode of failure in any of the loading cases, it is more likely to occur in many loading cases than originally designed.

This buckling analysis shows that the presence of a small bending moment greatly increases the chances that the member will fail due to buckling. The analysis also shows how the conservative buckling estimates were necessary to ensure no buckling failures in operation. The proper buckling analysis allows future suspension designers to properly account for buckling as a failure mode and conservative guesses at required buckling factors of safety are no longer necessary.

An important point to note is that while member MN has a 3.54 factor of safety in buckling, it has a 1.49 factor of safety in yielding and a 5.85 factor of safety with the axial force only. This example illustrates the need for a thorough structural analysis performed by a FE model as opposed to simply hand calculations. The presence of a bending moment greatly reduces the factor of safety, but the bending moment does this most significantly in yielding, and not bending.

While yielding is the primary failure mode in the example with member MN above, other members are more likely to buckle than to yield. Member JK is more likely to buckle in every loading scenario as shown in Table 5.5. Figure 5.2 highlights member JK. The worst case scenario for both occurs in the braking with full load transfer scenario where the factor of safety in yielding is 6.56 and the factor of safety in buckling is 4.08.

Table 5.5. Yielding and buckling factors of safety in member JK.

Member JK			
Steer Angle	Loading Scenario	FS, yield	FS, buckle
	1.5g Skid	18.34	11.16
	5g Bump	25.71	11.52
	Braking	9.14	5.68
	Braking FLT	6.56	4.08
0	LH Corner Braking	7.48	4.62
5.5	LH Corner Braking	7.39	4.57
11	LH Corner Braking	7.38	4.57
16.5	LH Corner Braking	7.45	4.62
22	LH Corner Braking	7.62	4.73
0	LH Corner	12.42	7.56
5.5	LH Corner	10.84	6.60
11	LH Corner	9.68	5.91
16.5	LH Corner	8.82	5.39
22	LH Corner	8.17	5.01
0	LH Corner FLT	11.77	7.17
5.5	LH Corner FLT	10.28	6.26
11	LH Corner FLT	9.18	5.61
16.5	LH Corner FLT	8.37	5.12
22	LH Corner FLT	7.76	4.76

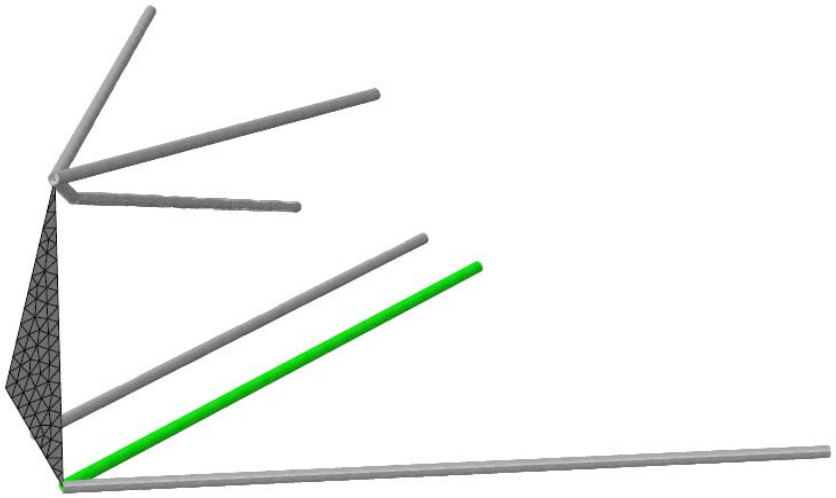

Figure 5.2. Member JK highlighted on the FE model.

The most important information from the buckling analysis in the FE model is shown in Table 5.6 where the minimum factor of safety for each member is shown for each loading scenario. In Table 5.6, the numbers highlighted in yellow represent situations where a member will fail in buckling before yielding. The lowest factor of safety for a given loading scenario is shown in red text. In all tested loading scenarios, the member most likely to fail would fail in a yielding mode, not a buckling mode. In 14 of 19 loading

scenarios, member ML has the lowest factor of safety with member JI having the lowest factor of safety in the other five scenarios.

Table 5.6. Factors of safety for all loading scenarios in each member. Yellow fill denotes failure in buckling. Red text represents the lowest factor of safety of a loading scenario.

Minimum Factors of Safety										
FS		1.5g Skid	5g Bump	Braking	Braking FLT	LH_Corner_Braking				
						0	**5.5**	**11**	**16.5**	**22**
FUCA (MN)		9.76	1.49	4.23	2.96	3.98	3.87	3.77	3.67	3.57
FUCA (ML)		**5.51**	**1.04**	4.30	3.02	**3.59**	**3.62**	3.55	3.50	3.45
FLCA (JK)		11.16	11.52	5.68	4.08	4.62	4.57	4.57	4.62	4.73
FLCA (JI)		12.50	8.44	**3.60**	**2.55**	4.01	3.68	**3.43**	**3.25**	**3.11**
FTR (PO)		91.64	59.63	96.47	57.15	11.52	11.69	11.94	12.27	12.71
FPR (QR)		10.47	1.96	7.06	4.94	5.10	5.17	5.28	5.43	5.51
	LH_Corner					LH_Corner_FLT				
	0	**5.5**	**11**	**16.5**	**22**	**0**	**5.5**	**11**	**16.5**	**22**
FUCA (MN)	5.21	5.12	5.02	4.91	4.80	4.89	4.81	4.72	4.62	4.51
FUCA (ML)	**2.93**	**3.03**	**3.13**	**3.24**	**3.34**	**2.76**	**2.85**	**2.95**	**3.04**	**3.14**
FLCA (JK)	7.56	6.60	5.91	5.39	5.01	7.17	6.26	5.61	5.12	4.76
FLCA (JI)	8.41	7.92	7.35	6.87	6.48	7.97	7.51	6.98	6.52	6.15
FTR (PO)	42.05	37.29	33.99	31.68	30.10	42.05	37.08	33.67	31.30	29.68
FPR (QR)	5.56	5.61	5.67	5.71	5.76	5.24	5.29	5.34	5.38	5.42

Continuing the comparison of the Beam Model with the hand calculations, Table 5.7 compares the axial force results of the Beam Model and the hand calculations with a percent difference calculation. There are two members, member JK in tension and member JI in compression, which see very large increases in the internal axial load when the FE model is modified to use beam elements. These members are shown in Figure 5.3 to reiterate the member labeling notation. While these increases are quite substantial, it is important to note that the critical design load for those members does not occur in those cases. For member JK, the tensile load increases by 292.24% with beam elements, but the load is only 1016.40 N. The maximum compressive load in member JK is -3924.87 N. This compressive load is the condition which the member must be designed to withstand. This load is actually a 7.11% *decrease* in load compared to the hand calculations, but as discussed earlier in this section, any existing bending moment can cause this lower axial force to result in a buckling failure. The same holds true for member JI, which is designed for the tensile case, and not the drastically higher compressive case seen with the beam elements. In terms of pure axial loads on each member, all except one see a decrease in axial load with the Beam Model compared to the hand calculations. The one exception is member PO, the front tie rod, which sees a 1.96% increase in compressive load as the critical design load. This small increase is easily accounted for by the current factors of safety.

Table 5.7. Comparison of hand calculations to the axial force in the beam element FE model with the percent difference of the beam element FE model to the hand calculations.

Member Loads - Axial Force						Percent Difference
Hand Calcs			Beam Model			
Tension			**Tension**			**Tension**
FUCA (MN)	527.821	N	FUCA (MN)	569.875	N	7.97%
FUCA (ML)	-267.745	N	FUCA (ML)	-250.695	N	-6.37%
FLCA (JK)	259.124	N	FLCA (JK)	1016.396	N	292.24%
FLCA (JI)	5949.970	N	FLCA (JI)	5828.549	N	-2.04%
FTR (PO)	325.612	N	FTR (PO)	254.403	N	-21.87%
FPR (QR)	9477.440	N	FPR (QR)	8779.588	N	-7.36%
Compression			**Compression**			**Compression**
FUCA (MN)	-4603.396	N	FUCA (MN)	-4495.284	N	-2.35%
FUCA (ML)	-4725.675	N	FUCA (ML)	-4634.469	N	-1.93%
FLCA (JK)	-4225.453	N	FLCA (JK)	-3924.871	N	-7.11%
FLCA (JI)	-140.936	N	FLCA (JI)	-444.261	N	215.22%
FTR (PO)	-1291.536	N	FTR (PO)	-1316.825	N	1.96%
FPR (QR)	1774.247	N	FPR (QR)	1643.658	N	-7.36%

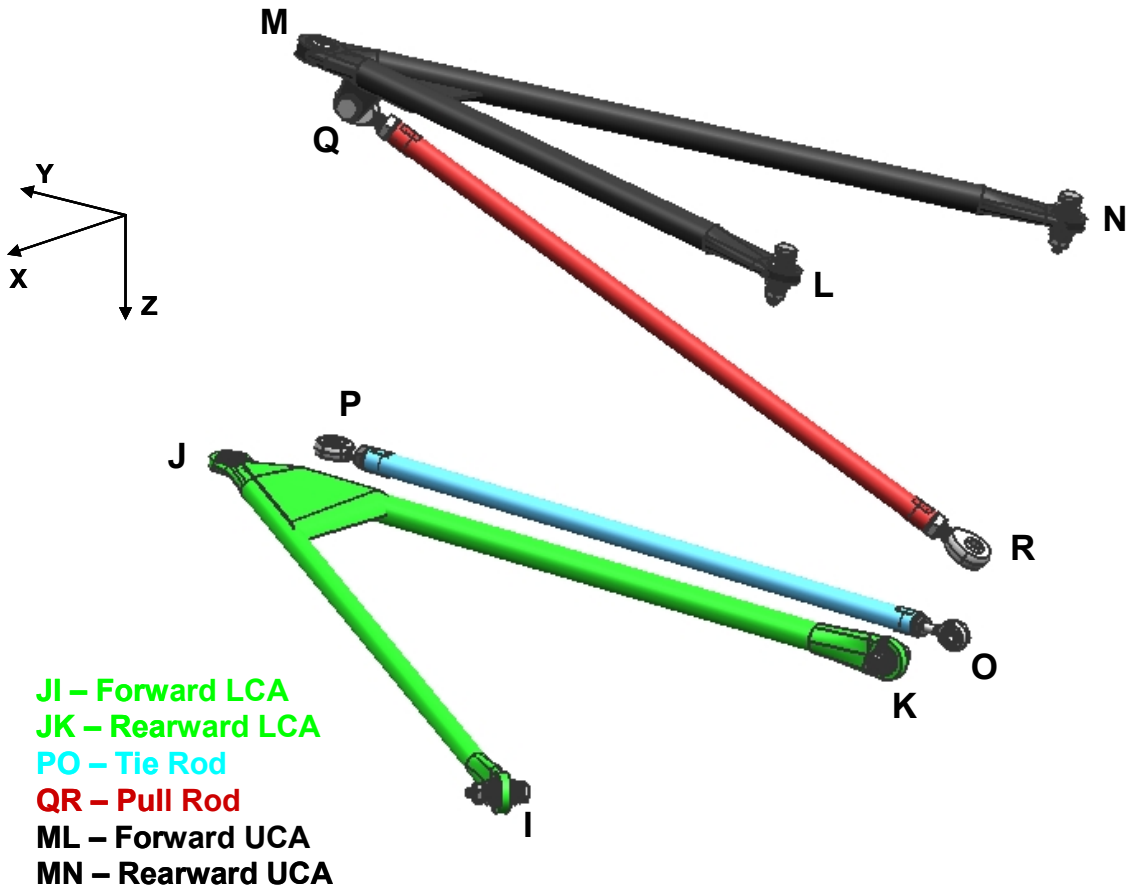

Figure 5.3. Diagram of suspension from the front middle labeling each member.

To summarize the results of the Beam Model compared to the hand calculations, the axial force in the critical design case for each member is either not significantly different or is less than that determined by the hand calculations. The hand calculations seem to be more conservative when looking at the axial force alone, however when accounting for any existing bending moment, several suspension members exhibit dramatically reduced buckling resistance and therefore the critical load for these members is markedly less than the critical load found using the hand calculations.

5.1.3 Steered Model

Starting from the Beam Model, the Steered Model includes the effects of steering angle on the member loads by changing the boundary condition on the inboard tie rod point. Displacing the tie rod end by various distances perpendicular to the chassis represents what happens when the driver turns the steering wheel and forces the steering rack to push the inboard tie rod mounting point laterally with respect to the axis of the vehicle. As mentioned earlier, starting in 2006, the hand calculations were adapted by rotating the forces and moments applied to the wheel center to account for a steering angle. These calculations showed increases in maximum member loads under cornering conditions. The same occurrence happens in the Steered Model when the upright and wheel center forces are rotated to account for steer angle.

The Steered Model not only accounts for the rotated forces, but also includes the changes in suspension geometry due to the articulation that occurs when steering angle is added to the model. This is one feature the hand calculations do not include. Also included in the radius of travel calculations for the Steered Model is the slip angle that each tire must assume in order to generate the lateral forces being applied. The results of this analysis are shown in Table 5.8 which is the same as Table 4.18 in Section 4.3.3.

Table 5.8. Summary of maximum axial forces in the suspension members through a steer angle sweep.

Axial Member Forces (all in N)												
Hand Calcs			**Abaqus - Beam Model**			**Abaqus - Steered Model, Max/Min**						
LH Corner Expected Load Transfer						**Tension**			**Compression**			
FUCA (MN)	-1651.46	N	FUCA (MN)	-1613.25	N	FUCA (MN)	-843.73	N	FUCA (MN)	-1415.15	N	
FUCA (ML)	-482.26	N	FUCA (ML)	-450.14	N	FUCA (ML)	-583.17	N	FUCA (ML)	-1041.06	N	
FLCA (JK)	-2382.05	N	FLCA (JK)	-2115.04	N	FLCA (JK)	-2423.10	N	FLCA (JK)	-3193.47	N	
FLCA (JI)	-78.18	N	FLCA (JI)	-185.14	N	FLCA (JI)	1637.22	N	FLCA (JI)	280.94	N	
FTR (PO)	-335.63	N	FTR (PO)	-360.74	N	FTR (PO)	-406.79	N	FTR (PO)	-504.06	N	
FPR (QR)	3341.76	N	FPR (QR)	3095.80	N	FPR (QR)	3065.26	N	FPR (QR)	2988.24	N	
LH Corner Full Load Transfer												
FUCA (MN)	-1752.76	N	FUCA (MN)	-1712.20	N	FUCA (MN)	-904.67	N	FUCA (MN)	-1504.32	N	
FUCA (ML)	-525.75	N	FUCA (ML)	-491.68	N	FUCA (ML)	-631.27	N	FUCA (ML)	-1111.77	N	
FLCA (JK)	-2514.97	N	FLCA (JK)	-2231.57	N	FLCA (JK)	-2554.85	N	FLCA (JK)	-3363.26	N	
FLCA (JI)	-83.00	N	FLCA (JI)	-196.52	N	FLCA (JI)	1715.84	N	FLCA (JI)	292.58	N	
FTR (PO)	-334.11	N	FTR (PO)	-360.76	N	FTR (PO)	-409.08	N	FTR (PO)	-511.16	N	
FPR (QR)	3546.67	N	FPR (QR)	3285.63	N	FPR (QR)	3253.58	N	FPR (QR)	3172.76	N	
LH Corner and Braking												
FUCA (MN)	-118.79	N	FUCA (MN)	-80.52	N	FUCA (MN)	346.21	N	FUCA (MN)	52.83	N	
FUCA (ML)	-2005.09	N	FUCA (ML)	-1972.70	N	FUCA (ML)	-2166.32	N	FUCA (ML)	-2724.15	N	
FLCA (JK)	-3728.04	N	FLCA (JK)	-3458.95	N	FLCA (JK)	-3381.59	N	FLCA (JK)	-3501.31	N	
FLCA (JI)	3823.03	N	FLCA (JI)	3714.91	N	FLCA (JI)	4793.23	N	FLCA (JI)	4045.27	N	
FTR (PO)	-1291.54	N	FTR (PO)	-1316.82	N	FTR (PO)	-1193.22	N	FTR (PO)	-1297.94	N	
FPR (QR)	3367.78	N	FPR (QR)	3119.86	N	FPR (QR)	3123.41	N	FPR (QR)	3113.74	N	

As Table 5.8 shows, most members experience an axial force increase with increased steering angle. While this may not increase the critical design load in each member, it does reveal that the current method of using hand calculations without accounting for steer and slip angles results is an inadequate representation of the member loads during cornering. In cases where the critical load for member design is not a scenario that involves cornering, the increased member loads during cornering will result in higher compliances in those members. Depending on the desired compliance in each member, this may change the design requirements of some parts. Should the increased member load from steer angle cause a larger compressive load with an internal bending moment, the increased strain in that member may cause the compliance to fall outside of the designed range. This may not result in the failure of the member, but excessive compliance compared to the expected design specification can result in excessive camber gain in the suspension, causing undesirable handling that may be difficult to correct.

Overall it is clear that the steer angle needs to be accounted for in calculating the suspension loads in cornering. Doing so results in significantly different forces from the original hand calculations and the stationary Beam Model, giving the suspension designer a more complete summary of the loads and associated compliances that must be considered in the sizing of the members. This result demonstrates that the current method of calculating member loads through hand calculations results in incomplete information. Future suspension designers should ensure that a sweep of steering angle is performed with appropriate slip angles to determine the true maximum member loads in cornering. In addition to designing for increased factor of safety, the higher loads in certain cornering positions may result in undesirable compliance outside the amount accounted for in the suspension geometry design. A compliance analysis using this new steered load information should be performed to validate that the necessary compliance will exist through the entire operating range of the suspension.

5.1.4 Sprung Model

Adding vertical movement to the FE model to create the Sprung Model allows the appropriate spring and ARB rates to be included in the quasi-static analysis. As discussed in Section 4.4.3, the member loads remained unchanged from the steered model with the addition of vertical movement. While the analysis could end here, the vertical movement of the suspension gives the designer a powerful tool in determining suspension tuning changes and a metric for validating the Sprung Model as a design tool.

By measuring the amount of vertical movement of the suspension, the installation ratio can be tested to see if it falls within the designed parameters. The distance the wheel moves vertically can be checked against the amount of spring compression to determine if there is an unexpected rising or falling wheel rate. The vertical displacement of the suspension can also be used to determine if the vehicle will hit the bump stops in any loading scenarios causing a sudden rise in the wheel rate and giving the vehicle unpredictable handling characteristics.

The vertical movement of the suspension in each of the loading scenarios shows that the magnitude of displacement is inline with the ± 25.4 mm of wheel movement the suspension is designed for. Table 4.23 from Section 4.4.3 is reproduced in Table 5.9 showing the wheel center displacement for each of the loading scenarios as well as through a steer angle sweep.

Table 5.9. Vertical articulation results for all loading scenarios.

Articulation Under Load (mm)															
Scenario	**Wheel Center - Purely Vertical**					**Spring - Compression**					**ARB - Movement/Compression**				
Steer Angle (degrees)	**0**	**5.5**	**11**	**16.5**	**22**	**0**	**5.5**	**11**	**16.5**	**22**	**0**	**5.5**	**11**	**16.5**	**22**
LH Corner 1.4g	21.1	21.4	21.7	22.0	22.4	16.5	16.3	16.2	16.0	15.9	22.2	22.0	21.8	21.6	21.4
LH Corner FLT	22.4	22.7	22.9	23.3	23.6	17.5	17.3	17.2	17.0	16.9	23.5	23.3	23.1	22.9	22.7
LH Corner and Braking	21.2	21.6	22.1	22.7	23.2	16.6	16.6	16.6	16.6	16.6	22.4	22.3	22.3	22.3	22.4
5g Bump	60.0					46.8					62.9				
Pure Braking 1.4g	16.5					13.0									
Pure Braking FLT	23.6					18.6									
1.5g Skid	14.2					11.3									

The displacement of the wheel center shows that all of the loading scenarios are within reasonable values of what is to be expected from the suspension with one exception, the 5g bump. This scenario is inherently dynamics and should not be represented by a constant vertical load on the tire, as it is in the Sprung Model and hand calculations. The full details of why this method of representing a bump scenario is quite vague are located in Section 4.3.3.1.

The vertical displacement of the wheel center shows that with increasing steer angle, the wheel center will displace further vertically. While this behavior is expected because the wheel center does not lie on the king-pin axis, an unexpected behavior occurs with the compression of the spring. The results of the vertical analysis show that the spring will compress less with steering angle for the same loading scenario. This causes a slight decreasing rate with steer angle. While this rate is very slight, a decreasing rate is undesirable as the suspension should increasingly resist body movement from roll as the roll angle increases. This not only keeps the vehicle off of the bump stops but also creates predictable handling for the driver.

The results from the vertical articulation of the Sprung Model show that there are a few behavioral nuances that need to be considered and potentially investigated further. This analysis also reveals that there is no change in member loads with vertical movement which simplifies the analysis of the internal loads in the suspension members. It must be noted that the similarity of member loads between the Steered Model and the Sprung Model is due to the quasi-static nature of the current analysis methods. Should the Sprung Model be modified to model the suspension loading dynamically, it is likely that the member loads will change with the vertical movement provided by the spring. The vertical analysis can now be used to validate the behavior of the FE model compared to the actual car.

5.1.5 Vertical Articulation from the Sprung Model Compared to On-Vehicle Measurements

As discussed in Section 4.5, the Sprung Model can be used with data collected from vehicle set up to determine the validity of the behavior of the FE model. It was shown that the Sprung Model operates in close relation to the idealized behavior of the suspension, which is fairly similar to the measured data of the finished vehicle. The high correlation of these results reveals that the FE model is properly representing the behavior of the suspension, which validates the behavioral characteristics the model has exhibited in the various loading cases.

A validated suspension model allows the team to determine if the contact patch loads are accurate as determined by the FSAE TTC data. Using strain gauges, the member loads can be determined for some of the loading scenarios seen in vehicle operation. Should these measured loads be significantly different than those determined by the FE model, the loading scenarios being used are most likely inaccurate and an investigation needs to be performed to determine the cause of the discrepancy. While the FE model has been validated as a means of representing the suspension characteristics of the vehicle, the stresses and loads in absolute terms have not been validated as the potential for inaccurate tire loads still exists and will need to be addressed in future research.

5.2 Discussion of Significant Effects

5.2.1 Concern between Hand Calculations and FE Model

The member loads found using the FE model, the final version of which is the Sprung Model, are significantly different than the loads determined from the hand calculations. The most prominent difference in loading occurs with the switch from truss to beam elements. The minimum factors of safety for each member in all of the loading scenarios in each stage of FE model development are shown in Table 5.10 to illustrate the differences between the various model stages. While the axial loads generally decrease with this switch, the added bending moments are cause for concern about member failure due to buckling. Once the increased axial forces due to steering angle are accounted for, the complete loading conditions show that the hand calculations are insufficient in determining the design requirements of the suspension members. Appendices B-1, B-2, B-3, B-4, and B-5 contain the full progression of member axial forces from the hand calculations through each individual FE model stages to the final Sprung Model.

Table 5.10. Minimum factors of safety for each member in each stage of FE model development.

	Factor of Safety (all with proper sections)						
	Truss	Beam	Beam PS	Steered	Sprung/Steered		
					Axial Only	Buckling	Yielding
FUCA (MN)	5.72	1.46	1.49	1.49	5.85	3.54	1.49
FUCA (ML)	3.21	0.72	1.04	1.04	3.27	4.34	1.04
FLCA (JK)	4.07	4.18	6.56	6.56	4.38	4.08	6.56
FLCA (JI)	3.94	3.90	2.55	2.55	4.02	5.72	2.55
FTR (PO)	11.75	11.52	11.52	11.69	11.52	5.10	11.69
FPR (QR)	2.78	3.00	1.96	1.96	3.00	N/A	1.96

5.2.2 The Significance of Bending and Factors to Address

Bending moments play a significant roll in the internal member loads of the suspension. The welded connections between each of the control arm members at the outboard points result in the ability to transmit bending forces due to loads that are not directed along the axes of the two control arm members. In the lower control arm, these loads are relatively small, although they are present, while in the upper control arm, these loads are significant. These moments should be included in any buckling analysis in order to determine if the presence of the moment will make the member excessively prone to buckling. The bending moments should also be included in a compliance analysis to determine if the deflection due to bending is high enough to warrant a change in either suspension member dimensions to decrease the compliance or the suspension camber curves to account for the increases compliance caused by the bending.

The bending in the upper control arm is partially due to the switch from truss elements to beam elements, but that is not the primary cause. If the switch from truss to beam elements was the only cause of internal bending moments, the lower control arm would have bending moments of similar magnitude to the upper control arm. The Sprung Model shows that the upper control arm has maximum bending moments an order of magnitude greater than the lower control arm. This large increase in internal bending moment is due to the way in which the pull rod acts on the upper control arm. The pull rod acts at an angle to the upper control arm bracket on which it is mounted. This results in a large bending moment in the pull-rod mount that must react on the upper control arm since the UCA is the only means of connection for the pull rod bracket other than the spherical bearing of the pull rod itself. The bending moment that is transferred to the UCA causes these members (members MN and ML) to be subjected to a large enough moment that failure due to buckling becomes a real concern with the axial loads that are expected in these members. The resulting factors of safety of the current design are 1.04 for yielding and 3.54 for buckling in member MN. In member ML, the safety factors are 1.49 for yielding and 4.34 for buckling.

The design of the upper control arm members should account for the bending moments. The tendency to buckle also needs to be calculated to determine if the large compressive loads seen in these members will fail under the expected loading. Once the members are designed against bending failure, the increased compliance for the bending of the

member should be calculated to determine if the control arm compliance will be large enough to cause the wheel and tire to deflect outside of the desired suspension settings.

It should also be noted that most of the buckling failure calculations show that the critical member is one of the lower control arm components. The factor of safety in most of these cases is relatively high. Ultimately the buckling calculations show that yielding due to the additional bending stresses is a more critical failure mode than true buckling. This fact makes members MN and ML more of a design concern than the lower control arm members given the current member size specifications.

5.2.3 The Effect of Vertical Suspension Movement

Vertical suspension movement does not have an effect on the member loads when loaded using quasi-static analysis techniques. This means that in terms of a structural analysis of the suspension, a vertical sweep of the suspension will not show any different results that at ride height for a static analysis. Dynamic analysis is not covered in this research and it is likely that this type of analysis would result in different internal member loads when the suspension is allowed to displace vertically. Despite this phenomenon, there are other reasons why performing a vertical sweep of suspension movement should be performed. Finding the amount of spring compression versus wheel center displacement can show the suspension designer what kind of wheel rate curves can be expected under a variety of loading scenarios and bellcrank designs. A vertical analysis also reveals how close to the bump stops the suspension will be under the expected loading conditions. This information is useful in determining if the springs are stiff enough to absorb road disturbances while also cornering at high lateral acceleration levels. This data can also be used to determine if the spring rates can be lowered to induce changes in the handling characteristics of the vehicle while avoiding excessive engagement of the bump stops.

Using the amount of wheel center movement, the suspension designer can determine how much vehicle roll to expect under cornering as well as the amount of dive and squat under braking and acceleration respectively. The amount of body roll and/or body pitch (squat and dive) allows the suspension designer to determine the camber angle of the tires with the road surface under the expected maneuvers. This information can be used to determine if the designed suspension points are going to provide proper tire attitude during all maneuvers or if the camber curve or wheel rates will need to be adjusted in order to maintain the optimal tire orientation throughout all dynamic events at competition.

The vertical movement of the suspension as determined from the Sprung Model is in line with the approximate vertical movement expected under the various loading scenarios. The one exception is the 5g-bump scenario in which a very large amount of vertical movement is predicted, an amount beyond the allowed travel of the suspension. This excessive movement is due to the flaws in the method used to simulate a 5g bump as discussed earlier in Section 4.3.3.1. All other loading scenarios shows vertical movement that is well within the range of suspension travel with a slight bit of room to utilize softer springs should the need arise in vehicle tuning.

Chapter 6
Conclusions and Recommendations

6.1 Discussion of Hand Calculation Assumptions

6.1.1 Pin-Pin Truss Members

The assumption that each suspension member can be approximated by a pinned-pinned truss member has been shown to be invalid based on the differences between the Truss Model to the Beam Model. While the Truss Model generated axial loads within 10% of most axial loads produced by the Beam model, the truss structure assumption in the hand calculations does not show the entire range of loads subjected to each suspension member. This truss member assumption makes hand calculations possible in a format that is quick and easy to perform for a variety of suspension designs. The truss representation of the suspension is not ideal, but the truss member assumption can allow the suspension designer to quickly determine if one set of suspension points will provide a large reduction in loading compared to a different set of points. This can be useful in determining if a certain design direction for the suspension geometry will result in smaller loads transmitted to the chassis and thus allow for less weight. If the truss member approach is used, it should be noted that this method is an idealization which should be used for comparison purposes only. This method should not be used for calculating the actual loads that are expected in each member as the differences can be large, especially in cases involving the critical design load.

6.1.2 Analysis Can Ignore Bending and Buckling in Members

The assumption that there is no bending in the suspension members has been shown to be incorrect. While it is not the dominant stress in the suspension members, the bending loads resulting from several of the loading scenarios are high enough to warrant concern in the design of the suspension members. A buckling analysis has always been performed in the past on the suspension members that have large compressive loads. These hand calculations add some resistance to buckling but they do not account for existing bending loads, nor do they perform a proper buckling analysis. In member MN, show in Figure 4.14 and reproduced here as Figure 6.1, the presence of a bending moment reduced the member's resistance to bending failure by over 82%. This kind of reduction in factor of safety against buckling has to be accounted for in the design.

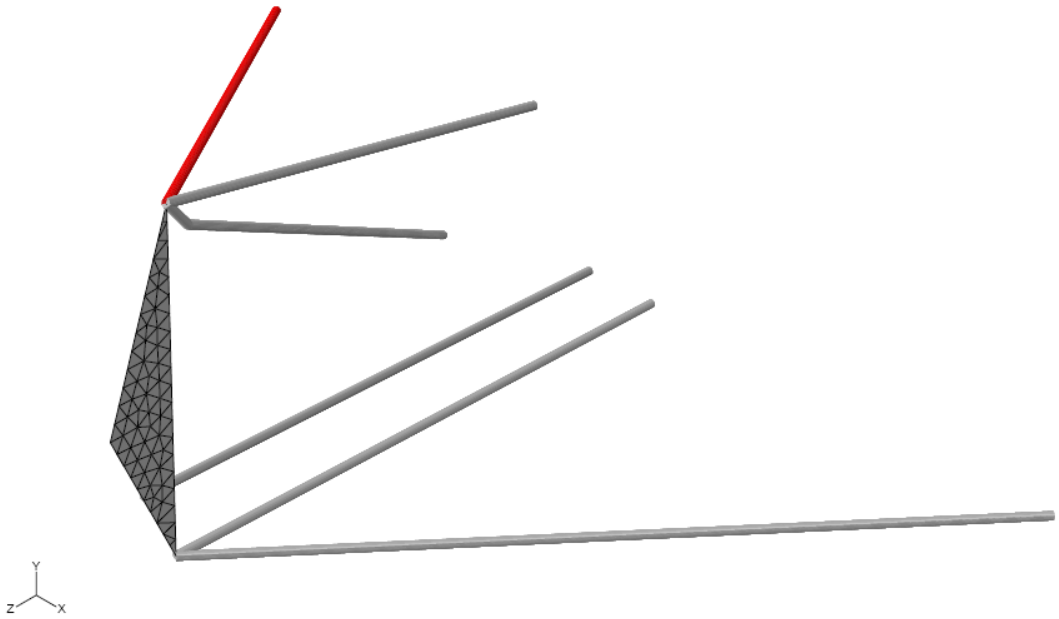

Figure 6.1. Highlighted member MN on FE model.

Factoring the bending moment into the buckling calculation will not only provide the suspension designer with a means of determining an appropriate factor of safety, but it will increase the safety of the driver and engineers who are around the vehicle during testing and vehicle operation. Adding an arbitrary factor of safety to the buckling loads for each member does not show any understanding of the behavior of the suspension and the loading to which it is subjected. A thorough buckling analysis for safety and compliance that factors in an existing bending moment should always be performed when analyzing a suspension.

6.1.3 Analysis Performed without Steer Angle

While the assumption that the suspension can be analyzed without accounting for steering angle has been dismissed in recent years at VT-FSAE, it has persisted as a design assumption for many years prior and should be addressed. Adding steer angle to the analysis of member loads greatly changes the maximum loads each member experiences in loading scenarios that involve cornering. There are several reasons why this is important to the performance of the car, including (1) improving the knowledge presented at the design competition, (2) designing the suspension members, bearings, and joints to withstand the actual loading they will see in cornering, and (3) having the capability to more accurately model the suspension member compliances in cornering.

The design competition judges consider the research that each team performed in determining how well a team has designed their vehicle. Performing a thorough analysis of the member loads under a variety of cornering conditions will aid the team in proving to the judges that the suspension analysis presented is complete in scope and provides as much information as possible for the designers to make the appropriate decisions.

There is a large increase in the member loads during cornering; the suspension parts must be designed to accommodate this. While it is more straightforward to design the body of the member to resist these forces, the joints and connections need to resist these increased loads as well. This topic is not covered in this research but should be investigated by future teams and graduate students. The bearings at each end of the suspension members will need to be capable of withstanding the increased forces in cornering as well as possessing the fatigue resistance that comes with the changing cornering loads.

Lastly, accounting for the changing cornering loads can give the car a performance advantage in the form of reduced compliance in common cornering conditions. The increased member loads which increase with steer angle reveal that the loads are carried in a different ways depending on the amount of steering added. The compliance is directly proportional to the internal loads in the members and this compliance needs to be reduced in cornering to optimize the tire attitude to the road surface. Teams in prior years have used the loads without accounting for steer angle to design against compliance in cornering. This has the potential to result in decreased compliance at small steer angles but increased compliance at higher steer angles. The courses that are used in the FSAE Competition are typically smaller in design and often incorporate tight corners; the vehicle often spends a higher percentage of lap time in smaller corners compared to larger and faster corners and straight-aways. It is also likely that the course will be designed such that some of the larger corners are in locations where the vehicle cannot get to a speed that approaches the limit of its handling. This further emphasizes the importance of maximizing mechanical tire grip in low speed corners. Reducing compliance at all steer angles will improve the mechanical grip of the car by optimizing the orientation of the contact patch to the road surface.

6.1.4 Analysis Performed at Ride Height

The Sprung Model showed no meaningful change in member loads with vertical movement of the suspension. It is important to note here that while the values for vertical displacement do not appear to be at levels that will engage the bump stops; this research does not include the properties of bump stops in any analysis. In negotiating a track, the vehicle is likely to encounter situations of combined loading where the bump stops are likely to be utilized. These situations may result in increased loading of the suspension members as the linkage moves to the extremes of the allowed travel.

It is also possible that dynamic loading of the suspension will vary with vertical wheel travel; in fact, this is extremely likely due to the behavior of the dampers. While this research has been limited to static loading scenarios, there are numerous conditions the vehicle will experience that are better suited to dynamic analysis techniques. In this case, the sprung and unsprung masses of the vehicle will have an effect on the suspension movement as will the characteristics of the damper curve, hysteresis in the member joints, and many other details not investigated in this research.

While the above areas are in need of further investigation, within the scope of this research, vertical movement of the suspension does not have any appreciable effect on suspension member loads for the static load scenarios tested.

6.2 Final Effects on Suspension Loading

6.2.1 Beam Members Change Loads

The use of beam elements in the Beam Model in place of truss elements provides a more accurate and thorough set of results for member loads. By refining the Truss Model into the Beam Model using beam elements, the axial forces as well as the bending moments can be calculated. The understanding of these forces gives the suspension designer a much broader and sturdier foundation from which future design decisions can be made.

The current right-front corner suspension model is a representation of the 2009 VT-FSAE suspension, but it can be adapted to future suspension points fairly easily. This research explained the techniques that can be used to create a model that reflects the behavior of the suspension. These techniques include the representation of spherical bearings by connector elements, the use of a rigid upright, and the utilization of connector elements to represent springs allowing vertical suspension articulation. The member loads developed in these FE models should be shared with all race engineers on a team to allow each part in the suspension to benefit from the improved understanding and representation of the internal loads. The chassis designer can now work with the suspension designer to determine a more accurate set of loading scenarios to apply to the chassis mounts.

The model developed in this research represents a better method of determining the internal member loads of the suspension when compared to the current hand calculations. Including bending moments in a structural analysis of the suspension members reveals how significant an effect these moments can have on the buckling resistance of suspension members. The improvements in determining internal moments made by the development of the Beam Model should be accounted for in all future suspension designs. This FE model and the methods described here can be used by future teams so long as the geometry is updated to reflect any changes to the suspension design that may occur.

Future use of this model and the techniques developed here could easily lead to a whole car model which would include a suspension system at each corner, fully modeled ARBs, and a deformable chassis. Inputs could be added to the wheel centers that simulate road surface irregularities and handling maneuvers to determine if the chassis has sufficient stiffness or if the chassis will have resonance problems under certain conditions. If access to a 7 or 8 post rig becomes an option, the team could even simulate the tests in the full car FE model and determine what the most important test conditions will be to running on the 7 post.

6.2.2 Suspension Steering Changes Loads

With a thorough understanding of the changes that occur with steer angle, it is relatively easy to calculate the suspension compliances at a variety of corner radii. This will ensure that the suspension is performing as desired through an entire range of cornering loads, something that up until now has been unknown. Maximizing the compliance resistance of the suspension members will increase the vehicle performance. Knowledge of the changes in member loads that occur with varying steer angles will improve the suspension design for all future teams.

6.3 Recommendations

6.3.1 Validate Loading with On-Car Testing and/or Test Rig

Measuring the loads in the suspension members through strain gauges is the single biggest improvement to gaining true knowledge of the vehicle suspension loads. While it was not possible to perform this test during the course of this research, the original intent was to design a test rig that would allow known inputs to be applied to the suspension and then member loads to be measured through strain gauges. The value of doing this in the future is not diminished by the research done here. If anything, the development of this FE model increases the need for testing than it has ever been.

Two things need to be accomplished in order to gain meaningful information from this future project. First, known loads need to be applied to the suspension. This can be performed on the car or on a test rig, the key factor is that the applied loads be known and not approximated. With known loads on the suspension, the strain gauges can be used to determine what member loads exist in each member. This information can then be compared to member loads determined by the FE model for the same applied forces. This approach provides the opportunity for validation of the FE model compared to the behavior of the actual suspension. If the correlation between the FE model and experimental data is poor, a process must be put in place to isolate the differences between the model and the data to determine and correct what is causing the discrepancy of the FE model.

The second part of this process is to install strain gauges on the suspension members of the vehicle connected to an appropriate data acquisition device, and measure the strains in the suspension members in a controlled driving environment. Driving on a skid pad at a variety of radii, accelerating and braking at the maximum possible rates, and driving over carefully designed road irregularities will give the representative member loads for a large number of loading scenarios. The important aspect with this project is that while the member loads have been measured, the designers now need to work backward to gain the most useful knowledge from this data. These loads can be compared to what the validated FE model says the member loads should be and the actual contact patch loads can be determined. Having knowledge of what the contact patch loads are is the single most important piece of design information to a racing team. This knowledge can only be acquired with a validated FE model. If the FE model used is not validated, there is no way to know whether the calculated loads at the contact patch are accurate. Currently,

the data provided by the FSAE TTC provides what should be reasonably accurate loads, but the camber angle and vertical load on the tire as measured in vehicle operation are estimated by the team. If incorrect, these estimates have the potential to result in incorrect suspension loading being read from the FSAE TTC data.

Perhaps comparing the contact patch loads to the FSAE TTC data will reveal that the tire is not operating at the ideal conditions. In this case, the suspension designer can change the approach used to specify the suspension points to fully take advantage of the potential grip in the tire. If the tire loads result in lower levels of suspension loads, the team would be able to lighten all of the suspension members. Less unsprung weight creates huge performance advantages by creating less mass that the springs and dampers must control, as well as reducing the mass that the tires must accelerate in all directions.

This research could be divided among two or three graduate students to fully complete the scope of the project. Designing the test rig and validating the FE model would take a large amount of work and there are many things that would need to be carefully measured and controlled in order to obtain meaningful and accurate results. The next stage of research would be measuring the member loads on the vehicle. This will require a good understanding of data acquisition systems and the possible modification of one of these systems to obtain the number of channels needed to record all the required data. Data on the total vehicle accelerations and spring movement would also have to be recorded in order to cross reference this data with the FE model. This section of the research would also require an extremely proficient driver to be able to replicate handling maneuvers as consistently as possible. The last section of this research would involve calculating what the contact patch loads are and why, if at all, they are different from what was expected based on the FSAE TTC data.

6.3.2 Improving the Realism of the Components in the Model (Gussets, Crimped Tubes, etc.)

The scope of this research was limited to a macroscopic beam finite element model of the suspension. Each part was defeatured to represent a simplified configuration, limiting the variables to isolate certain suspension behavior characteristic. Future research into the effects of including appropriate details of the structural design of the suspension members would yield results for local effects such as stress concentrations. Currently, the chassis side suspension members are swaged and bearing cups are welded to the ends into which spherical bearings are pressed. This method of construction reduces some of the stress concentrations seen in earlier designs that did not transition the member bodies to the bearing cups as smoothly. Despite this, each connection point on the suspension members should be analyzed to determine if there are any high levels of stress that could be causing excessive fatigue in the welded sections of the suspension members.

This research also does not include the gussets added to each control arm at the outboard end. The gussets act as a means of reducing the tendency of the members to buckle by created a fixed support at one end of the suspension member. While this was looked at in a simplified manner in the Euler-Johnson buckling analysis by including the fixed-pinned

end-condition constraint, the gussets have the potential to increase the amount of bending moment to which each control arm member is subjected. If one member has a properly oriented bending moment, the gusset will cause the other member in the control arm to bend. If this second member is already carrying a large compressive load, instead of strengthening the structure, this could cause the second member to buckle. This analysis has the potential to reduce the bending on each member and improve the factor of safety of the control arm against buckling.

The recommended way of performing this research is to create realistic control arms in a continuum shell finite element model complete with gussets, swaged tubes, bearing cups, and pull-rod brackets. Using the FE model and the techniques described in this thesis, the realistic suspension would be subjected to the expected loading and the changes in the internal bending moments would be investigated. Similarly, this analysis or any research into the gussets and brackets would lead into the next recommendation on including the dynamic loading of the suspension assembly. The gussets not only change how each of the members are connected to one another, they also add mass to the part that would affect the frequencies at which the part would react.

Improving the realism of the suspension members and other components would allow for a sensitivity study to be performed. VT-FSAE has analyzed the sensitivity of manufacturing tolerances on the performance of the suspension; however these analyses utilize hand calculations to determine the behavior. The FE model could be used in future sensitivity studies in which not only manufacturing tolerances, but also member compliance could be analyzed. A study of how member compliances changes the suspension behavior from a kinematic standpoint would allow the suspension designer to account for the compliance in the kinematic design in a more thorough way than simply increasing the aggressiveness of the camber curve. This information would allow the structural optimization of each component for the loading scenarios of interest to ensure that as few compromised are made in the structural design of the suspension. Characteristics like bump steer, compliance steer, and camber compliance could all be analyzed and accounted for in the structural and kinematic designs, creating a vehicle that exhibits predictable behavior in highly loaded conditions.

6.3.3 Dynamic Loading of Suspension

Dynamic loading of the suspension goes well beyond the inclusion of gussets and brackets in the representation of the suspension components. Dynamic loading of the suspension would allow the designer to see if there are any harmonics that the suspension members are susceptible to during typical handling maneuvers. The resonant frequencies may cause unexpected vibration in the suspension members that cause unpredictable handling or excessive compliances. If a resonance in the suspension causes the suspension to oscillate, the interference in the feedback to the driver through the steering wheel is likely to prevent the driver from properly interpreting what the vehicle is doing. Proper driver feedback is an aspect of suspension design that should always be accounted for whenever designing a vehicle.

As discussed earlier, the 5g-bump loading scenario is inherently a dynamic load case. Representing the 5g-bump loading as a quasi-static loading scenario is not entirely representative. The member forces that result from treating this loading scenario as a quasi-static load result in an excessive amount of movement in the suspension. Modeling this scenario properly would best be accomplished by modifying the FE model to accommodate dynamic loading. This is something that Abaqus is fully capable of handling. The model would require that the boundary conditions at the chassis be revised such that the chassis has a mass associated with it and has the ability to displace vertically. An unsprung mass for the wheel and tire would need to be created and a damper would also need to be added to act along the same line as the ride spring. A step input displacement (or whatever function is determined to most accurately represent a road surface imperfection) would then be applied to the wheel center. In this case, the model would represent the vehicle driving over a bump and the input forces would remain unknown. An analysis would then be performed on the structure to determine the maximum loads seen in each member. Stress waves and their propagation through the suspension members would need to be investigated as would any harmonics resulting from the impact, both in the individual suspension members and in the system as a whole.

An alternate approach to the 5g bump would be to set up the model as described above, but instead of adding a defined movement to the wheel center, the 5g bump force could be added and subsequently removed after a finite amount of wheel travel or a finite amount of time. This scenario would more accurately represent a 5g bump than the static load currently used, given that as the wheel displaces vertically, the force caused by the road would decrease once the wheel and/or chassis had displaced vertically enough to ride over the disturbance.

The dynamic response of the suspension would not be limited to the internal propagation of stress waves within each individual member. The dynamic response should also not be limited to cases where the vehicle drives over a bump. The action of taking a set when entering a corner could be investigated to determine the time it will take for a given spring/damper combination to take a set more quickly and oscillate less on corner entry. The same research could be performed for corner exit to optimize acceleration grip onto a straight. The internal response of each suspension member as well as of the suspension system as a whole would yield a wealth of knowledge to improve vehicle handling.

Lastly, the suspension movement through an entire course could be modeled. This would provide information on the dynamic response of the suspension to the large variety of loading seen in a typical endurance or autocross course and would allow issues with transient handling characteristics to be addressed. Also, this type of modeling would help produce a more accurate determination of the number of cycles each suspension member is subject to during a typical course. Doing so would permit a more exact fatigue analysis to be performed on the suspension, as there is not currently an accurate record of how many cycles the suspension experiences in a competition.

6.3.4 Bearing Hysteresis

The last major recommendation necessary to discuss is the hysteresis that can be present in spherical bearings. In this research the bearing mechanics were neglected and each bearing was assumed to behave in an idealized manner. This was done to limit the scope of the project. Modeling bearing behavior can be a thesis in and of itself. Future graduate students interested in optimizing the performance of the FE model should include bearing hysteresis as a potential area of research. After the 2005 competition, the 2005 VT-FSAE car was tested on the Suspension Parameter Measuring Machine (SPMM) at The Goodyear Tire & Rubber Co. test facility in Akron, Ohio. It was discovered that bearing hysteresis accounted for a large percentage of the total force in the suspension during movement. From the 2006 VT-FSAE car onwards, higher quality spherical bearings meeting aircraft and military specification have been used. Recommendations to the team by alumni and race engineers were performed wherever possible. All of this was done to try and reduce this hysteresis.

Bearing hysteresis force will resist the movement of the suspension members during suspension movement. This resisting force has the potential to cause a bending moment to be generated in the suspension members during articulation. If the suspension moves from ride height to a loaded position and is subjected to high compressive forces, the bending moment caused by hysteresis may add to any existing bending moment to create a situation where a member that was unlikely to buckle has become highly prone to this type of failure. Another point along these lines is that in the pull rod and tie rod, bending was previously prevented by idealized spherical bearings. If hysteresis in the rod ends was high enough, these members would be subjected to bending loads and a member previously not designed to carry a bending moment, may have a failure due to buckling. Smart design decisions can make this negligible, but if these decisions are not properly made or bearing hysteresis is high enough, these bending moments will need to be included in any analysis. Large amount of hysteresis in a vehicle suspension also cause poor handling characteristics that will make driving the vehicle at the limit of the tires difficult.

At this time it is unknown how much hysteresis the current bearings used cause and what the associated bending moment on the suspension members would be. To determine this information, it is necessary to measure the hysteresis in sample bearings and then apply it to the connectors in the FE model to determine the increase in bending moments. If enough information were obtained from the measurements of the bearing characteristics, fully modeled bearings could be added to the suspension and the designers would be able to determine the effects of bearing play, internal friction, and bearing compliance on the overall suspension compliance and loads.

This type of research, combined with the other recommendations above, would generate knowledge of suspension design approaching the level of professional racing teams. With this level of research applied to suspension design, the handling performance of a vehicle can be noticeably improved over current levels.

References

1. SAE International, “Vehicle Dynamics Terminology – SAE J670e”, SAE International, 1976
2. Meriam, J., Kraige, L., *Engineering Mechanics: Statics, Fifth Edition*, John Wiley & Sons, Inc., 2002
3. Gillespie, T., *Fundamentals of Vehicle Dynamics*, Society of Automotive Engineers, Inc., 1992
4. SAE International, “2009 Formula SAE Rules”, SAE International, 2009
5. Smith, C., *Tune to Win*, Aero Publishers, Inc., 1978
6. Milliken, W., Milliken, D., *Race Car Vehicle Dynamics*, Society of Automotive Engineers, Inc., 1995
7. SAE International, “Formula SAE 2008 – Skidpad Event Results”, SAE International, 2008
8. Abaqus 6.8-2 Analysis User’s Manual
9. Calspan Tire Research Facility (TIRF), www.calspan.com/tire.htm
10. Shigley, J., Mischke, C., Budynas, R., *Mechanical Engineering Design, Seventh Edition*, The McGraw-Hill Companies, Inc., 2004
11. Abaqus 6.8-2 Example Problems Manual
12. National Crash Analysis Center (NCAC), www.ncac.gwu.edu
13. Smith, C., *Racing Chassis and Suspension Design*, Society of Automotive Engineers, Inc., 2004
14. Milliken Research Associates, Inc., Formula SAE Tire Test Consortium, www.millikenresearch.com/fsaettc.html
15. Puhn, F., *How to Make Your Car Handle*, The Berkley Publishing Group, 1981
16. MATWEB: Material Property Data, www.matweb.com

Appendix A: Programming Code

A-1 MATLAB m-file to Calculate Member Loads

```
function [Front_Loads,Rear_Loads,F_Geometry_Mat_Front,F_Geometry_Mat_Rear] = ...
      Member_Loads(Front_Points,Rear_Points,Ftire_front,Mtire_front,...
      Ftire_rear,Mtire_rear)

%   Member_Loads     Outputs Suspension Member Loads and Unit Vectors
%
%   [Front_Loads,Rear_Loads,F_Geometry_Mat_Front,F_Geometry_Mat_Rear] = ...
%     Member_Loads(Front_Points,Rear_Points,Ftire_front,Mtire_front,...
%     Ftire_rear,Mtire_rear)
%
%   Outputs suspension member loads and unit vectors from points, force and moment inputs.
%
%   John D. Fratello
%   Last Updated 3/10/08



T_front = [Ftire_front; Mtire_front];
T_rear = [Ftire_rear; Mtire_rear];

%   Right Rear Points
e = Rear_Points(1:3,1);
f = Rear_Points(1:3,2);
d = Rear_Points(1:3,3);
b = Rear_Points(1:3,4);
c = Rear_Points(1:3,5);
a = Rear_Points(1:3,6);
h = Rear_Points(1:3,7);
g = Rear_Points(1:3,8);
s = Rear_Points(1:3,9);
t = Rear_Points(1:3,10);
rear_wc = Rear_Points(1:3,11);

%   Right Front Points
j = Front_Points(1:3,1);
i = Front_Points(1:3,2);
k = Front_Points(1:3,3);
m = Front_Points(1:3,4);
l = Front_Points(1:3,5);
n = Front_Points(1:3,6);
p = Front_Points(1:3,7);
      o= Front_Points(1:3,8);
q = Front_Points(1:3,9);
r = Front_Points(1:3,10);
front_wc = Front_Points(1:3,11);

%Magnitudes
OP = norm(p-o);
ML = norm(m-l);
```

```
MN = norm(m-n);
JI = norm(j-i);
JK = norm(j-k);
QR = norm(q-r);
BC = norm(b-c);
BA = norm(b-a);
EF = norm(e-f);
ED = norm(e-d);
HG = norm(h-g);
ST = norm(s-t);

%r-vectors (from wc to inboard point)
rp = p - front_wc;
rm = m - front_wc;
rq = q - front_wc;
rj = j - front_wc;

rb = b - rear_wc;
re = e - rear_wc;
rh = h - rear_wc;
rs = s - rear_wc;

%Find all the unit vectors (inboard - outboard)/magnitude
n_op = (o - p)./OP;
n_ml = (l - m)./ML;
n_mn = (n - m)./MN;
n_ji = (i - j)./JI;
n_jk = (k - j)./JK;
n_qr = (r - q)./QR;

n_bc = (c - b)./BC;
n_ba = (a - b)./BA;
n_ef = (f - e)./EF;
n_ed = (d - e)./ED;
n_hg = (g - h)./HG;
n_st = (t - s)./ST;

% Unit Moments
M_op = (cross(rp,n_op));
M_ml = (cross(rm,n_ml));
M_mn = (cross(rm,n_mn));
M_ji = (cross(rj,n_ji));
M_jk = (cross(rj,n_jk));
M_qr = (cross(rq,n_qr));

M_bc = (cross(rb,n_bc));
M_ba = (cross(rb,n_ba));
M_ef = (cross(re,n_ef));
M_ed = (cross(re,n_ed));
M_hg = (cross(rh,n_hg));
M_st = (cross(rs,n_st));

% Geometry matrices (unit vectors and unit moments)
F_Geometry_Mat_Front = [n_mn,n_ml,n_jk,n_ji,n_op,n_qr];
F_Geometry_Mat_Rear = [n_bc,n_ba,n_ef,n_ed,n_hg,n_st];
M_Geometry_Mat_Front = [M_mn,M_ml,M_jk,M_ji,M_op,M_qr];
```

```
M_Geometry_Mat_Rear = [M_bc,M_ba,M_ef,M_ed,M_hg,M_st];

Geometry_Mat_Front = [F_Geometry_Mat_Front ;
M_Geometry_Mat_Front];
Geometry_Mat_Rear = [F_Geometry_Mat_Rear ; M_Geometry_Mat_Rear];

% Solve for loads (Just solving a system of 6 equations in matrix form)
Front_Loads = (Geometry_Mat_Front)\(-T_front);
Rear_Loads = (Geometry_Mat_Rear)\(-T_rear);
```

Appendix B: Member Load Data

B-1 Member Load Comparison of Hand Calculations and Truss Model

Table B.1. Axial loads as calculated by the Truss Model compared to the hand calculations with the percent difference for all loading scenarios.

Magnitude of Axial Member Force (N)			
Members	**Hand Calcs**	**Truss Model**	**% Difference**
1.4g Pure Lateral			
Force in member FUCA (MN)	-1651.464	-1651.358	-0.01%
Force in member FUCA (ML)	-482.257	-482.156	-0.02%
Force in member FLCA (JK)	-2382.053	-2382.032	0.00%
Force in member FLCA (JI)	-78.180	-78.181	0.00%
Force in member FTR (OP)	-335.633	-335.661	0.01%
Force in member FPR (QR)	3341.764	3341.562	-0.01%
Pure Lateral FLT	0.000	0.000	
Force in member FUCA (MN)	-1752.755	-1752.644	-0.01%
Force in member FUCA (ML)	-525.755	-525.646	-0.02%
Force in member FLCA (JK)	-2514.968	-2514.936	0.00%
Force in member FLCA (JI)	-83.002	-83.004	0.00%
Force in member FTR (OP)	-334.109	-334.140	0.01%
Force in member FPR (QR)	3546.671	3546.460	-0.01%
Pure Braking FLT	0.000	0.000	
Force in member FUCA (MN)	527.821	527.999	0.03%
Force in member FUCA (ML)	-3732.692	-3732.521	0.00%
Force in member FLCA (JK)	-4225.453	-4225.415	0.00%
Force in member FLCA (JI)	5949.970	5949.941	0.00%
Force in member FTR (OP)	-237.185	-237.213	0.01%
Force in member FPR (QR)	3761.825	3761.474	-0.01%
1.4g Pure Braking	0.000	0.000	
Force in member FUCA (MN)	390.898	391.022	0.03%
Force in member FUCA (ML)	-2628.032	-2627.916	0.00%
Force in member FLCA (JK)	-3027.755	-3027.731	0.00%
Force in member FLCA (JI)	4218.018	4218.017	0.00%
Force in member FTR (OP)	-137.486	-137.507	0.02%
Force in member FPR (QR)	2631.093	2630.852	-0.01%
LH Turn and Braking	0.000	0.000	
Force in member FUCA (MN)	-118.787	-118.654	-0.11%
Force in member FUCA (ML)	-2005.087	-2004.974	-0.01%
Force in member FLCA (JK)	-3728.044	-3728.023	0.00%
Force in member FLCA (JI)	3823.028	3823.015	0.00%
Force in member FTR (OP)	-1291.536	-1291.546	0.00%
Force in member FPR (QR)	3367.775	3367.540	-0.01%
1.5g Full Skid	0.000	0.000	
Force in member FUCA (MN)	-884.121	-884.066	-0.01%
Force in member FUCA (ML)	-267.745	-267.693	-0.02%
Force in member FLCA (JK)	-1574.858	-1574.853	0.00%
Force in member FLCA (JI)	-48.864	-48.865	0.00%
Force in member FTR (OP)	178.872	178.862	-0.01%
Force in member FPR (QR)	1774.247	1774.142	-0.01%
5g Bump	0.000	0.000	
Force in member FUCA (MN)	-4603.396	-4602.931	-0.01%
Force in member FUCA (ML)	-4725.675	-4725.257	-0.01%
Force in member FLCA (JK)	259.124	259.208	0.03%
Force in member FLCA (JI)	-140.936	-140.953	0.01%
Force in member FTR (OP)	325.612	325.537	-0.02%
Force in member FPR (QR)	9477.440	9476.536	-0.01%

B-2 Complete Member Load Comparison of Hand Calculations, Truss Model, and Beam Model

Table B.2. Comparison of the hand calculations, the Truss Model, and the Beam Model with unit sections for all loading scenarios.

Internal Member Loads						
Members	**Region**	**Hand Calcs (N)**	**Truss Model (N)**	**Beam Model, Axial Force (N)**	**% Diff HC-Truss**	**% Diff HC-Beam**
1.4g Pure Lateral						
Force in member FUCA (MN)	2	-1651.464	-1651.358	-1613.379	-0.01%	-2.31%
Force in member FUCA (ML)	3	-482.257	-482.156	-450.138	-0.02%	-6.66%
Force in member FLCA (JK)	2	-2382.053	-2382.032	-2115.036	0.00%	-11.21%
Force in member FLCA (JI)	1	-78.180	-78.181	-185.127	0.00%	136.80%
Force in member FTR (OP)		-335.633	-335.661	-360.745	0.01%	7.48%
Force in member FPR (QR)		3341.765	3341.562	3095.798	-0.01%	-7.36%
Pure Lateral FLT						
Force in member FUCA (MN)	2	-1752.755	-1752.644	-1712.338	-0.01%	-2.31%
Force in member FUCA (ML)	3	-525.755	-525.646	-491.671	-0.02%	-6.48%
Force in member FLCA (JK)	2	-2514.968	-2514.936	-2231.570	0.00%	-11.27%
Force in member FLCA (JI)	1	-83.002	-83.004	-196.507	0.00%	136.75%
Force in member FTR (OP)		-334.109	-334.140	-360.761	0.01%	7.98%
Force in member FPR (QR)		3546.671	3546.460	3285.626	-0.01%	-7.36%
Pure Braking FLT						
Force in member FUCA (MN)	2	527.821	527.999	569.875	0.03%	7.97%
Force in member FUCA (ML)	3	-3732.692	-3732.521	-3696.454	0.00%	-0.97%
Force in member FLCA (JK)	2	-4225.453	-4225.415	-3924.871	0.00%	-7.11%
Force in member FLCA (JI)	1	5949.970	5949.941	5828.549	0.00%	-2.04%
Force in member FTR (OP)		-237.185	-237.213	-265.448	0.01%	11.92%
Force in member FPR (QR)		3761.825	3761.474	3484.821	-0.01%	-7.36%
1.4g Pure Braking						
Force in member FUCA (MN)	2	390.898	391.022	420.302	0.03%	7.52%
Force in member FUCA (ML)	3	-2628.032	-2627.916	-2602.690	0.00%	-0.96%
Force in member FLCA (JK)	2	-3027.755	-3027.731	-2817.526	0.00%	-6.94%
Force in member FLCA (JI)	1	4218.018	4218.017	4133.096	0.00%	-2.01%
Force in member FTR (OP)		-137.486	-137.507	-157.256	0.02%	14.38%
Force in member FPR (QR)		2631.093	2630.852	2437.359	-0.01%	-7.36%
LH Turn and Braking						
Force in member FUCA (MN)	2	-118.787	-118.654	-80.943	-0.11%	-31.86%
Force in member FUCA (ML)	3	-2005.087	-2004.974	-1972.688	-0.01%	-1.62%
Force in member FLCA (JK)	2	-3728.044	-3728.023	-3458.950	0.00%	-7.22%
Force in member FLCA (JI)	1	3823.028	3823.015	3714.581	0.00%	-2.84%
Force in member FTR (OP)		-1291.536	-1291.546	-1316.825	0.00%	1.96%
Force in member FPR (QR)		3367.775	3367.540	3119.863	-0.01%	-7.36%
1.5g Full Skid						
Force in member FUCA (MN)	2	-884.121	-884.066	-863.898	-0.01%	-2.29%
Force in member FUCA (ML)	3	-267.745	-267.693	-250.695	-0.02%	-6.37%
Force in member FLCA (JK)	2	-1574.858	-1574.853	-1433.097	0.00%	-9.00%
Force in member FLCA (JI)	1	-48.864	-48.865	-105.644	0.00%	116.20%
Force in member FTR (OP)		178.872	178.862	165.545	-0.01%	-7.45%
Force in member FPR (QR)		1774.247	1774.142	1643.658	-0.01%	-7.36%
5g Bump						
Force in member FUCA (MN)	2	-4603.396	-4602.931	-4495.284	-0.01%	-2.35%
Force in member FUCA (ML)	3	-4725.675	-4725.257	-4634.469	-0.01%	-1.93%
Force in member FLCA (JK)	2	259.124	259.208	1016.396	0.03%	292.24%
Force in member FLCA (JI)	1	-140.936	-140.953	-444.261	0.01%	215.22%
Force in member FTR (OP)		325.612	325.537	254.403	-0.02%	-21.87%
Force in member FPR (QR)		9477.440	9476.536	8779.588	-0.01%	-7.36%

B-3 Full Data for Beam Models

Table B.3. Complete internal member loads for the Beam Model with unit sections.

Internal Member Loads								
Members	Region	Beam Model, Axial Force (N)	Beam Model - Beams, SF2 (N)	Beam Model - Beams, SF3 (N)	Beam Model, Shear Force Magnitude (N)	Beam Model - Beams, SM1 (Nm)	Beam Model - Beams, SM2 (Nm)	Beam Model, Bending Moment Magnitude (Nm)
1.4g Pure Lateral								
Force in member FUCA (MN)	2	-1613.379	-2.058	52.392	52.433	0.819	20.851	20.867
Force in member FUCA (ML)	3	-450.138	-5.509	-54.876	55.152	-1.690	16.834	16.919
Force in member FLCA (JK)	2	-2115.036	-0.051	0.000	0.051	0.022	0.000	0.022
Force in member FLCA (JI)	1	-185.127	0.040	0.000	0.040	0.022	0.000	0.022
Force in member FTR (OP)		-360.745	0.000	0.000	0.000	0.000	0.000	0.000
Force in member FPR (QR)		3095.798	0.000	0.000	0.000	0.000	0.000	0.000
Pure Lateral FLT								
Force in member FUCA (MN)	2	-1712.338	-2.184	55.605	55.648	0.869	22.130	22.147
Force in member FUCA (ML)	3	-491.671	-5.846	-58.241	58.534	-1.793	17.867	17.956
Force in member FLCA (JK)	2	-2231.570	-0.054	0.000	0.054	0.023	0.000	0.023
Force in member FLCA (JI)	1	-196.507	0.043	0.000	0.043	0.023	0.000	0.023
Force in member FTR (OP)		-360.761	0.000	0.000	0.000	0.000	0.000	0.000
Force in member FPR (QR)		3285.626	0.000	0.000	0.000	0.000	0.000	0.000
Pure Braking FLT								
Force in member FUCA (MN)	2	569.875	-3.374	58.976	59.073	1.343	23.471	23.510
Force in member FUCA (ML)	3	-3696.454	-4.827	-61.772	61.961	-1.481	18.950	19.007
Force in member FLCA (JK)	2	-3924.871	1.601	0.000	1.601	-0.018	0.000	0.018
Force in member FLCA (JI)	1	5828.549	-1.265	0.000	1.265	-0.685	0.000	0.685
Force in member FTR (OP)		-265.448	0.000	0.000	0.000	0.000	0.000	0.000
Force in member FPR (QR)		3484.821	0.000	0.000	0.000	0.000	0.000	0.000
1.4g Pure Braking								
Force in member FUCA (MN)	2	420.302	-236.948	41.249	240.512	0.943	16.416	16.443
Force in member FUCA (ML)	3	-2602.690	-3.364	-43.205	43.336	-1.032	13.254	13.294
Force in member FLCA (JK)	2	-2817.526	1.136	0.000	1.136	-0.486	0.000	0.486
Force in member FLCA (JI)	1	4133.096	-0.897	0.000	0.897	-0.486	0.000	0.486
Force in member FTR (OP)		-157.256	0.000	0.000	0.000	0.000	0.000	0.000
Force in member FPR (QR)		2437.359	0.000	0.000	0.000	0.000	0.000	0.000
LH Turn and Braking								
Force in member FUCA (MN)	2	-80.943	-2.753	52.800	52.871	1.096	21.013	21.042
Force in member FUCA (ML)	3	-1972.688	-4.669	-55.303	55.500	-1.432	16.965	17.025
Force in member FLCA (JK)	2	-3458.950	1.021	0.000	1.021	-0.437	0.000	0.437
Force in member FLCA (JI)	1	3714.581	-0.806	0.000	0.806	-0.437	0.000	0.437
Force in member FTR (OP)		-1316.825	0.000	0.000	0.000	0.000	0.000	0.000
Force in member FPR (QR)		3119.863	0.000	0.000	0.000	0.000	0.000	0.000
1.5g Full Skid								
Force in member FUCA (MN)	2	-863.898	-1.090	27.817	27.838	0.433	11.071	11.079
Force in member FUCA (ML)	3	-250.695	-2.929	-29.136	29.282	8.938	0.000	8.938
Force in member FLCA (JK)	2	-1433.097	-0.029	0.000	0.029	0.012	0.000	0.012
Force in member FLCA (JI)	1	-105.644	0.023	0.000	0.023	0.012	0.000	0.012
Force in member FTR (OP)		165.545	0.000	0.000	0.000	0.000	0.000	0.000
Force in member FPR (QR)		1643.658	0.000	0.000	0.000	0.000	0.000	0.000
5g Bump								
Force in member FUCA (MN)	2	-4495.284	-5.904	148.583	148.700	2.349	59.133	59.180
Force in member FUCA (ML)	3	-4634.469	-15.533	-155.628	156.401	-4.765	47.741	47.979
Force in member FLCA (JK)	2	1016.396	-0.122	0.000	0.122	0.052	0.000	0.052
Force in member FLCA (JI)	1	-444.261	0.096	0.000	0.096	0.052	0.000	0.052
Force in member FTR (OP)		254.403	0.000	0.000	0.000	0.000	0.000	0.000
Force in member FPR (QR)		8779.588	0.000	0.000	0.000	0.000	0.000	0.000

Table B.4. Complete member loads for the Beam Model with proper designed cross-sections.

Internal Member Loads								
Members	**Region**	**Beam Model - Proper Sections, Axial Force (N)**	**Beam Model - Proper Sections, SF2 (N)**	**Beam Model - Proper Sections, SF3 (N)**	**Beam Model - Proper Sections, Shear Force Magnitude (N)**	**Beam Model - Proper Sections, SM1 (Nm)**	**Beam Model - Proper Sections, SM2 (Nm)**	**Proper Sections, Bending Moment Magnitude (Nm)**
1.4g Pure Lateral								
Force in member FUCA (MN)	2	-1613.250	-1.903	52.392	52.427	0.757	20.851	20.865
Force in member FUCA (ML)	3	-450.142	-5.710	-54.876	55.173	-1.752	16.834	16.925
Force in member FLCA (JK)	2	-2115.036	-0.024	0.000	0.024	0.010	0.000	0.010
Force in member FLCA (JI)	1	-185.143	0.019	0.000	0.019	0.010	0.000	0.010
Force in member FTR (OP)		-360.745	0.000	0.000	0.000	0.000	0.000	0.000
Force in member FPR (QR)		3095.798	0.000	0.000	0.000	0.000	0.000	0.000
Pure Lateral FLT								
Force in member FUCA (MN)	2	-1712.201	-2.020	55.605	55.642	0.803	22.130	22.144
Force in member FUCA (ML)	3	-491.675	-6.060	-58.241	58.556	-1.859	17.867	17.963
Force in member FLCA (JK)	2	-2231.570	-0.025	0.000	0.025	0.011	0.000	0.011
Force in member FLCA (JI)	1	-196.525	0.020	0.000	0.020	0.011	0.000	0.011
Force in member FTR (OP)		-360.761	0.000	0.000	0.000	0.000	0.000	0.000
Force in member FPR (QR)		3285.626	0.000	0.000	0.000	0.000	0.000	0.000
Pure Braking FLT								
Force in member FUCA (MN)	2	570.480	-2.642	58.976	59.035	1.051	23.471	23.495
Force in member FUCA (ML)	3	-3696.472	-5.777	-61.772	62.042	-1.772	18.950	19.032
Force in member FLCA (JK)	2	-3924.871	0.751	0.000	0.751	-0.321	0.000	0.321
Force in member FLCA (JI)	1	5829.083	-0.594	0.000	0.594	-0.321	0.000	0.321
Force in member FTR (OP)		-265.448	0.000	0.000	0.000	0.000	0.000	0.000
Force in member FPR (QR)		3484.821	0.000	0.000	0.000	0.000	0.000	0.000
1.4g Pure Braking								
Force in member FUCA (MN)	2	420.730	-1.852	41.249	41.291	0.737	16.416	16.433
Force in member FUCA (ML)	3	-2602.703	-4.035	-43.205	43.393	-1.238	13.254	13.311
Force in member FLCA (JK)	2	-2817.526	0.532	0.000	0.532	-0.228	0.000	0.228
Force in member FLCA (JI)	1	4133.465	-0.421	0.000	0.421	-0.228	0.000	0.228
Force in member FTR (OP)		-157.256	0.000	0.000	0.000	0.000	0.000	0.000
Force in member FPR (QR)		2437.359	0.000	0.000	0.000	0.000	0.000	0.000
LH Turn and Braking								
Force in member FUCA (MN)	2	-80.518	-2.239	52.800	52.847	0.891	21.013	21.032
Force in member FUCA (ML)	3	-1972.702	-5.336	-55.303	55.560	-1.637	16.965	17.044
Force in member FLCA (JK)	2	-3458.950	0.478	0.000	0.478	-0.205	0.000	0.205
Force in member FLCA (JI)	1	3714.914	-0.379	0.000	0.379	-0.205	0.000	0.205
Force in member FTR (OP)		-1316.825	0.000	0.000	0.000	0.000	0.000	0.000
Force in member FPR (QR)		3119.863	0.000	0.000	0.000	0.000	0.000	0.000
1.5g Full Skid								
Force in member FUCA (MN)	2	-863.831	-1.008	27.817	27.835	0.401	11.071	11.078
Force in member FUCA (ML)	3	-250.697	-3.033	-29.136	29.293	-0.931	8.938	8.986
Force in member FLCA (JK)	2	-1433.097	-0.014	0.000	0.014	0.006	0.000	0.006
Force in member FLCA (JI)	1	-105.654	0.011	0.000	0.011	0.006	0.000	0.006
Force in member FTR (OP)		165.545	0.000	0.000	0.000	0.000	0.000	0.000
Force in member FPR (QR)		1643.658	0.000	0.000	0.000	0.000	0.000	0.000
5g Bump								
Force in member FUCA (MN)	2	-4494.883	-5.427	148.583	148.682	2.159	59.133	59.172
Force in member FUCA (ML)	3	-4634.469	-16.153	-155.628	156.464	-4.955	47.741	47.998
Force in member FLCA (JK)	2	1016.396	-0.057	0.000	0.057	0.024	0.000	0.024
Force in member FLCA (JI)	1	-444.300	0.045	0.000	0.045	0.024	0.000	0.024
Force in member FTR (OP)		254.403	0.000	0.000	0.000	0.000	0.000	0.000
Force in member FPR (QR)		8779.588	0.000	0.000	0.000	0.000	0.000	0.000

B-4 Complete Member Loads using the Steered Model

Table B.5. Internal axial forces, bending moment magnitudes, and shear force magnitudes for the suspension members as calculated by the Steered Model. Note that all the non-steered loading scenarios result in the same values as for the Beam Model.

Magnitude and Components of Section Forces and Moments in Elements

Steer Angle		0			5.5			11			16.5			22		
Member	Region	Steered Model, Axial Force (N)	Steered Model, Shear Force Magnitude (N)	Steered Model, Bending Moment Magnitude (Nm)	Steered Model, Axial Force (N)	Steered Model, Shear Force Magnitude (N)	Steered Model, Bending Moment Magnitude (Nm)	Steered Model, Axial Force (N)	Steered Model, Shear Force Magnitude (N)	Steered Model, Bending Moment Magnitude (Nm)	Steered Model, Axial Force (N)	Steered Model, Shear Force Magnitude (N)	Steered Model, Bending Moment Magnitude (Nm)	Steered Model, Axial Force (N)	Steered Model, Shear Force Magnitude (N)	Steered Model, Bending Moment Magnitude (Nm)
1.4g Pure Lateral																
FUCA (MN)	2	-1613.250	52.427	20.865	-1415.153	51.911	20.660	-1219.671	51.434	20.470	-1028.607	50.999	20.297	-843.730	50.611	20.142
FUCA (ML)	3	-450.142	55.173	16.925	-583.166	54.623	16.757	-726.888	54.115	16.600	-879.992	53.651	16.458	-1041.057	53.236	16.331
FLCA (JK)	2	-2115.036	0.024	0.010	-2423.102	0.036	0.015	-2707.232	0.096	0.041	-2964.815	0.154	0.066	-3193.472	0.211	0.090
FLCA (JI)	1	-185.143	0.019	0.010	280.940	0.029	0.015	742.853	0.076	0.041	1196.336	0.122	0.066	1637.221	0.167	0.090
FTR (PO)		-360.745	0.000	0.000	-406.793	0.000	0.000	-446.259	0.000	0.000	-478.784	0.000	0.000	-504.068	0.000	0.000
FPR (QR)		3095.798	0.000	0.000	3065.261	0.000	0.000	3036.988	0.000	0.000	3011.233	0.000	0.000	2988.240	0.000	0.000
Pure Lateral FLT																
FUCA (MN)	2	-1712.201	55.642	22.144	-1504.317	55.101	21.929	-1299.183	54.599	21.729	-1098.688	54.143	21.548	-904.675	53.736	21.386
FUCA (ML)	3	-491.675	58.556	17.963	-631.269	57.979	17.786	-782.086	57.446	17.622	-942.747	56.959	17.473	-1111.771	56.524	17.340
FLCA (JK)	2	-2231.570	0.025	0.011	-2554.849	0.038	0.016	-2853.009	0.100	0.043	-3123.310	0.161	0.069	-3363.265	0.221	0.095
FLCA (JI)	1	-196.525	0.020	0.011	292.578	0.030	0.016	777.300	0.079	0.043	1253.184	0.128	0.069	1715.839	0.175	0.095
FTR (PO)		-360.761	0.000	0.000	-409.081	0.000	0.000	-450.498	0.000	0.000	-484.634	0.000	0.000	-511.158	0.000	0.000
FPR (QR)		3285.626	0.000	0.000	3253.585	0.000	0.000	3223.911	0.000	0.000	3196.888	0.000	0.000	3172.761	0.000	0.000
LH Turn and Braking																
FUCA (MN)	2	-80.518	52.847	21.032	52.826	52.763	20.999	169.074	52.745	20.992	267.177	52.795	21.011	346.214	52.911	21.058
FUCA (ML)	3	-1972.702	55.560	17.044	-2166.320	55.467	17.015	-2357.255	55.444	17.008	-2543.773	55.493	17.023	-2724.149	55.612	17.060
FLCA (JK)	2	-3458.950	0.478	0.205	-3500.435	0.521	0.223	-3501.306	0.559	0.239	-3461.575	0.591	0.253	-3381.587	0.617	0.264
FLCA (JI)	1	3714.914	0.379	0.205	4045.275	0.413	0.223	4336.838	0.442	0.239	4586.917	0.468	0.253	4793.226	0.489	0.264
FTR (PO)		-1316.825	0.000	0.000	-1297.942	0.000	0.000	-1270.875	0.000	0.000	-1235.858	0.000	0.000	-1193.222	0.000	0.000
FPR (QR)		3119.863	0.000	0.000	3114.832	0.000	0.000	3113.742	0.000	0.000	3116.606	0.000	0.000	3123.408	0.000	0.000

B-5 Complete Member Loads using the Sprung Model

Table B.6. Internal axial forces, bending moment magnitudes, and shear force magnitudes for the suspension members as calculated by the Sprung Model for the steered scenarios. Note that the yellow highlighted cell is the only change from the Steered Model.

Magnitude and Components of Section Forces and Moments in Elements

Steer Angle		0			5.5			11			16.5			22		
Member	Region	Steered Model, Axial Force (N)	Steered Model, Shear Force Magnitude (N)	Steered Model, Bending Moment Magnitude (Nm)	Steered Model, Axial Force (N)	Steered Model, Shear Force Magnitude (N)	Steered Model, Bending Moment Magnitude (Nm)	Steered Model, Axial Force (N)	Steered Model, Shear Force Magnitude (N)	Steered Model, Bending Moment Magnitude (Nm)	Steered Model, Axial Force (N)	Steered Model, Shear Force Magnitude (N)	Steered Model, Bending Moment Magnitude (Nm)	Steered Model, Axial Force (N)	Steered Model, Shear Force Magnitude (N)	Steered Model, Bending Moment Magnitude (Nm)
1.4g Pure Lateral																
FUCA (MN)	2	-1613.250	52.427	20.865	-1415.153	51.911	20.660	-1219.671	51.434	20.470	-1028.607	50.999	20.297	-843.730	50.611	20.142
FUCA (ML)	3	-450.142	55.173	16.925	-583.166	54.623	16.757	-726.888	54.115	16.600	-879.992	53.651	16.458	-1041.057	53.236	16.331
FLCA (JK)	2	-2115.036	0.024	0.010	-2423.102	0.036	0.015	-2707.232	0.096	0.041	-2964.815	0.154	0.066	-3193.472	0.211	0.090
FLCA (JI)	1	-185.143	0.019	0.010	280.940	0.029	0.015	742.853	0.076	0.041	1196.336	0.122	0.066	1637.221	0.167	0.090
FTR (PO)		-360.745	0.000	0.000	-406.793	0.000	0.000	-446.259	0.000	0.000	-478.784	0.000	0.000	-504.064	0.000	0.000
FPR (QR)		3095.798	0.000	0.000	3065.261	0.000	0.000	3036.988	0.000	0.000	3011.233	0.000	0.000	2988.240	0.000	0.000
Pure Lateral FLT																
FUCA (MN)	2	-1712.201	55.642	22.144	-1504.317	55.101	21.929	-1299.183	54.599	21.729	-1098.688	54.143	21.548	-904.675	53.736	21.386
FUCA (ML)	3	-491.675	58.556	17.963	-631.269	57.979	17.786	-782.086	57.446	17.622	-942.747	56.959	17.473	-1111.771	56.524	17.340
FLCA (JK)	2	-2231.570	0.025	0.011	-2554.849	0.038	0.016	-2853.009	0.100	0.043	-3123.310	0.161	0.069	-3363.265	0.221	0.095
FLCA (JI)	1	-196.525	0.020	0.011	292.578	0.030	0.016	777.300	0.079	0.043	1253.184	0.128	0.069	1715.839	0.175	0.095
FTR (PO)		-360.761	0.000	0.000	-409.081	0.000	0.000	-450.498	0.000	0.000	-484.634	0.000	0.000	-511.158	0.000	0.000
FPR (QR)		3285.626	0.000	0.000	3253.585	0.000	0.000	3223.911	0.000	0.000	3196.888	0.000	0.000	3172.761	0.000	0.000
LH Turn and Braking																
FUCA (MN)	2	-80.518	52.847	21.032	52.826	52.763	20.999	169.074	52.745	20.992	267.177	52.795	21.011	346.214	52.911	21.058
FUCA (ML)	3	-1972.702	55.560	17.044	-2166.320	55.467	17.015	-2357.255	55.444	17.008	-2543.773	55.493	17.023	-2724.149	55.612	17.060
FLCA (JK)	2	-3458.960	0.478	0.205	-3500.435	0.521	0.223	-3501.306	0.559	0.239	-3461.575	0.591	0.253	-3381.587	0.617	0.264
FLCA (JI)	1	3714.914	0.379	0.205	4045.275	0.413	0.223	4336.838	0.442	0.239	4586.917	0.468	0.253	4793.226	0.489	0.264
FTR (PO)		-1316.825	0.000	0.000	-1297.942	0.000	0.000	-1270.875	0.000	0.000	-1235.858	0.000	0.000	-1193.222	0.000	0.000
FPR (QR)		3119.863	0.000	0.000	3114.832	0.000	0.000	3113.742	0.000	0.000	3116.606	0.000	0.000	3123.408	0.000	0.000

Table B.7. Internal axial forces, bending moment magnitudes, and shear force magnitudes for the suspension members as calculated by the Sprung Model for the non-steered scenarios.

Internal Member Loads								
Members	**Region**	**ABAQUS - Vertical Movement, Axial Force (N)**	**ABAQUS - Proper Sections, SF2 (N)**	**ABAQUS - Proper Sections, SF3 (N)**	**ABAQUS - Vertical Movement, Shear Force Magnitude (N)**	**ABAQUS - Proper Sections, SM1 (Nm)**	**ABAQUS - Proper Sections, SM2 (Nm)**	**Vertical Movement, Bending Moment Magnitude (Nm)**
1.4g Pure Lateral								
Force in member FUCA (MN)	2	-1613.250	-1.903	52.392	52.427	0.757	20.851	20.865
Force in member FUCA (ML)	3	-450.142	-5.710	-54.876	55.173	-1.752	16.834	16.925
Force in member FLCA (JK)	2	-2115.036	-0.024	0.000	0.024	0.010	0.000	0.010
Force in member FLCA (JI)	1	-185.143	0.019	0.000	0.019	0.010	0.000	0.010
Force in member FTR (OP)		-360.745	0.000	0.000	0.000	0.000	0.000	0.000
Force in member FPR (QR)		3095.798	0.000	0.000	0.000	0.000	0.000	0.000
Pure Lateral FLT								
Force in member FUCA (MN)	2	-1712.201	-2.020	55.605	55.642	0.803	22.130	22.144
Force in member FUCA (ML)	3	-491.675	-6.060	-58.241	58.556	-1.859	17.867	17.963
Force in member FLCA (JK)	2	-2231.570	-0.025	0.000	0.025	0.011	0.000	0.011
Force in member FLCA (JI)	1	-196.525	0.020	0.000	0.020	0.011	0.000	0.011
Force in member FTR (OP)		-360.761	0.000	0.000	0.000	0.000	0.000	0.000
Force in member FPR (QR)		3285.626	0.000	0.000	0.000	0.000	0.000	0.000
Pure Braking FLT								
Force in member FUCA (MN)	2	570.480	-2.642	58.976	59.035	1.051	23.471	23.495
Force in member FUCA (ML)	3	-3696.472	-5.777	-61.772	62.042	-1.772	18.950	19.032
Force in member FLCA (JK)	2	-3924.871	0.751	0.000	0.751	-0.321	0.000	0.321
Force in member FLCA (JI)	1	5829.083	-0.594	0.000	0.594	-0.321	0.000	0.321
Force in member FTR (OP)		-265.448	0.000	0.000	0.000	0.000	0.000	0.000
Force in member FPR (QR)		3484.821	0.000	0.000	0.000	0.000	0.000	0.000
1.4g Pure Braking								
Force in member FUCA (MN)	2	420.730	-1.852	41.249	41.291	0.737	16.416	16.433
Force in member FUCA (ML)	3	-2602.703	-4.035	-43.205	43.393	-1.238	13.254	13.311
Force in member FLCA (JK)	2	-2817.526	0.532	0.000	0.532	-0.228	0.000	0.228
Force in member FLCA (JI)	1	4133.465	-0.421	0.000	0.421	-0.228	0.000	0.228
Force in member FTR (OP)		-157.256	0.000	0.000	0.000	0.000	0.000	0.000
Force in member FPR (QR)		2437.359	0.000	0.000	0.000	0.000	0.000	0.000
LH Turn and Braking								
Force in member FUCA (MN)	2	-80.518	-2.239	52.800	52.847	0.891	21.013	21.032
Force in member FUCA (ML)	3	-1972.702	-5.336	-55.303	55.560	-1.637	16.965	17.044
Force in member FLCA (JK)	2	-3458.950	0.478	0.000	0.478	-0.205	0.000	0.205
Force in member FLCA (JI)	1	3714.914	-0.379	0.000	0.379	-0.205	0.000	0.205
Force in member FTR (OP)		-1316.825	0.000	0.000	0.000	0.000	0.000	0.000
Force in member FPR (QR)		3119.863	0.000	0.000	0.000	0.000	0.000	0.000
1.5g Full Skid								
Force in member FUCA (MN)	2	-863.831	-1.008	27.817	27.835	0.401	11.071	11.078
Force in member FUCA (ML)	3	-250.697	-3.033	-29.136	29.293	-0.931	8.938	8.986
Force in member FLCA (JK)	2	-1433.097	-0.014	0.000	0.014	0.006	0.000	0.006
Force in member FLCA (JI)	1	-105.654	0.011	0.000	0.011	0.006	0.000	0.006
Force in member FTR (OP)		165.545	0.000	0.000	0.000	0.000	0.000	0.000
Force in member FPR (QR)		1643.658	0.000	0.000	0.000	0.000	0.000	0.000
5g Bump								
Force in member FUCA (MN)	2	-4494.883	-5.427	148.583	148.682	2.159	59.133	59.172
Force in member FUCA (ML)	3	-4634.469	-16.153	-155.628	156.464	-4.955	47.741	47.998
Force in member FLCA (JK)	2	1016.396	-0.057	0.000	0.057	0.024	0.000	0.024
Force in member FLCA (JI)	1	-444.300	0.045	0.000	0.045	0.024	0.000	0.024
Force in member FTR (OP)		254.403	0.000	0.000	0.000	0.000	0.000	0.000
Force in member FPR (QR)		8779.588	0.000	0.000	0.000	0.000	0.000	0.000

Appendix C: Complete Wheel Load Data

C-1 Wheel Center Loads for All Wheels and All Loading Scenarios

Table C.1. Wheel center loads for left hand cornering at 1.4g with expected load transfer.

	PURE CORNERING 1.4g						
		LF		RF		LR		RR
Force (N)	X	0.00		**0.00**		0.00		0.00
	Y	-123.64		**-1802.29**		-451.17		-1916.53
	Z	-68.72		**-1134.97**		-255.77		-1209.48
Moment (Nm)	Mz (aligning torque)	1.40		**-12.69**		6.01		-9.13
	My (braking and engine torque)	0.00		**0.00**		0.00		0.00
	Mx (overturning moment)	31.40		**457.78**		114.60		486.80

Table C.2. Wheel center loads for left hand cornering with full load transfer.

	PURE LATERAL FLT						
		LF		RF		LR		RR
Force (N)	X	0.00		**0.00**		0.00		0.00
	Y	0.00		**-1891.30**		0.00		-2214.45
	Z	0.00		**-1203.69**		0.00		-1465.24
Moment (Nm)	Mz (aligning torque)	0.00		**-14.32**		0.00		-12.42
	My (braking and engine torque)	0.00		**0.00**		0.00		0.00
	Mx (overturning moment)	0.00		**480.39**		0.00		562.47

Table C.3. Wheel center loads for pure braking at 1.4g with expected load transfer.

	PURE BRAKING 1.4g						
		LF		RF		LR		RR
Force (N)	X	-1585.06		**-1585.06**		-431.21		-431.21
	Y	0.00		**0.00**		0.00		0.00
	Z	-934.71		**-934.71**		-399.76		-399.76
Moment (Nm)	Mz (aligning torque)	13.06		**-12.85**		7.61		-7.53
	My (braking and engine torque)	-402.60		**-402.60**		0.00		0.00
	Mx (overturning moment)	0.00		**0.00**		0.00		0.00

Table C.4. Wheel center loads for pure braking with full load transfer.

	PURE BRAKING FLT						
		LF		RF		LR		RR
Force (N)	X	-2235.80		**-2235.80**		0.00		0.00
	Y	0.00		**0.00**		0.00		0.00
	Z	-1334.47		**-1334.47**		0.00		0.00
Moment (Nm)	Mz (aligning torque)	15.66		**-15.43**		0.00		0.00
	My (braking and engine torque)	-567.89		**-567.89**		0.00		0.00
	Mx (overturning moment)	0.00		**0.00**		0.00		0.00

Table C.5. Wheel center loads for combined left hand cornering and braking.

	LH TURN AND BRAKING						
		LF		**RF**		**LR**		**RR**
Force (N)	X	-401.07		**-1442.88**		-282.28		-1024.29
	Y	-570.46		**-1342.93**		-30.49		-994.06
	Z	-460.24		**-1214.19**		-160.06		-834.44
Moment (Nm)	Mz (aligning torque)	18.23		**30.61**		7.42		27.83
	My (braking and engine torque)	-101.87		**-366.49**		0.00		0.00
	Mx (overturning moment)	144.90		**341.11**		7.74		252.49

Table C.6. Wheel center loads for a 1.5g full vehicle skid.

	1.5g FULL VEHICLE SKID						
		LF		**RF**		**LR**		**RR**
Force (N)	X	0.00		**0.00**		0.00		0.00
	Y	-946.57		**-932.88**		-1135.66		-1116.54
	Z	-601.84		**-601.84**		-732.62		-732.62
Moment (Nm)	Mz (aligning torque)	-3.23		**-27.60**		-5.05		-33.51
	My (braking and engine torque)	0.00		**0.00**		0.00		0.00
	Mx (overturning moment)	240.43		**236.95**		288.46		283.60

Table C.7. Wheel center loads for a 5g bump at each corner.

	5G BUMP						
		LF		**RF**		**LR**		**RR**
Force (N)	X	0.00		**0.00**		0.00		0.00
	Y	0.00		**0.00**		0.00		0.00
	Z	-3009.22		**-3009.22**		-3663.11		-3663.11
Moment (Nm)	Mz (aligning torque)	0.00		**0.00**		0.00		0.00
	My (braking and engine torque)	0.00		**0.00**		0.00		0.00
	Mx (overturning moment)	0.00		**0.00**		0.00		0.00

Appendix D: Steer Angle Calculations

D-1 Steer Angle versus Lateral Movement of Tie Rod Calculations

To properly model a steered suspension, the tie rod must be displaced laterally (car Y-axis) to induce a steer angle on the upright/tire assembly. A process of trigonometry, similar to that used to find that radius of travel, is used to determine the amount of tie rod movement for each steer angle. Beginning with the steering geometry in the top view shown in Figure D.1, the steering arm on the tie rod is isolated for inspection.

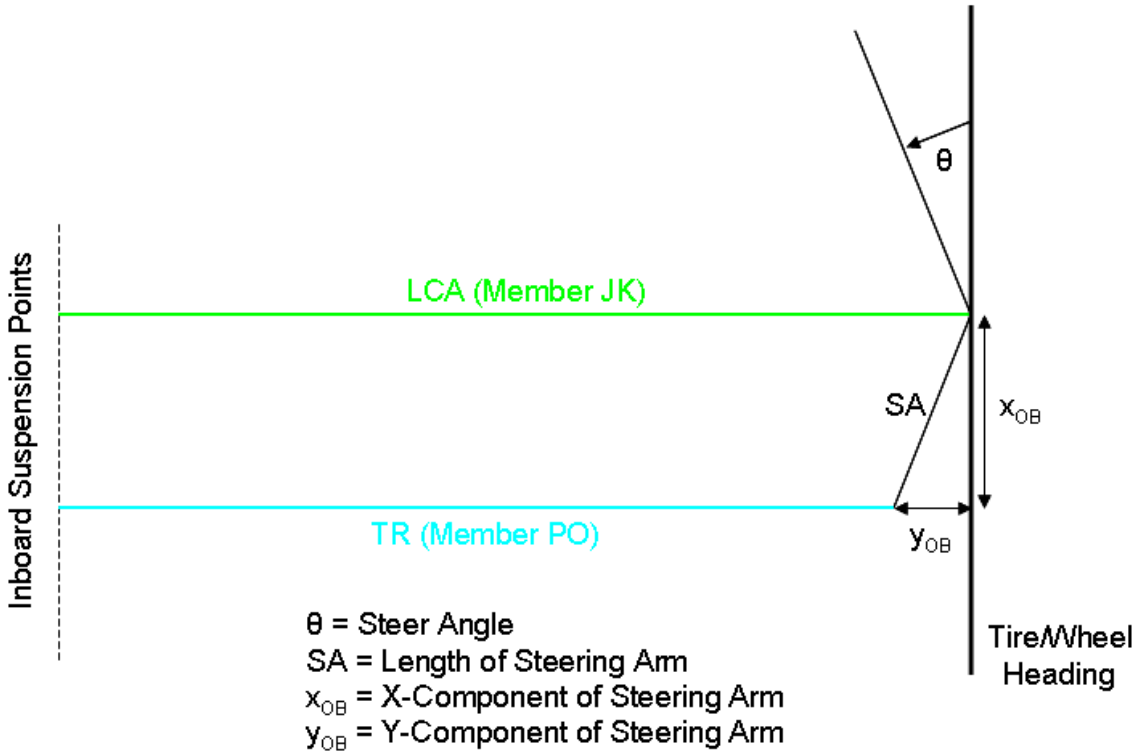

Figure D.1. Geometry of steering linkage in the top view (not to scale).

From the data provided by the suspension designer, the static position of the suspension with no steering input, results in x_{OB} = 59.7 mm and y_{OB} = 23.2 mm. This yields a value for *SA* of 64.1 mm. Figure D.2 is a closer view of the steering arm with notation for steering input.

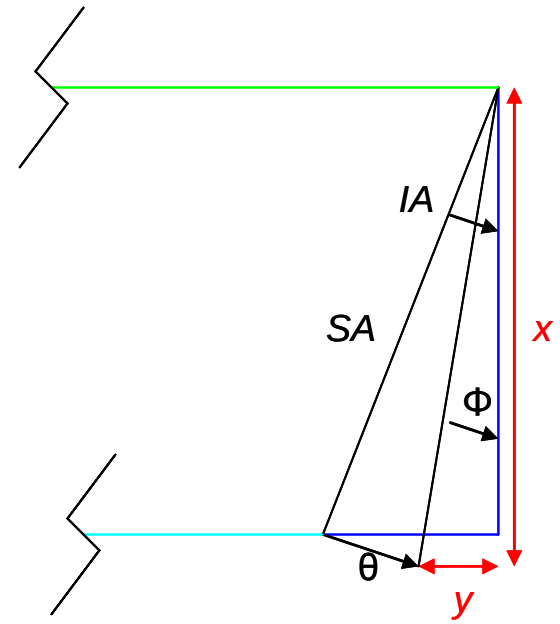

θ = Steer Angle
Φ = Angle of Steering Arm to Car X-Axis
SA = Length of Steering Arm
IA = Angle of Steering Arm in Non-Steered Position to X-axis

Figure D.2. Steering arm detail showing the notation for steered calculations.

The angle Φ is defined in Equation (D.1) as

$$\Phi = \theta - IA\,, \tag{D.1}$$

where angle *IA* is the fixed angle representing the steering arm in the non-steered position to the X-axis. The values for *x* and *y* can then be calculated by

$$\sin\Phi = \frac{y}{SA}\,, \tag{D.2}$$

$$y = SA\sin\Phi\,, \tag{D.3}$$

and

$$\cos\Phi = \frac{x}{SA}\,, \tag{D.4}$$

$$x = SA\cos\Phi\,. \tag{D.5}$$

Next, the movement of the outboard tie rod point (Suspension Point P) is determined by using Figure D.3 as reference.

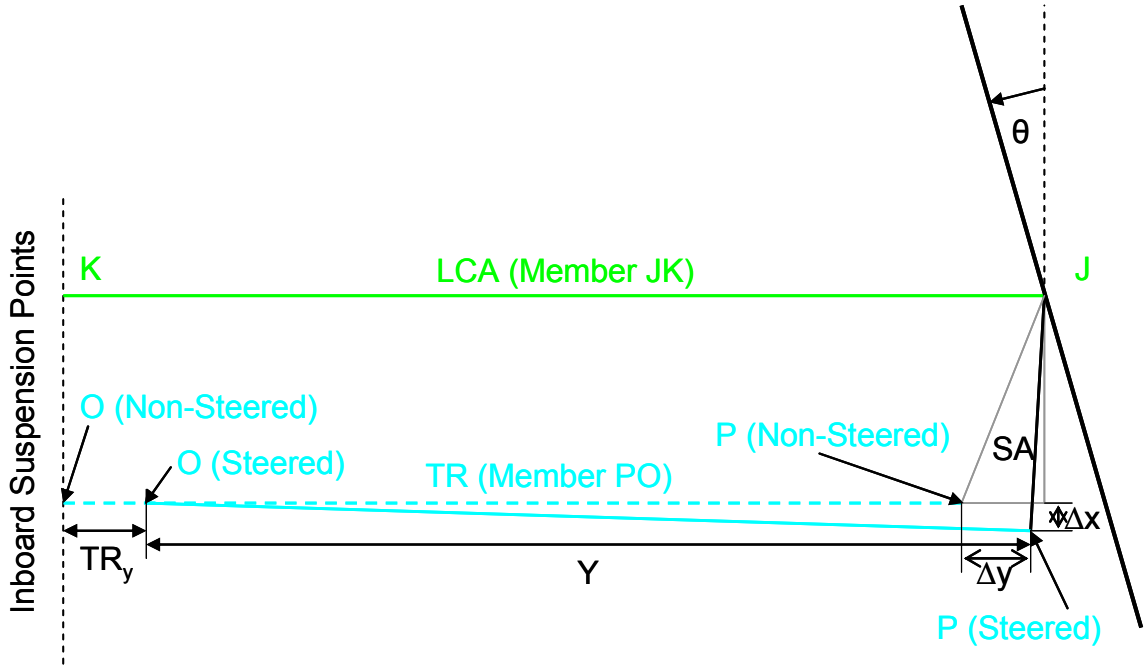

Figure D.3. Diagram of the tie rod movement under steering in the top view.

Using the non-steered values for x_{OB} and y_{OB}, Δx and Δy are defined as

$$\Delta x = x - x_{OB}\,, \tag{D.6}$$

and

$$\Delta y = y_{OB} - y\,. \tag{D.7}$$

Substituting Equation (D.3) and Equation (D.5) into Equation (D.7) and Equation (D.6) respectively yields

$$\Delta y = y_{OB} - SA\sin\Phi\,, \tag{D.8}$$

and

$$\Delta x = SA\cos\Phi - x_{OB}\,. \tag{D.9}$$

The amount of lateral movement at the inboard tie rod point is defined as the length of the tie rod minus the value Y plus the outboard y movement (Δy) shown by

$$TR_y = TR - Y + \Delta y\,. \tag{D.10}$$

Figure D.4 shows a detailed view of the triangle formed by the tie rod when steered. This geometry is used to determine the unknown variable *Y* in order to calculate the inboard tie rod movement.

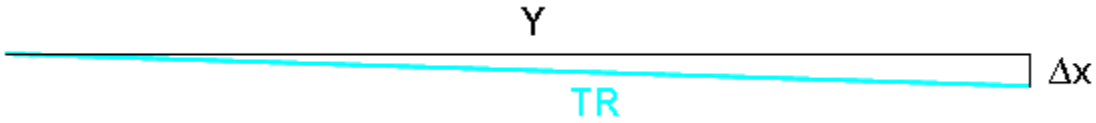

Figure D.4. Geometry of the triangle formed when the tie rod is displaced due to a steering input.

This geometry is a simple right triangle that allows the Pythagorean Theorem to be used to define *Y* as

$$\Delta x^2 + Y^2 = TR^2, \tag{D.11}$$

$$Y = \sqrt{TR^2 - \Delta x^2}\ . \tag{D.12}$$

Substituting Equation (D.9) into Equation (D.12) results in

$$Y = \sqrt{TR^2 - \left(SA\cos\Phi - 59.7\right)^2}\ . \tag{D.13}$$

Using Equation (D.13) in Equation (D.10) allows the calculation of the tie rod movement to be written as

$$TR_y = TR - \sqrt{TR^2 - \left(SA\cos\Phi - 59.7\right)^2} + 23.2 - SA\sin\Phi\ . \tag{D.14}$$

Equation (D.14) is the far left column in all tables in Appendix D-2. This is the amount by which the inboard tie rod point (Point O) was displaced laterally in each of the steered loading scenarios.

D-2 Steer Angle versus Radius of Travel Data

Table D.1. Steer angle and radius of travel data for the left hand corner loading scenario.

LH_Corner

Steer Angle, θ	Slip Angle, α	Angle of Travel, θ_T	β	Slip of Rear, α	L (m)	R (m)	Δy (mm)	Δx (mm)	Y (mm)	**TR_y (mm)**
0	**13.3486**	**-13.3486**	**103.349**	**-13.349**	**-1.6E+16**	**1.6E+16**	0.000	0.000	415.4929	**0.00**
1	13.3486	-12.3486	102.349	-13.349	90.935	90.322	1.045	0.397	415.4928	**1.05**
2	13.3486	-11.3486	101.349	-13.349	45.641	45.028	2.097	0.775	415.4922	**2.10**
3	13.3486	-10.3486	100.349	-13.349	30.537	29.924	3.156	1.135	415.4914	**3.16**
4	13.3486	-9.3486	99.349	-13.349	22.981	22.367	4.220	1.476	415.4903	**4.22**
5.5	**13.3486**	**-7.8486**	**97.849**	**-13.349**	**16.792**	**16.178**	5.828	1.953	415.4884	**5.83**
6	13.3486	-7.3486	97.349	-13.349	15.415	14.801	6.367	2.102	415.4876	**6.37**
7	13.3486	-6.3486	96.349	-13.349	13.249	12.636	7.448	2.387	415.4861	**7.45**
8	13.3486	-5.3486	95.349	-13.349	11.623	11.009	8.533	2.654	415.4845	**8.54**
9	13.3486	-4.3486	94.349	-13.349	10.355	9.742	9.624	2.901	415.4828	**9.63**
10	13.3486	-3.3486	93.349	-13.349	9.340	8.726	10.718	3.129	415.4812	**10.73**
11	**13.3486**	**-2.3486**	**92.349**	**-13.349**	**8.507**	**7.893**	11.816	3.338	415.4795	**11.83**
12	13.3486	-1.3486	91.349	-13.349	7.812	7.198	12.918	3.528	415.4780	**12.93**
13	13.3486	-0.3486	90.349	-13.349	7.222	6.608	14.023	3.698	415.4765	**14.04**
14	13.3486	0.6514	89.349	-13.349	6.715	6.101	15.131	3.849	415.4751	**15.15**
15	13.3486	1.6514	88.349	-13.349	6.274	5.660	16.241	3.981	415.4739	**16.26**
16.5	**13.3486**	**3.1514**	**86.849**	**-13.349**	**5.712**	**5.097**	17.910	4.143	415.4723	**17.93**
17	13.3486	3.6514	86.349	-13.349	5.545	4.931	18.467	4.187	415.4719	**18.49**
18	13.3486	4.6514	85.349	-13.349	5.240	4.625	19.583	4.260	415.4711	**19.60**
19	13.3486	5.6514	84.349	-13.349	4.966	4.351	20.699	4.315	415.4705	**20.72**
20	13.3486	6.6514	83.349	-13.349	4.718	4.103	21.817	4.349	415.4702	**21.84**
21	13.3486	7.6514	82.349	-13.349	4.493	3.878	22.935	4.364	415.4700	**22.96**
22	**13.3486**	**8.6514**	**81.349**	**-13.349**	**4.288**	**3.672**	24.053	4.360	415.4701	**24.08**
23	13.3486	9.6514	80.349	-13.349	4.099	3.483	25.170	4.336	415.4703	**25.1929**
24	13.3486	10.6514	79.349	-13.349	3.925	3.310	26.287	4.292	415.4708	**26.3096**
25	13.3486	11.6514	78.349	-13.349	3.765	3.149	27.404	4.230	415.4714	**27.4251**

Slip Angle	
LH_Corner	13.3486 deg
Wheelbase, l	1663.70 mm
Half Track Front, t_f	609.60 mm
Rear Axle to CG, b	728.35 mm
Half Track Difference, t_r-t_f	25.40 mm
Steering	
y_{OB}	23.24 mm
x_{OB}	59.69 mm
IA	21.27 deg
SA	64.05 mm
TR Length	415.49 mm

d (m)	r (m)	CG r (m)
	18.25	9.125
	15.25	7.625 8.3235
	21.25	10.625 9.9265
Half Track Front, t_f (m)	0.6985	

Table D.2. Steer angle and radius of travel data for the left hand corner with full load transfer loading scenario.

LH_Corner_FLT

Steer Angle, θ	Slip Angle, α	Angle of Travel, θ+α	β	Slip of Rear, α	L	R (m)	Δy	Δx	Y	TR_y (in)
0	14.0992	-14.0992	104.099	-14.099	7.5E+15	7.5E+15	0.000	0.000	415.4929	**0.00**
1	14.0992	-13.0992	103.099	-14.099	90.396	89.783	1.045	0.397	415.4928	**1.05**
2	14.0992	-12.0992	102.099	-14.099	45.381	44.768	2.097	0.775	415.4922	**2.10**
3	14.0992	-11.0992	101.099	-14.099	30.371	29.757	3.156	1.135	415.4914	**3.16**
4	14.0992	-10.0992	100.099	-14.099	22.861	22.247	4.220	1.476	415.4903	**4.22**
5.5	14.0992	-8.5992	98.599	-14.099	16.710	16.096	5.828	1.953	415.4884	**5.83**
6	14.0992	-8.0992	98.099	-14.099	15.341	14.728	6.367	2.102	415.4876	**6.37**
7	14.0992	-7.0992	97.099	-14.099	13.189	12.575	7.448	2.387	415.4861	**7.45**
8	14.0992	-6.0992	96.099	-14.099	11.573	10.959	8.533	2.654	415.4845	**8.54**
9	14.0992	-5.0992	95.099	-14.099	10.313	9.699	9.624	2.901	415.4828	**9.63**
10	14.0992	-4.0992	94.099	-14.099	9.304	8.690	10.718	3.129	415.4812	**10.73**
11	14.0992	-3.0992	93.099	-14.099	8.477	7.862	11.816	3.338	415.4795	**11.83**
12	14.0992	-2.0992	92.099	-14.099	7.785	7.171	12.918	3.528	415.4780	**12.93**
13	14.0992	-1.0992	91.099	-14.099	7.199	6.585	14.023	3.698	415.4765	**14.04**
14	14.0992	-0.0992	90.099	-14.099	6.695	6.081	15.131	3.849	415.4751	**15.15**
15	14.0992	0.9008	89.099	-14.099	6.258	5.643	16.241	3.981	415.4739	**16.26**
16.5	14.0992	2.4008	87.599	-14.099	5.698	5.083	17.910	4.143	415.4723	**17.93**
17	14.0992	2.9008	87.099	-14.099	5.533	4.918	18.467	4.187	415.4719	**18.49**
18	14.0992	3.9008	86.099	-14.099	5.230	4.614	19.583	4.260	415.4711	**19.60**
19	14.0992	4.9008	85.099	-14.099	4.957	4.342	20.699	4.315	415.4705	**20.72**
20	14.0992	5.9008	84.099	-14.099	4.711	4.095	21.817	4.349	415.4702	**21.84**
21	14.0992	6.9008	83.099	-14.099	4.487	3.871	22.935	4.364	415.4700	**22.96**
22	14.0992	7.9008	82.099	-14.099	4.283	3.667	24.053	4.360	415.4701	**24.08**
23	14.0992	8.9008	81.099	-14.099	4.096	3.480	25.170	4.336	415.4703	**25.1929**
24	14.0992	9.9008	80.099	-14.099	3.923	3.307	26.287	4.292	415.4708	**26.3096**
25	14.0992	10.9008	79.099	-14.099	3.764	3.147	27.404	4.230	415.4714	**27.4251**

Slip Angle	
LH_Corner	14.0992 deg
Wheelbase, l	1663.7 mm
Half Track Front, tf	609.6 mm
Rear Axle to CG, b	728.345 mm
Half Track Difference, tf-tr	25.4 mm
Steering	
yOB	23.241 mm
xOB	59.69 mm
IA	21.27403 deg
SA	64.05498 mm
TR Length	415.4929 mm

d (m)	r (m)	CG r (m)
	18.25	9.125
	15.25	7.625 8.3235
	21.25	10.625 9.9265
Half Track Front, tf (m)		0.6985

Table D.3. Steer angle and radius of travel data for the left hand corner and braking combined loading scenario.

LH_Braking_Combined

Steer Angle, θ	Slip Angle, α	Angle of Travel, θ-α	β	Slip of Rear, α	L	R (m)	Δy	Δx	Y	TR_y (in)
0	3.4504	-3.4504	93.450	-3.450	-4.1E+16	4.1E+16	0.000	0.000	415.4929	**0.00**
1	3.4504	-2.4504	92.450	-3.450	95.156	94.545	1.045	0.397	415.4928	**1.05**
2	3.4504	-1.4504	91.450	-3.450	47.613	47.003	2.097	0.775	415.4922	**2.10**
3	3.4504	-0.4504	90.450	-3.450	31.759	31.149	3.156	1.135	415.4914	**3.16**
4	3.4504	0.5496	89.450	-3.450	23.828	23.217	4.220	1.476	415.4903	**4.22**
5.5	3.4504	2.0496	87.950	-3.450	17.331	16.721	5.828	1.953	415.4884	**5.83**
6	3.4504	2.5496	87.450	-3.450	15.886	15.275	6.367	2.102	415.4876	**6.37**
7	3.4504	3.5496	86.450	-3.450	13.613	13.002	7.448	2.387	415.4861	**7.45**
8	3.4504	4.5496	85.450	-3.450	11.906	11.295	8.533	2.654	415.4845	**8.54**
9	3.4504	5.5496	84.450	-3.450	10.576	9.964	9.624	2.901	415.4828	**9.63**
10	3.4504	6.5496	83.450	-3.450	9.510	8.898	10.718	3.129	415.4812	**10.73**
11	3.4504	7.5496	82.450	-3.450	8.636	8.024	11.816	3.338	415.4795	**11.83**
12	3.4504	8.5496	81.450	-3.450	7.906	7.294	12.918	3.528	415.4780	**12.93**
13	3.4504	9.5496	80.450	-3.450	7.287	6.675	14.023	3.698	415.4765	**14.04**
14	3.4504	10.5496	79.450	-3.450	6.755	6.143	15.131	3.849	415.4751	**15.15**
15	3.4504	11.5496	78.450	-3.450	6.292	5.680	16.241	3.981	415.4739	**16.26**
16.5	3.4504	13.0496	76.950	-3.450	5.701	5.089	17.910	4.143	415.4723	**17.93**
17	3.4504	13.5496	76.450	-3.450	5.527	4.915	18.467	4.187	415.4719	**18.49**
18	3.4504	14.5496	75.450	-3.450	5.207	4.594	19.583	4.260	415.4711	**19.60**
19	3.4504	15.5496	74.450	-3.450	4.919	4.306	20.699	4.315	415.4705	**20.72**
20	3.4504	16.5496	73.450	-3.450	4.659	4.046	21.817	4.349	415.4702	**21.84**
21	3.4504	17.5496	72.450	-3.450	4.422	3.809	22.935	4.364	415.4700	**22.96**
22	3.4504	18.5496	71.450	-3.450	4.207	3.594	24.053	4.360	415.4701	**24.08**
23	3.4504	19.5496	70.450	-3.450	4.009	3.396	25.170	4.336	415.4703	**25.1929**
24	3.4504	20.5496	69.450	-3.450	3.827	3.213	26.287	4.292	415.4708	**26.3096**
25	3.4504	21.5496	68.450	-3.450	3.658	3.045	27.404	4.230	415.4714	**27.4251**

LH_Corner	Slip Angle	3.4504	deg
Wheelbase, l		1663.7	mm
Half Track Front, tf		609.6	mm
Rear Axle to CG, b		728.345	mm
Half Track Difference, tf-tr		25.4	mm
Steering			
yOB		23.241	mm
xOB		59.69	mm
IA		21.27403	deg
SA		64.05498	mm
TR Length		415.4929	mm

d (m)	r (m)	CG r (m)
	18.25	9.125
	15.25	7.625
	21.25	10.625
Half Track Front, tf (m)		0.6985

8.3235
9.9265